The deubiquitinase Otud7b suppresses cone photoreceptor cell degeneration in mouse models of retinal degenerative diseases

脱ユビキチン化酵素 Otud7b は網膜変性疾患マウスモデルにおける錐体視細胞変性を抑制する

大阪大学 理学研究科 生物科学専攻

分子発生学研究室

(PI: 古川 貴久 教授)

Leah Rie Varner

Abstract

The retina, a light-sensitive tissue that is located in the back of the eyes, is crucial for our vision. Light penetrates the eyes and reaches the retinal photoreceptor cells, which convert the light into an electrical signal that is transmitted to the brain. These retinal photoreceptor cells can be categorized into two types: rods and cones. Rod photoreceptor cells are essential for dim light vision, whereas cone photoreceptor cells are essential for daylight, high acuity, and color vision. Primary and secondary cone photoreceptor cell death in retinal degenerative diseases, including age-related macular degeneration and retinitis pigmentosa, leads to severe visual impairment and blindness. Although the protection of cone photoreceptor cells under stress conditions, such as retinal degenerative diseases, is crucial for maintaining vision, the underlying molecular mechanisms are unclear.

Through our microarray analysis, Otud7b/Cezanne was identified as a candidate molecule which regulates photoreceptor development and maintenance. Otud7b is a multifunctional deubiquitinase that is involved in several cell signaling pathways; however, its role in the retina is not known. In this study, we investigated the function of the deubiquitinase Otud7b in the retina. We found that Otud7b is predominantly expressed in photoreceptor cells in the mouse retina. While the ablation of *Otud7b* did not cause a significant defect in the development and maturation of the mouse retina, *Otud7b*$^{-/-}$ mice subjected to light-induced damage, a dry age-related macular degeneration model, exhibited increased cone photoreceptor degeneration. In addition, *Otud7b* deficiency in *Mak*$^{-/-}$ mice, a mouse model of retinitis pigmentosa, resulted in further cone photoreceptor degeneration. Moreover, neuronal cells deficient in *Otud7b* were susceptible to serum starvation, resulting in cell death. Using RNA-sequencing and

bioinformatics analysis, we found that NF-κB activity was increased in *Otud7b*$^{-/-}$ retinas exposed to light. A luciferase reporter assay also demonstrated increased NF-κB activation in *Otud7b*-deficient neuronal cells under stress. Neuronal cell death resulting from *Otud7b* deficiency was suppressed by NF-κB inhibition. Furthermore, inhibition of NF-κB attenuated cone photoreceptor degeneration in light-exposed *Otud7b*$^{-/-}$ retina.

Together, our findings suggest that Otud7b deubiquitinase protects cone photoreceptor cells under stress conditions by modulating NF-κB activity.

Table of Contents

Introduction

Humans rely on sight to perceive their surroundings. Studies have found that people regard sight as the most valuable sense[1,2]. Humans depend on sight to learn, to avoid danger, to complete tasks, and to interact with others. The eyes are the organs responsible for sight. The outermost part of the eyes, include the cornea, a transparent outer coat, and the sclera, fibrous membrane. The middle layer contains three continuous structures: the iris, ciliary body, and choroid. The iris, which is visible through the cornea, is a pigmented tissue that regulates the amount of light that passes through the pupil, the hole in the middle of the iris[3]. The ciliary body is composed of the ciliary processes and ciliary muscles which hold the lens in place or changes the shape of the lens, respectively[3]. The choroid functions to provide nutrients to the retina through the blood vessels and to absorb excess light[3]. The lens is like a bi-convex lens that focuses light onto the retina. It is kept in place by the ciliary body[3,4]. The innermost layer is the retina[3]. In between the retina and lens is a vitreous body that holds the retina against the choroid[3].

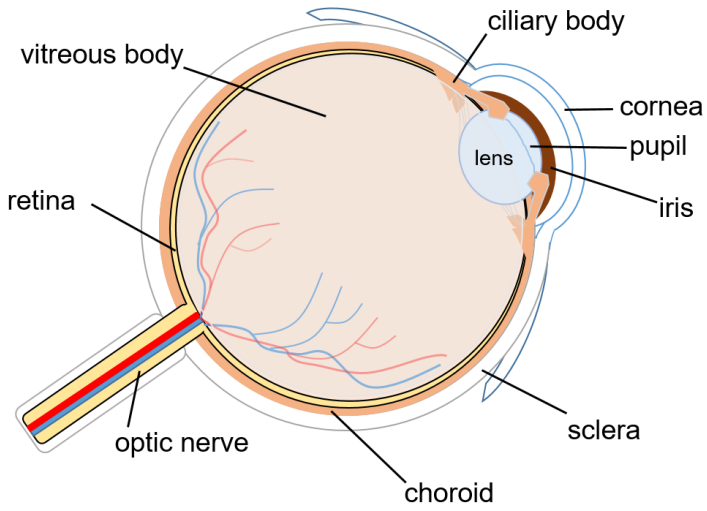

Figure 1. Anatomy of the eye.
Sensory organ that is connect to the brain through the optic nerve. Outermost layer: cornea and sclera. Middle layer: iris, ciliary body, and choroid. Innermost layer: retina.

The retina is a light-sensitive tissue that is located in the back of the eye. The retina is comprised of several layers: retinal pigmented epithelium (RPE), outer segment (OS), inner segment (IS), outer nuclear layer (ONL) outer plexiform layer (OPL), inner nuclear layer (INL), inner plexiform layer (IPL), and ganglion cell layer (GCL). The RPE is comprised of cuboidal post-mitotic epithelial cells that acts as the outer blood-retinal barrier regulating ion passage to and from the retina [5]. The retina consists of five types of neurons: photoreceptor cells, bipolar cells, amacrine cells, horizontal cells, and ganglion cells and glial cells, Müller glial cells[1]. Retinal photoreceptor cells are specialized neurons that perceive light and convert it into electrical signals that are transmitted to retinal ganglion cells, which send signals through the optic nerve to the brain. Photoreceptor cells consist of membrane-bound discs, abundance of mitochondria, a cell body, and a synaptic terminal which are located in the OS, IS, ONL, and OPL, respectively.

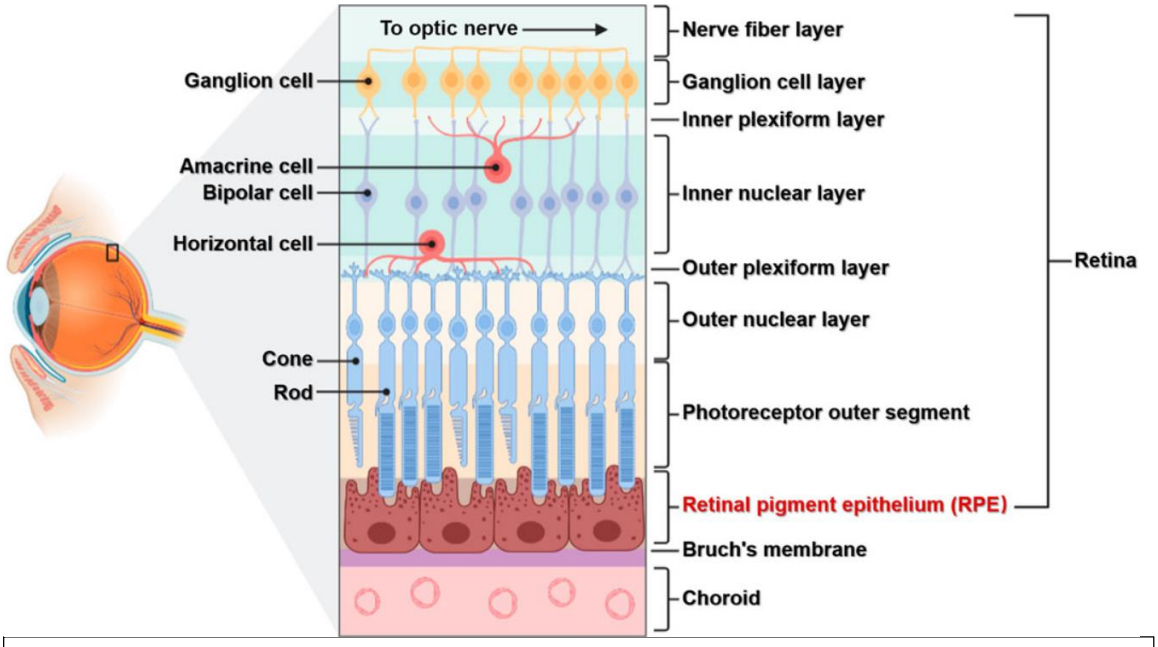

Figure 2. Retina structure.
Schematic representation of the retina. The retina is comprised two types of photoreceptor cells: rods and cones, bipolar cells, horizontal cells, amacrine cells, and ganglion cells.

Photoreceptor cells in the vertebrate retina can be categorized into rods and cones. Around 6 million cones and more than 100 million rods exist within the human retina[6]. Mice have around 6.4 million rods which accounts for 97.2% of all photoreceptors in their retina[7]. Rod photoreceptor cells are sensitive to lower-range light intensities and are essential for vision under dim light, whereas cone photoreceptor cells operate at brighter intensities and are essential for daylight, high acuity, and color vision. In humans, color is perceived by short-wavelength cones, middle-wavelength cones, or long wavelength cones; however, mice only have short-wavelength cones and middle-wavelength cones[8]. The INL is composed of the cell bodies of bipolar cells, horizontal cells, Müller glial cells, and amacrine cells[6,9,10]. Bipolar cells receive the electrical signal from photoreceptor cells and transmits the signal to the ganglion cells[6,10,11]. Horizontal cells regulate feedback signals between rods and cone cells[6,10,11]. Bipolar cells and amacrine cells synaptic connections to the ganglion cells occur in the IPL. The GCL is comprised of the ganglion cell bodies. The axons of the ganglion cells make up the optic nerve[6,10,11]. Degeneration of retinal cells have been known to cause certain retinal diseases.

Retinitis pigmentosa (RP) and age-related macular degeneration (AMD) are retinal degenerative diseases that lead to progressive vision loss because of retinal photoreceptor cell degeneration. RP affects approximately 1.5 million individuals worldwide[12-14]. RP is the most common inherited retinal dystrophy[13,15]. In RP, rod photoreceptor cell degeneration, which initially leads to night blindness, is followed by cone photoreceptor deterioration, eventually resulting in blindness[16,17]. Progression of RP usually occurs from

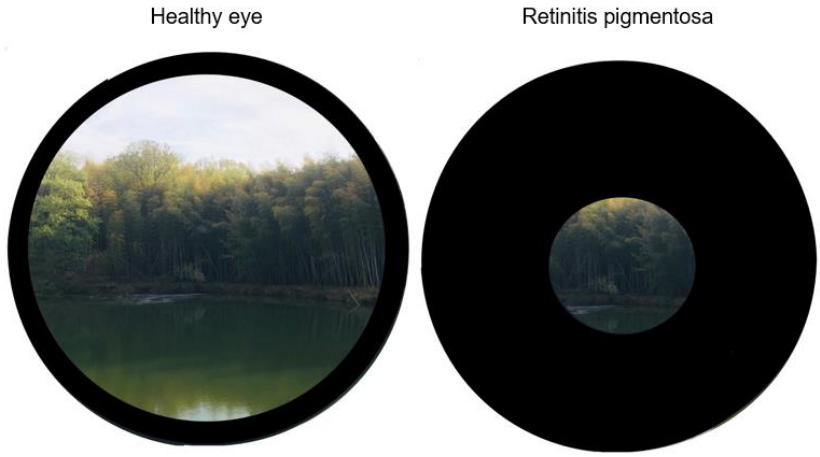

Figure 3. Visual field of a person with retinitis pigmentosa.
Left shows the visual field of a healthy eye. Right shows one that is afflicted with retinitis pigmentosa. Only the central retinal photoreceptors retains the ability to process light.

the midperiphery of the retina to the central retina[18]. This results in tunnel vision where a small central part of the visual field is left (Figure 3). RP affects one in 4000 worldwide[13,15,19]. There are two types of RP, nonsyndromic and syndromic. Nonsyndromic RP refers to the disease when it involves vision loss alone while syndromic RP refers to RP that occurs with a systemic disease[20]. Two frequent syndromes that are associated with RP is Usher syndrome and Bardet Biedl syndrome. Around 14% of all RP cases are Usher syndrome where people suffer from neurosensory deafness[13]. RP is associated with obesity, mental retardation, post-axial polydactyly, and renal abnormalities in Bardet Biedl syndrome[13,20]. Prevalence of syndromic RP for Usher syndrome is 1.8 to 6.2/100,000 individuals while syndromic RP for Bardet Biedl syndrome is 1/150,000[13]. Mode of inheritance include, autosomal dominant forms, autosomal recessive form, X-linked forms, and digenic forms[13,19]. In the autosomal dominant form, a person will receive the trait if either of their parents have the mutations in the genes that cause RP. Autosomal dominant cases of RP have been reported to be a

mild form where people exhibit symptoms after their 20s and retain central vision[13,15,20]. Around 10 to 20% of RP cases are autosomal dominant[20]. Autosomal recessive inheritance occurs when an individual receives two copies of a gene with a mutation. Autosomal recessive RP symptoms begin to manifest in the early teen years[13,20]. In the X-linked inheritance, mutations in genes that cause RP are on the X chromosome. Thereby, males, XY, only need one mutant allele to inherit the disease. Females, XX, can become carriers of the disease if they inherit a mutant allele. X-linked RP start early are associated with myopia, nearsightedness[13]. Digenic forms are rare as it results from heterozygous mutations in *ROM1* in combination with heterozygous mutations in *RDS*[13]. Since the identification of the first gene associated with RP in 1990, around 80 genes have been implicated with RP (Figure 4)[13,15]. After almost all the rod photoreceptor cells have died, cone photoreceptor degeneration occurs in RP; however, cone cell death can occur for years[21]. The reason for the delay in cone cell death is still unclear.

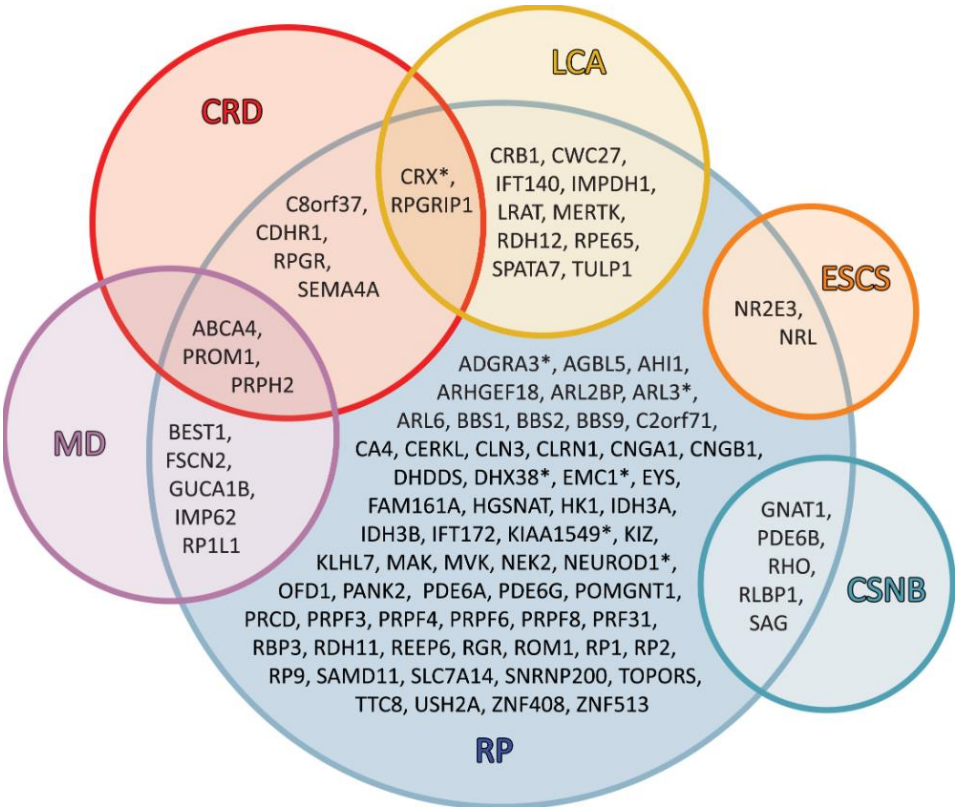

Figure 4. Venn diagram of genes associated with retinitis pigmentosa and other retinal dystrophies.

Abbreviations: MD: macular dystrophy, CRD: cone-rod dystrophy, CSNB: congenital stationary night blindness, ESCS: enhanced S-cone syndrome, LCA: Leber congenital amaurosis, RP: retinitis pigmentosa

AMD affects the central vision. In AMD, deterioration of the macula, the central part of the retina that contains the highest concentration of cone photoreceptor cells, causes loss of central vision (Figure 5)[22]. Rod photoreceptor cells are completely absent from the fovea. People who have AMD will still have their periphery vision. 9% of all cases of blindness are due to AMD[23]. AMD affects approximately 200 million individuals worldwide[24] AMD is classified into two types, dry or atrophic and wet or neovascular (Figure 6)[25]. Choroidal neovascularization is a hallmark of wet AMD whereas degeneration of the retinal pigmented epithelium and photoreceptor cells occur in dry AMD[26]. Dry AMD progresses slowly and can go unnoticed for years while the wet AMD can cause vision loss within a few months. The majority of people who suffer from AMD have dry AMD[27]. Dry AMD, however, can progress to wet AMD[28]. In wet AMD, blood vessels grow abnormally and penetrate the RPE of the retina. Leakage or hemorrhage can result in RPE detachment can cause rapid vision loss[26,29]. The rate of progression vary among individuals due to the environmental and demographic risk factors[29]. These risk factors, include age, hyperthyroidism, diabetes, smoking, and sunlight exposure[29]. Aside from age, the others have been reported to induce oxidative stress which results in reactive oxygen species[29]. Photoreceptor cells are susceptible to oxidative stress due to their high metabolic activity[29].

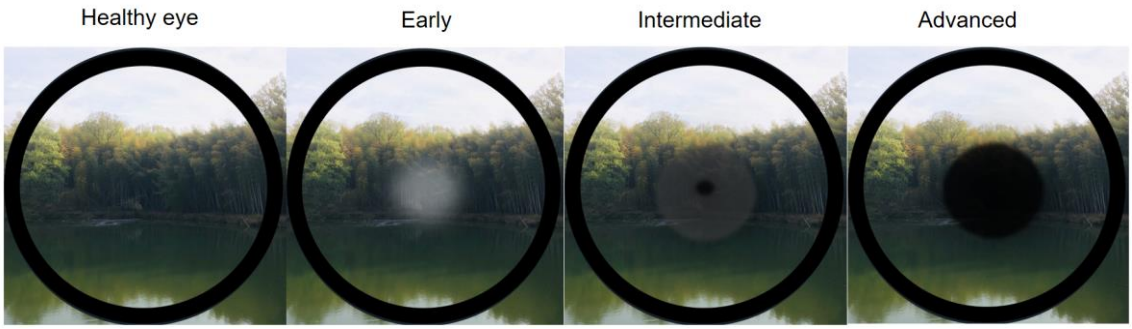

Figure 5. Visual field of age-related macular degeneration at different stages.
Healthy eye visual field. Early: minimal blurring vision. Intermediate: blurring with loss of vision. Advanced: loss of vision in the center.

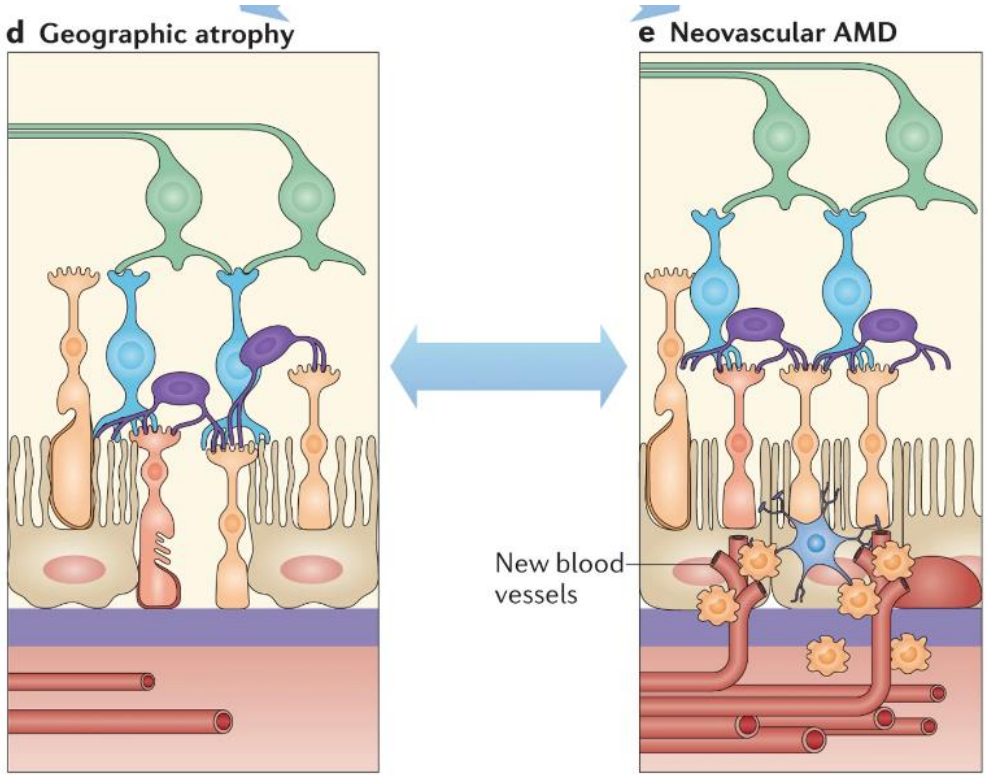

Figure 6. Two types of age-related macular degeneration.
Left shows the geographic atrophy or dry AMD. Choroidal blood vessels constrict and confluent regions of RPE. Right shows neovascular AMD or wet AMD where the blood vessels enter into the RPE.

We aim to elucidate the molecular mechanisms that protect cone photoreceptor cells from degeneration under stress conditions, such as in retinal degenerative diseases. To understand the mechanisms of photoreceptor degeneration, we investigated enzymes that are part of the ubiquitin proteasome pathway. The ubiquitin proteasome pathway is involved in protein quality control, signal transduction, proliferation, and development[30]. Ubiquitin, which was first discovered in 1975 by Gideon Goldstein, is a 76 amino acid essential protein that is highly conserved in eukaryotes and involved in the post-translational modification of proteins[31-36]. Ubiquitination process is a reversible protein modification that is regulated by E3 ubiquitin ligases and deubiquitinases (DUBs) (Figure 7A)[34-38]. E1, an ubiquitin-activating enzyme, activates ubiquitin which is then transferred to E2, an ubiquitin-conjugating enzyme. E2 forms a complex with an E3 ubiquitin ligase (Figure 7A). E3 ubiquitin ligases are responsible for ligating ubiquitin to the lysine residues of a substrate (Figure 7A). Around 600 E3 ubiquitin ligases have been identified in the human genome[39]. Various types of ubiquitination exist, since ubiquitin can be conjugated by another ubiquitin through the lysine (Lys) residues (Lys6, Lys11, Lys27, Lys29, Lys33, Lys48, and Lys63) or Methionine1 (Met1)[34,40]. Different lysine chains result in different processes. Monoubiquitination of a substrate results in protein interactions, localization, trafficking, activity modulation, or proteasomal degradation[34]. Lys11 and Lys48 often result in proteasomal degradation. Lys48, Lys63, and possibly Lys6 autophagy degradation[34]. Linkages of Lys6, Lys27, Lys29, Lys33, and Met1 have not been well studied[34].

DUBs remove or trim the ubiquitin chains on the substrate (Figure 7A)[32,34,36,37]. Three main role of DUBs is the maintenance of ubiquitin levels, maintenance of protein homeostasis and signaling in cells and process of ubiquitin chains[36,37]. Around 100 DUBs

exist within the human genome. These DUBs are classified into seven families: ubiquitin-specific proteases (USP), ubiquitin carboxyl-terminal hydrolases (UCH), Machado-Josephin domain-containing proteases (MJD), ovarian tumor proteases (OTU), motif-interacting with ubiquitin-containing novel DUB family (MINDY), JAB1/MPN/MOV34 family (JAMM), ZUFSP/Mug105 family (ZUP1) (Figure 7B)[32,34-38,41]. USP, UCH, MJD, OTU, MINDY, and ZUP1 are cysteine proteases, on the other hand, JAMM is the only metalloprotease[32,34,41]. The enzymatic activity relies on the thiol of the cysteine which is stabilized by nearby histidine aspartic acid residues[41,42]. This catalytic triad cuts the ubiquitin from the target protein[41,42]. DUBs are known to regulate biological processes such as endocytosis, DNA damage repair, chromatin remodeling, signaling pathways, and inflammatory processes[32,35,36,41,42]. It was reported that mutations in *KLHL7*, substrate adaptor for the CUL3-based E3 ligase, cause autosomal-dominant retinitis pigmentosa[43,44]. In addition, we previously found that the knockout of *Klhl18* could suppress light-induced photoreceptor damage[45]. We used a previously generated microarray to search for other genes involved in ubiquitin metabolism. In this study, we examined the role of the DUB Otud7b/Cezanne in the retina.

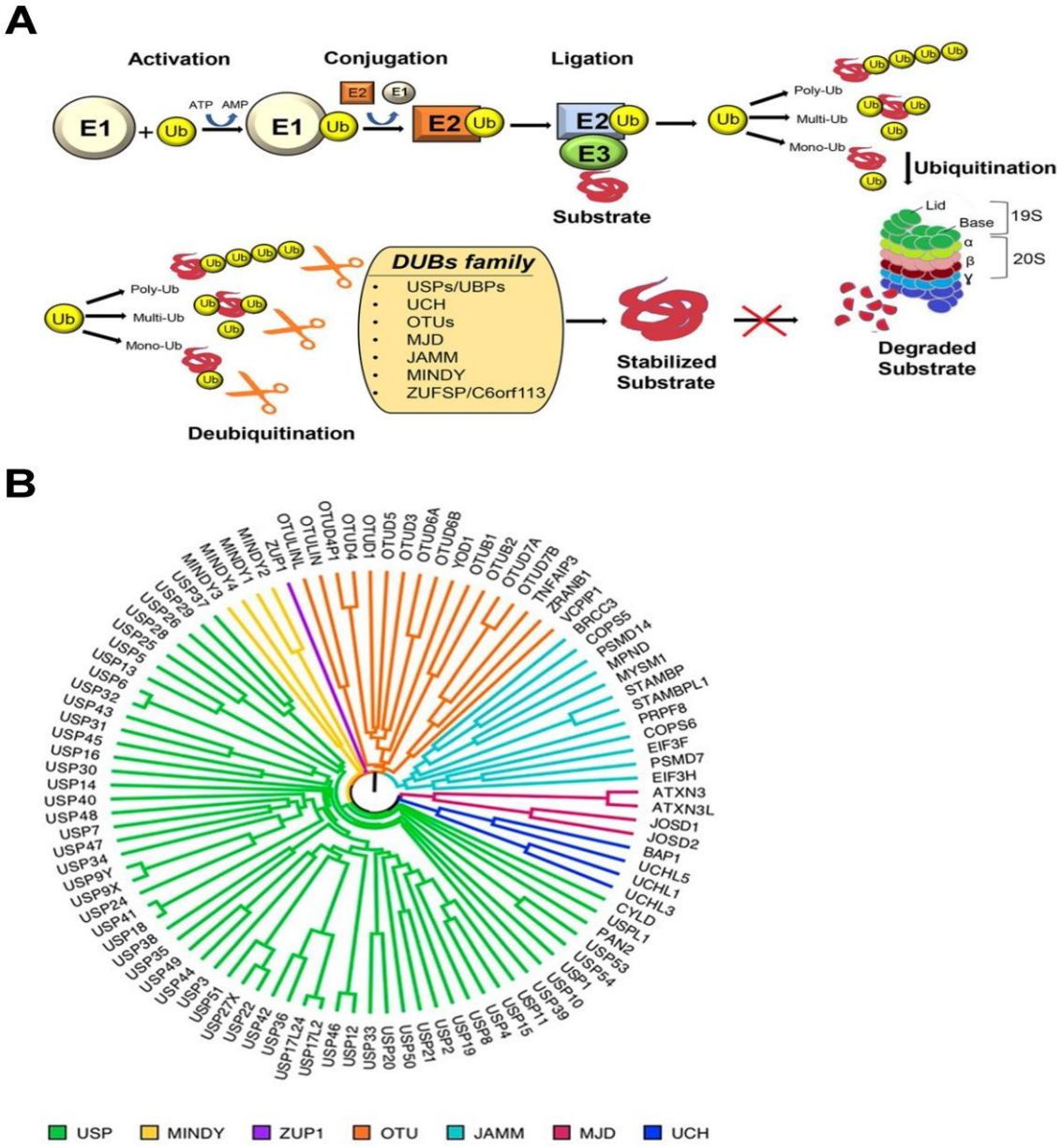

Figure 7. The ubiquitination cascade and deubiquitinases.

(A) Schematic diagram of ubiquitination and deubiquitination. E1 enzyme activates ubiquitin. Ubiquitin is then transferred to E2 which forms a complex with E3. The complex targets a specific substrate for ubiquitination. The ubiquitination becomes a signal for the substrate degradation. DUBs trim the ubiquitin chains, thereby stabilizing the substrate and preventing its degradation. **(B)** Phylogenic tree of deubiquitinases found in human genome.

Results

Otud7b is expressed in retinal photoreceptor cells

We previously reported that the ubiquitin ligase Cul3-Klhl18 regulates transducin translocation during light-dark adaptation in rod photoreceptor cells[45]. To identify other enzymes that are involved in ubiquitin metabolism in the retina and that may regulate photoreceptor function and/or development, we searched for genes enriched in photoreceptor cells. We compared transcripts between control and *Otx2* conditional knockout retinas, in which the cell fate is altered from photoreceptor cells to amacrine-like cells[46,47]. Among the candidate genes identified, we focused on *Otud7b*, the function of which in the retina has not yet been elucidated. Otud7b belongs to the OTU protease family. The OTU is further separated into four subclasses, including otubains, OTUD, A20-like OTU, and OTULIN (Figure 8)[36]. Otud7b consists of an ubiquitin association domain, OTU domain, and zinc-finger domain. Otud7b interacts with its substrate through the ubiquitin association domain and deubiquitinates its substrate with the OTU domain[36]. To confirm the expression of *Otud7b* in the retina, RT-PCR was performed using various tissues from 4-week-old mice. *Otud7b* was ubiquitously expressed but was highly enriched in the retina (Figure 9A). To investigate the localization of the Otud7b protein in the retina, immunofluorescence analysis was performed on adult mouse retinal sections using an antibody against Otud7b. Otud7b immunofluorescence signals were observed in the IS, ONL, and OPL (Figure 9B). Furthermore, we observed Otud7b signals at the cone photoreceptor synapses marked with peanut agglutinin (PNA) (Figure 9C). In addition, we found the expression of *OTUD7B* in the human retina using RT-PCR (Figure 9D). These results suggest that Otud7b is expressed in rod and cone photoreceptor cells.

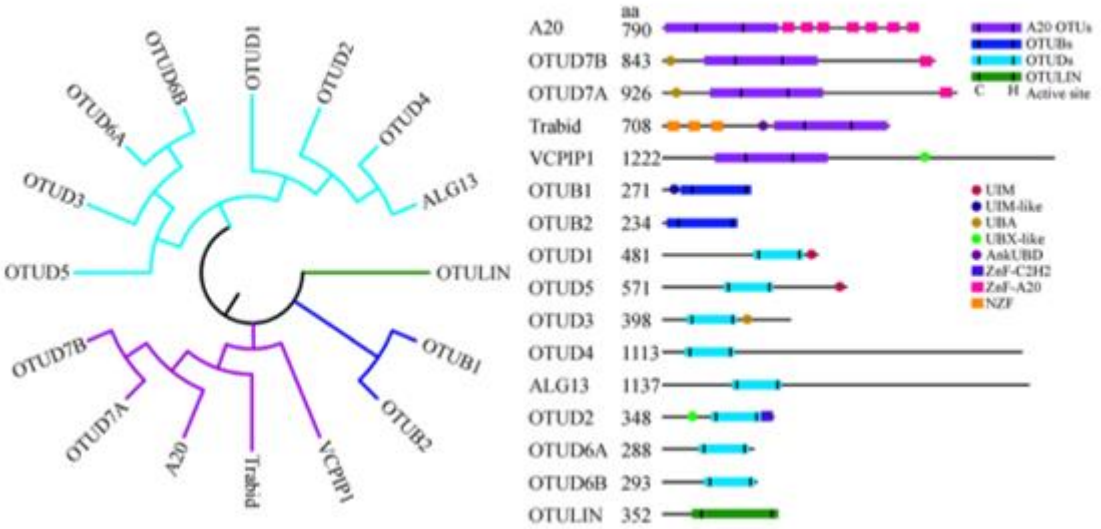

Figure 8. Phylogenic tree of ovarian tumor proteases

(A) Sixteen ovarian tumor proteases in four subclasses (left). Domain structure of each ovarian tumor protease (right).

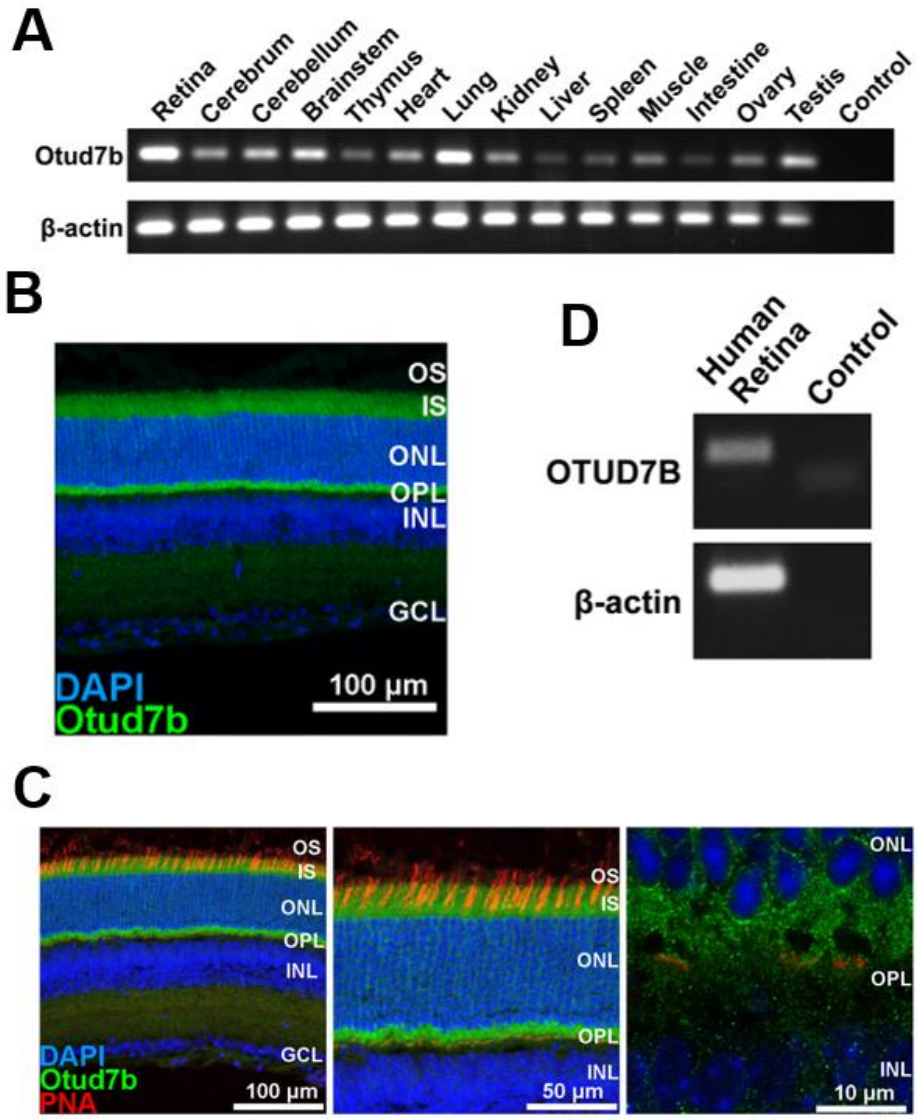

Figure 9. Expression pattern of *Otud7b*.

(A) RT-PCR analysis of the *Otud7b* transcript in mouse tissues at 4 weeks. *Otud7b* was expressed ubiquitously with strong expression in the retina. *β-actin* was used as a loading control. **(B)** Immunofluorescence analysis of the wild-type retina using an anti-Otud7b antibody. Nuclei were stained with DAPI. Otud7b was localized to the photoreceptor inner segment, cell body, and synapse. **(C)** Immunofluorescence analysis of the wild-type retina using the anti-Otud7b antibody and PNA (a marker for cone outer segments and synapses). Nuclei were stained with DAPI. Otud7b signals were observed in the vicinity of PNA signals in the OPL. **(D)** RT-PCR analysis of the *OTUD7B* transcript in the human retina. *β-actin* was used as a loading control.

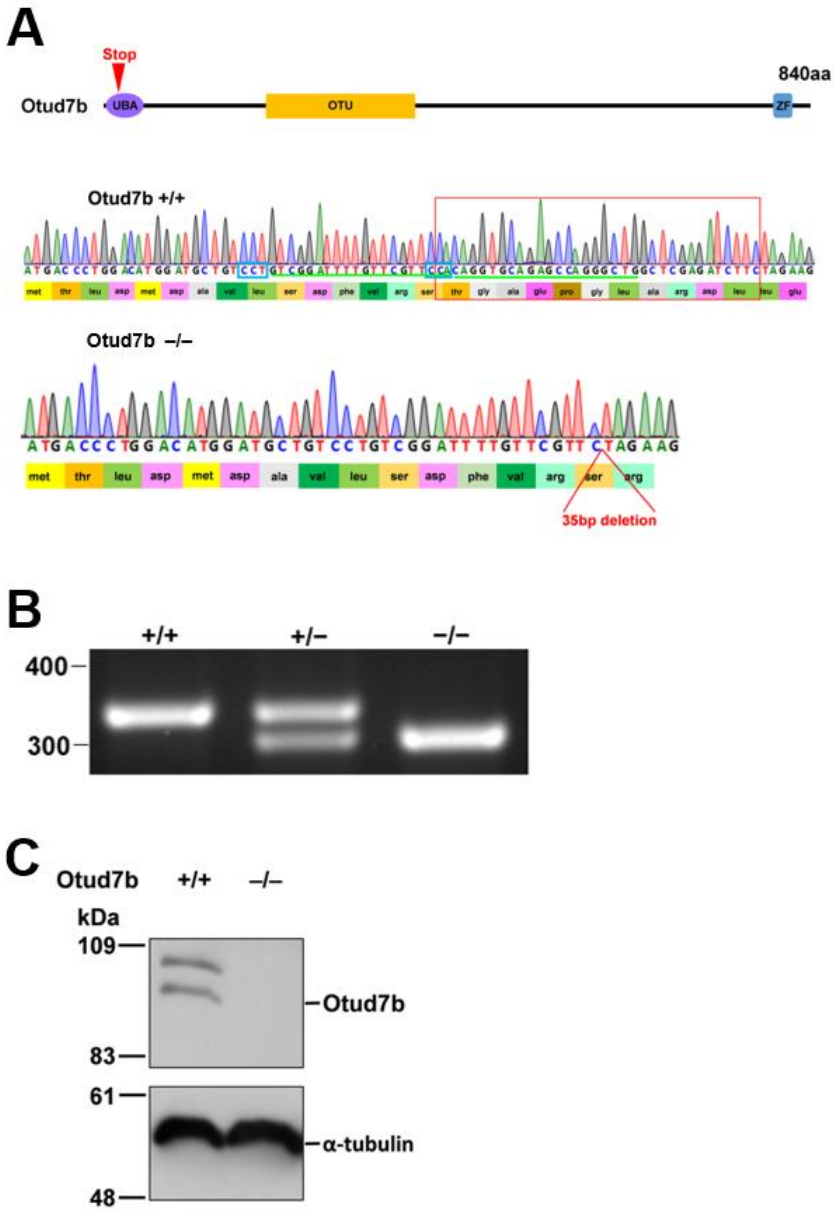

Figure 10. Generation of *Otud7b*$^{-/-}$ mice.

(A) Schematic representation (upper panel) and DNA sequence of exon 2 (lower panel) in *Otud7b*$^{-/-}$ mice. *Otud7b*$^{-/-}$ mice were generated using CRISPR/Cas9-mediated genome editing. Thirty-five base-pair deletions, boxed in red in *Otud7b*$^{+/+}$, results in a translational frameshift and a premature stop codon. The gRNA regions are underlined in green. Blue boxes represent the PAM sequences. **(B)** PCR products of 338 and 303 bp were amplified from wild-type and 35-bp deleted alleles, respectively. **(C)** Western blotting of the Otud7b protein in *Otud7b*$^{+/+}$ and *Otud7b*$^{-/-}$ retinas. No Otud7b bands were detected in the *Otud7b*$^{-/-}$ retina. α-tubulin was used as a loading control.

Histological and functional analysis of the retina in *Otud7b*$^{-/-}$ mice

To investigate the functional role of Otud7b in retinal photoreceptor cells, we generated conventional *Otud7b*$^{-/-}$ mice using CRISPR/Cas9 genome editing (Figures 10A and 10B). To confirm the loss of Otud7b in the *Otud7b*$^{-/-}$ mouse retina, we performed western blotting and immunofluorescence analysis using an anti-Otud7b antibody (Figures 10C and 11A). Immunostaining revealed that Otud7b signals were not detected in the *Otud7b*$^{-/-}$ retina, and western blotting revealed that the protein bands observed in the *Otud7b*$^{+/+}$ retina were missing in the *Otud7b*$^{-/-}$ retina (Figures 10C and 11A). *Otud7b*$^{-/-}$ mice were viable, fertile, and showed no gross morphological abnormalities. To examine the effects of *Otud7b* deficiency on the retina, we performed immunofluorescence analysis on mouse retinal sections at 1 month of age using antibodies against Rhodopsin (a marker for rod outer segments), S-opsin (a marker for S-cone outer segments), and M-opsin (a marker for M-cone outer segments); no obvious differences were observed between *Otud7b*$^{+/+}$ and *Otud7b*$^{-/-}$ retinas (Figure 11A). We examined the synapses of photoreceptor cells by immunostaining using antibodies against Pikachurin (a marker for photoreceptor synaptic terminals) and Ctbp2 (a marker for synaptic ribbons); no obvious differences were observed between *Otud7b*$^{+/+}$ and *Otud7b*$^{-/-}$ retinas (Figure 11B). We also examined other cell types using antibodies against Chx10 (a marker for bipolar cells), Pax6 (a marker for amacrine and ganglion cells), Calbindin (a marker for horizontal and a subset of amacrine cells), Rbpms (a marker for ganglion cells), and S100β (a marker for Müller glia) and found no substantial differences between *Otud7b*$^{+/+}$ and *Otud7b*$^{-/-}$ retinas (Figures 12A–12E). To investigate the physiological effects of *Otud7b* deficiency, we performed electroretinograms (ERGs) under dark (scotopic) and light-adapted (photopic) conditions. The electrical activities of rod

photoreceptor cells and rod bipolar cells in response to light stimuli were visualized using the amplitudes of a-waves and b-waves, respectively, under scotopic conditions. In contrast, under photopic conditions, the amplitudes of the a-waves and b-waves reflect the population activity of cone photoreceptors (a-waves) and cone ON-bipolar cells (b-waves). We observed no significant differences in a- and b-wave amplitudes under the scotopic and photopic conditions between *Otud7b*$^{+/+}$ and *Otud7b*$^{-/-}$ mice (Figures 13 and 14). Next, we examined *Otud7b*$^{+/+}$ and *Otud7b*$^{-/-}$ mouse retinas at 6 months of age to investigate whether *Otud7b* deficiency leads to retinal degeneration. Similar to the mouse retinas at 1 month, no substantial differences between *Otud7b*$^{+/+}$ and *Otud7b*$^{-/-}$ mouse retinas were observed when immunofluorescence analysis was performed using antibodies against Rhodopsin, S-opsin, and M-opsin (Figure 15), or when ERGs were recorded (Figures 16 and 17).

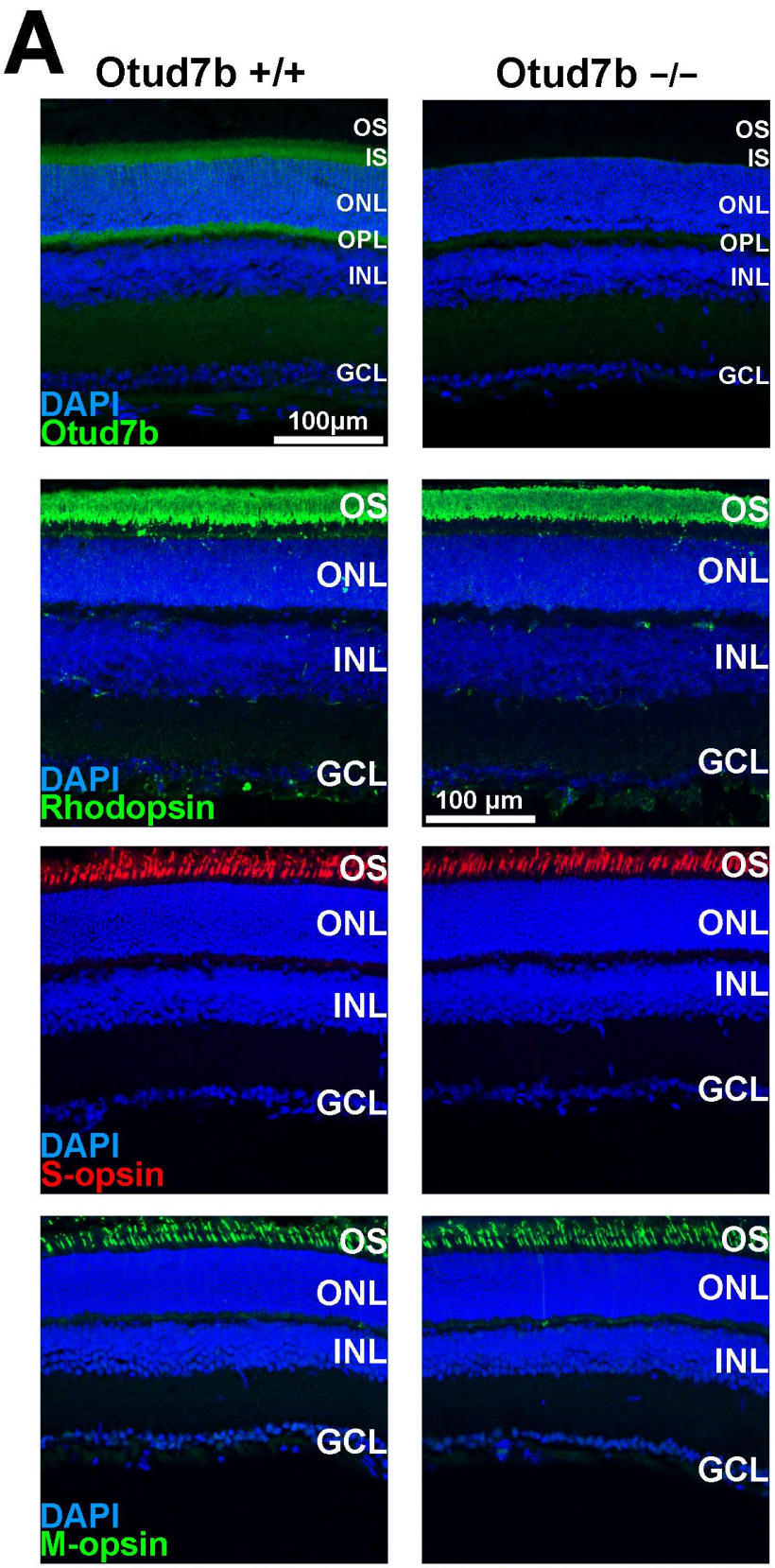
A
Otud7b +/+
Otud7b −/−
OS
IS
ONL
OPL
INL
GCL
DAPI
Otud7b
100μm
DAPI
Rhodopsin
100 μm
DAPI
S-opsin
DAPI
M-opsin

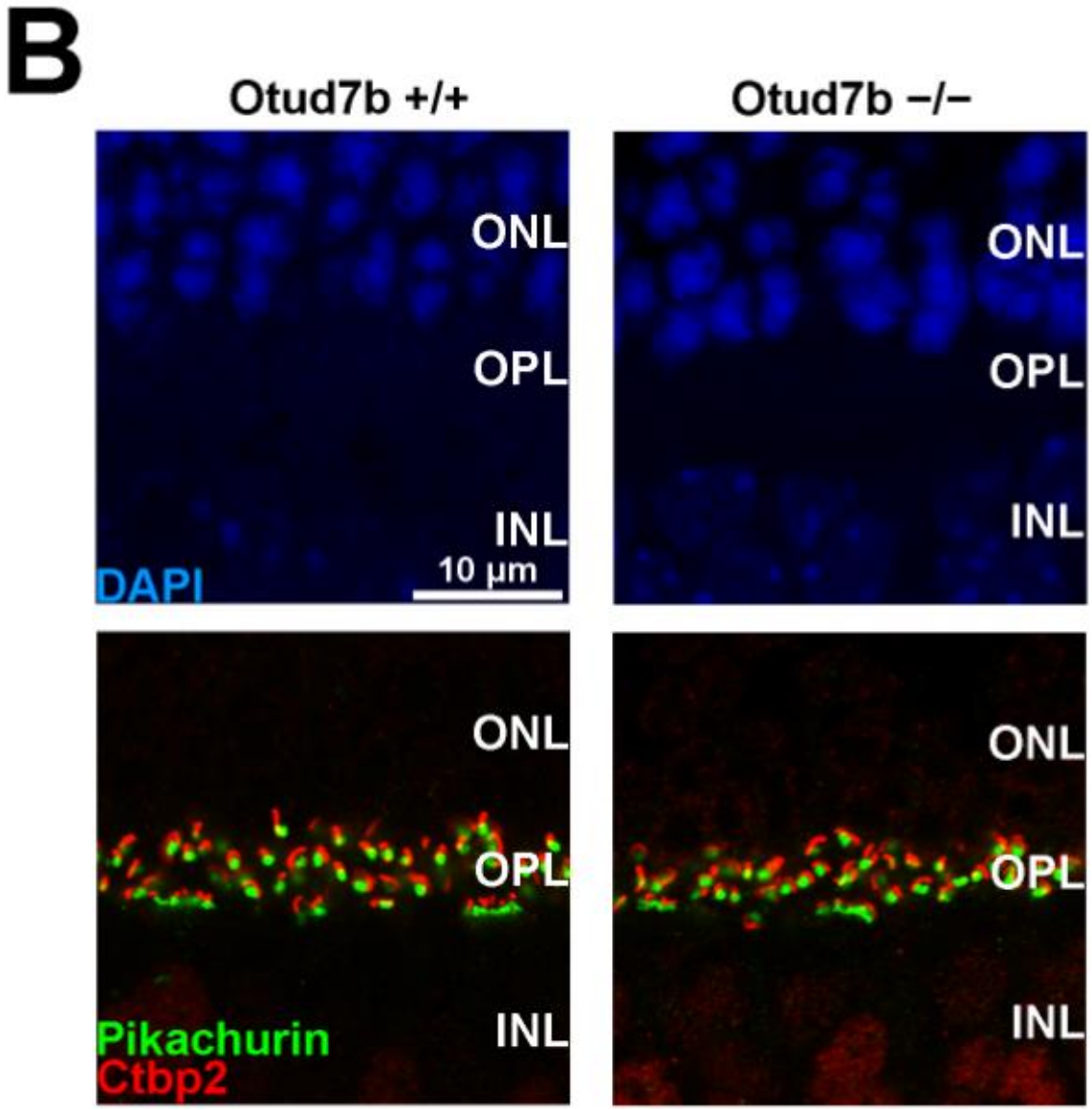

Figure 11. Phenotypic analysis of the *Otud7b*$^{-/-}$ mouse retina at 1 month.
(A) Immunofluorescence analysis of retinal sections from *Otud7b*$^{+/+}$ and *Otud7b*$^{-/-}$ mice at 1 month using antibodies against Otud7b, Rhodopsin (a marker for rod outer segments), S-opsin (a marker for S-cone outer segments), and M-opsin (a marker for M-cone outer segments). Nuclei were stained with DAPI. No obvious difference was observed comparing the photoreceptor cells of *Otud7b*$^{+/+}$ and *Otud7b*$^{-/-}$ retinas. **(B)** Immunofluorescence analysis of the synaptic regions of *Otud7b*$^{+/+}$ and *Otud7b*$^{-/-}$ retinas at 1 month using antibodies against Pikachurin (a marker for photoreceptor synaptic terminals) and Ctbp2 (a marker for synaptic ribbons).

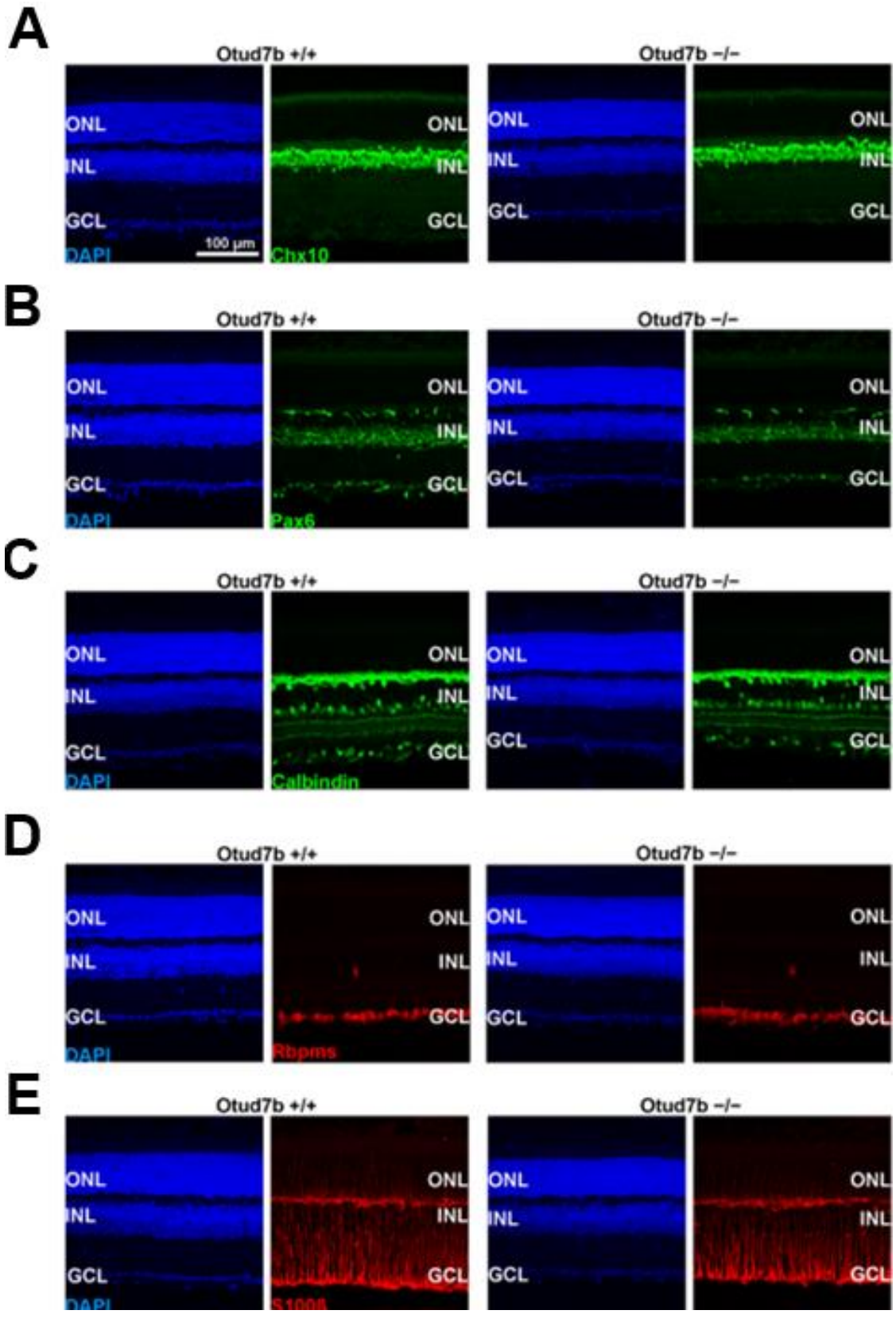
A
Otud7b +/+
Otud7b −/−
ONL
INL
GCL
DAPI
100 µm
Chx10
B
Pax6
C
Calbindin
D
Rbpms
E
S100β

Figure 12. Phenotypic analysis of the *Otud7b*$^{-/-}$ mouse retina at 1 month.
(A–E) Immunofluorescence analysis of *Otud7b*$^{+/+}$ and *Otud7b*$^{-/-}$ retinas at 1 month using antibodies against Chx10 (a marker for bipolar cells, **A**), Pax6 (a marker for amacrine and ganglion cells, **B**), Calbindin (a marker for horizontal and a subset of amacrine cells, **C**), Rbpms (a marker for ganglion cells, **D**), and S100β (a marker for Müller glia, **E**). Nuclei were stained with DAPI.

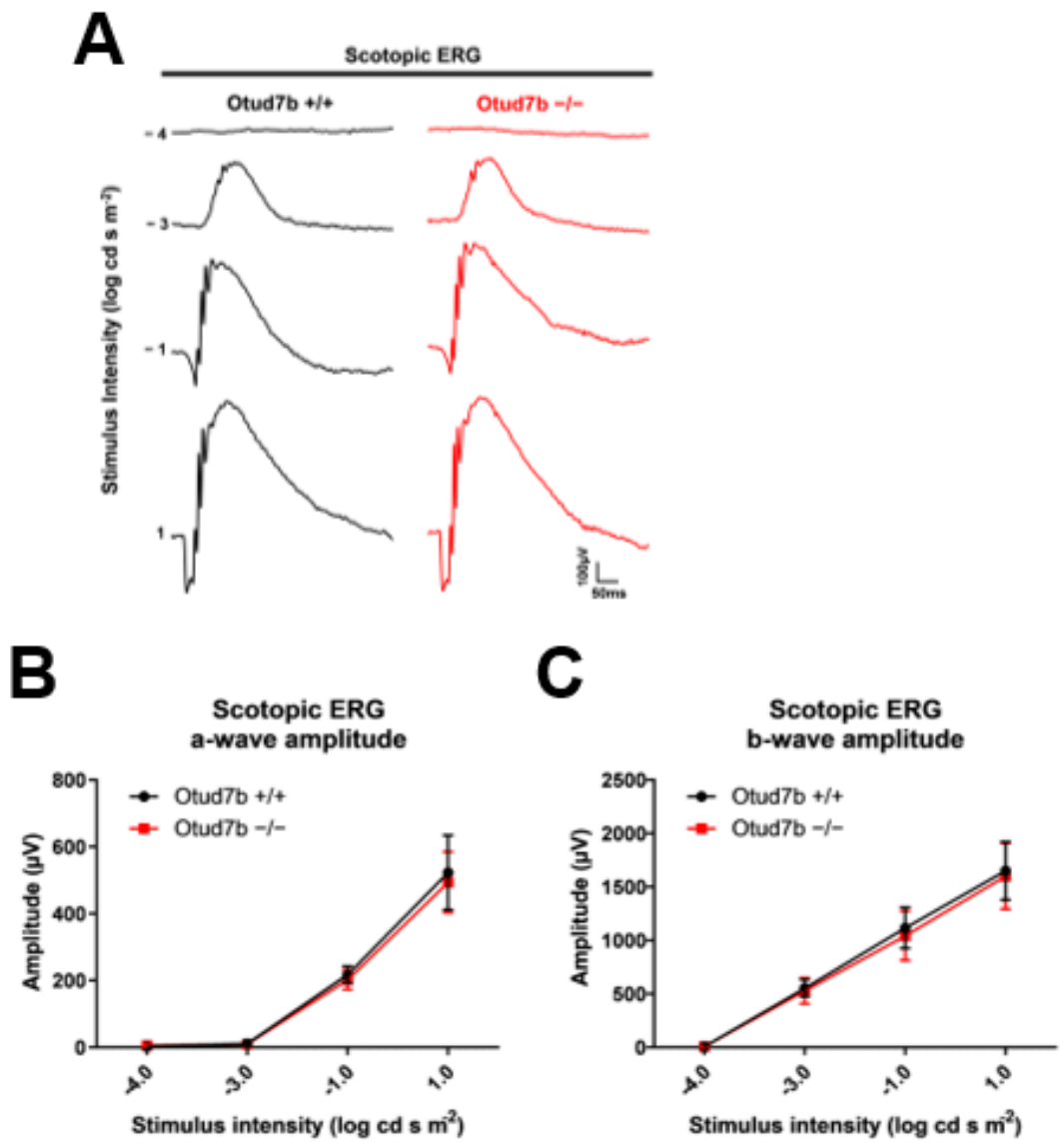

Figure 13. Scotopic ERG analysis of *Otud7b*$^{+/+}$ and *Otud7b*$^{-/-}$ mice at 1 month. **(A)** Representative photopic ERGs elicited by four stimulus intensities (−4 to 1.0 log cd s/m^2). Scotopic a-wave **(B)** and b-wave **(C)** amplitudes are shown as functions of stimulus intensity. Data are presented as the mean ± SD (unpaired t-test). n = 4 per genotype.

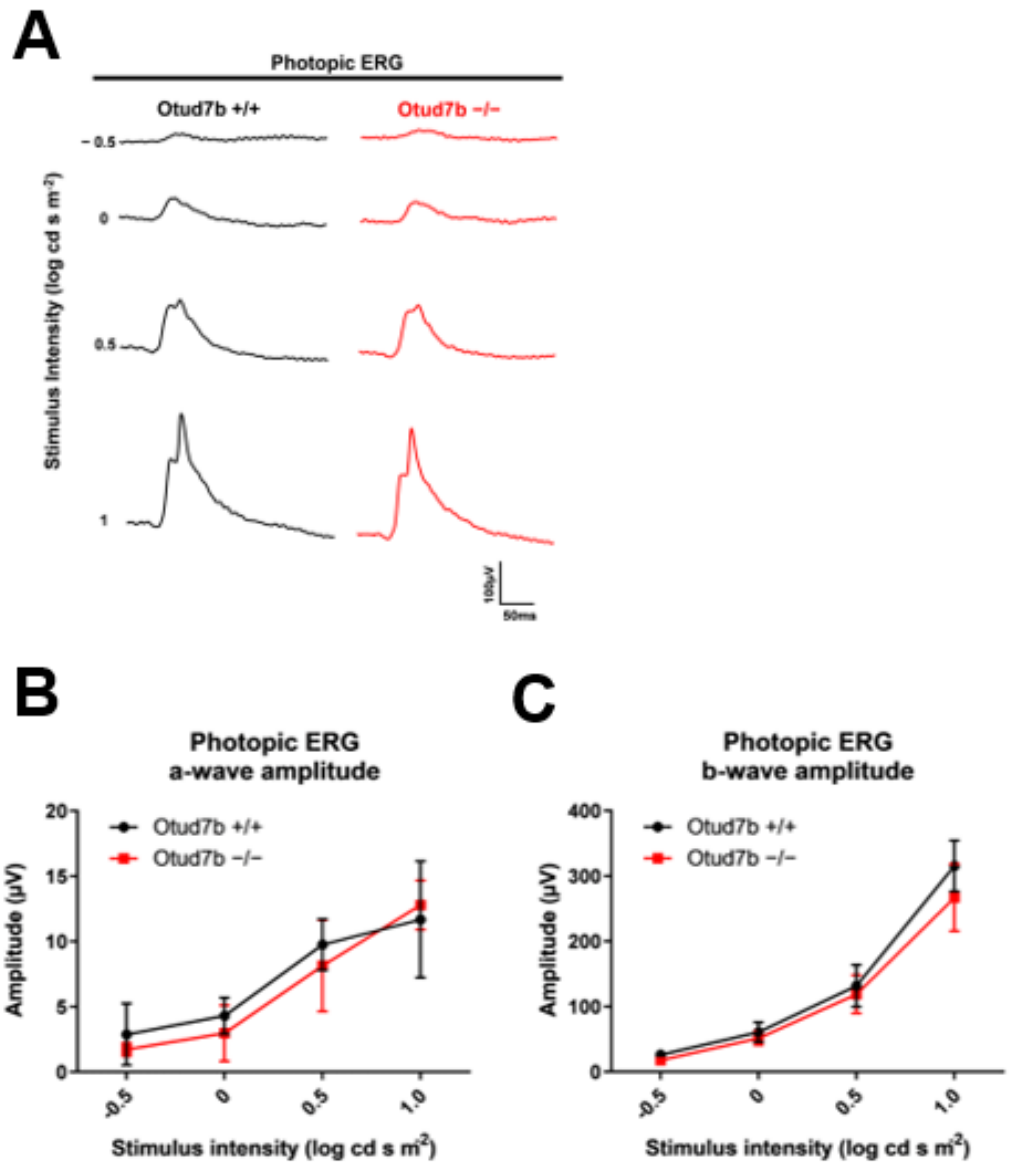

Figure 14. Photopic ERG analysis of *Otud7b*$^{+/+}$ and *Otud7b*$^{-/-}$ mice at 1 month. **(A)** Representative photopic ERGs elicited by four stimulus intensities (−0.5 to 1.0 log cd s/m^2). Photopic a-wave **(B)** and b-wave **(C)** amplitudes are shown as functions of stimulus intensity. Data are presented as the mean ± SD (unpaired t-test). n = 4 per genotype.

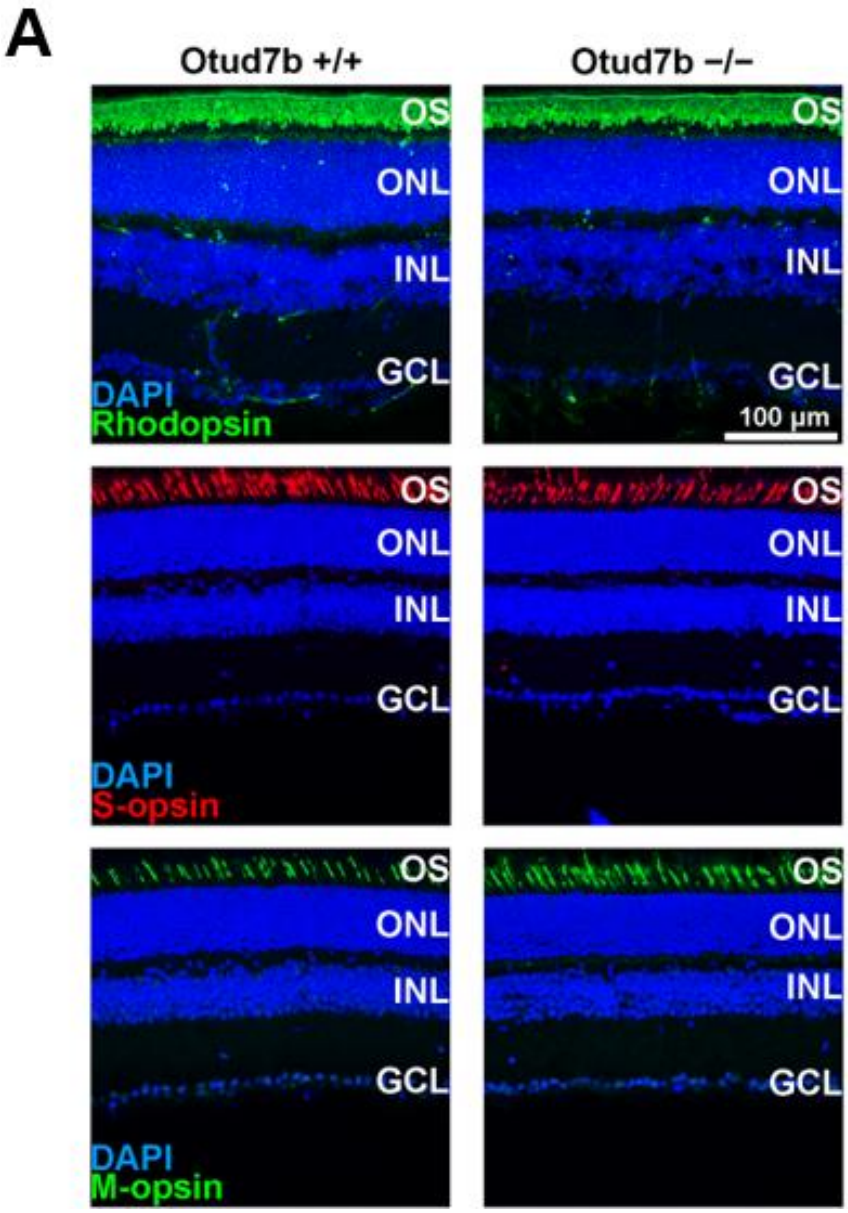

Figure 15. Phenotypic analysis of the *Otud7b*$^{-/-}$ mouse retina at 6 months.
(A) Immunofluorescence analysis of retinal sections from *Otud7b*$^{+/+}$ and *Otud7b*$^{-/-}$ mice at 6 months using antibodies against Rhodopsin (a marker for rod outer segments), S-opsin (a marker for S-cone outer segments), and M-opsin (a marker for M-cone outer segments). Nuclei were stained with DAPI. No obvious difference was observed between *Otud7b*$^{+/+}$ and *Otud7b*$^{-/-}$ retinas.
Data are presented as the mean ± SD (unpaired t-test). n = 6 and 7 for *Otud7b*$^{+/+}$ and *Otud7b*$^{-/-}$ respectively.

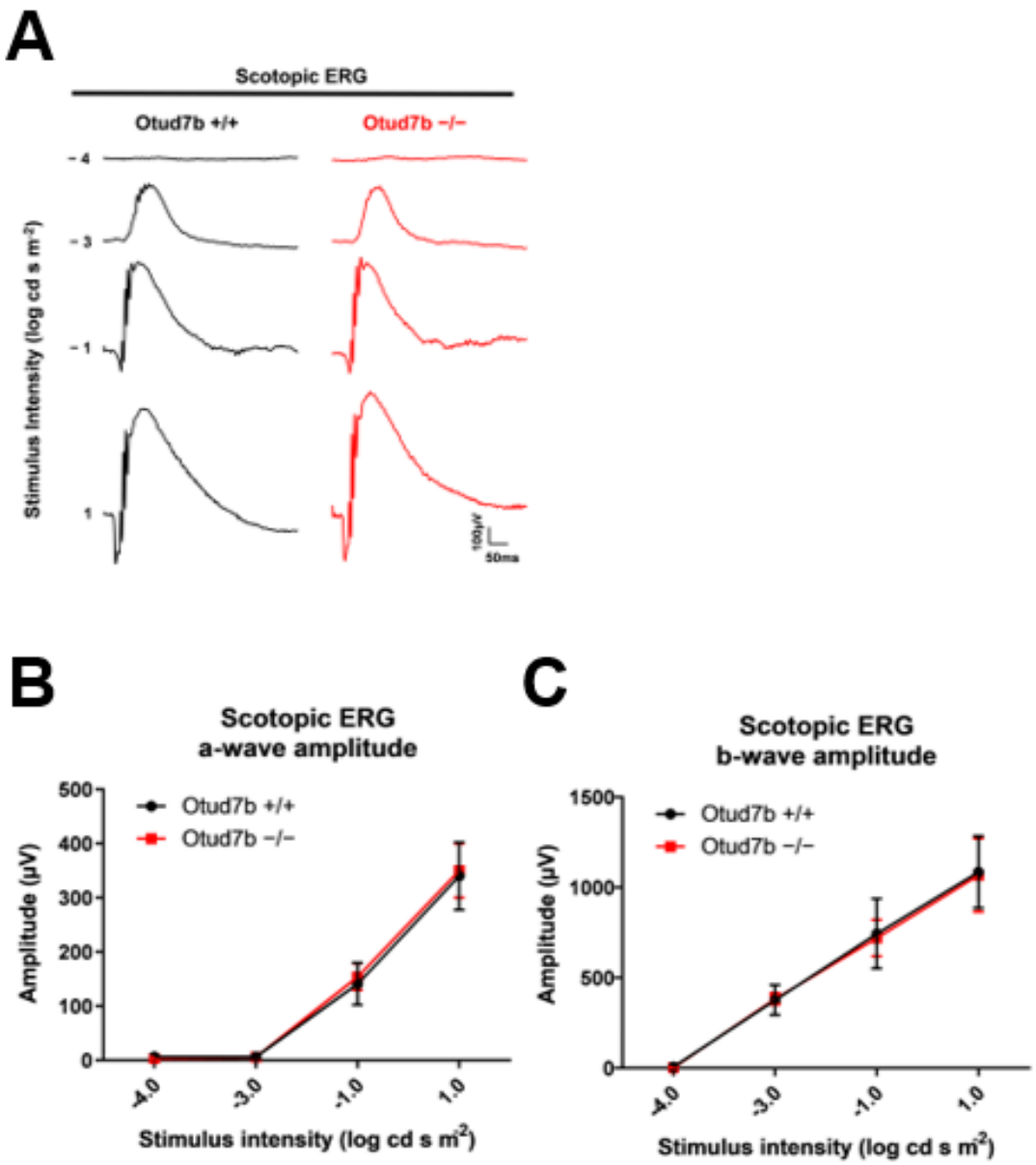

Figure 16. Scotopic ERG analysis of *Otud7b*$^{+/+}$ and *Otud7b*$^{-/-}$ mice at 6 months.
(A) Representative scotopic ERGs elicited by four stimulus intensities (−4.0 to 1.0 log cd s/m2). Scotopic a-wave **(B)** and b-wave **(C)** amplitudes are shown as functions of stimulus intensity. Data are presented as the mean ± SD (unpaired t-test). n = 6 and 7 for *Otud7b*$^{+/+}$ and *Otud7b*$^{-/-}$ respectively.

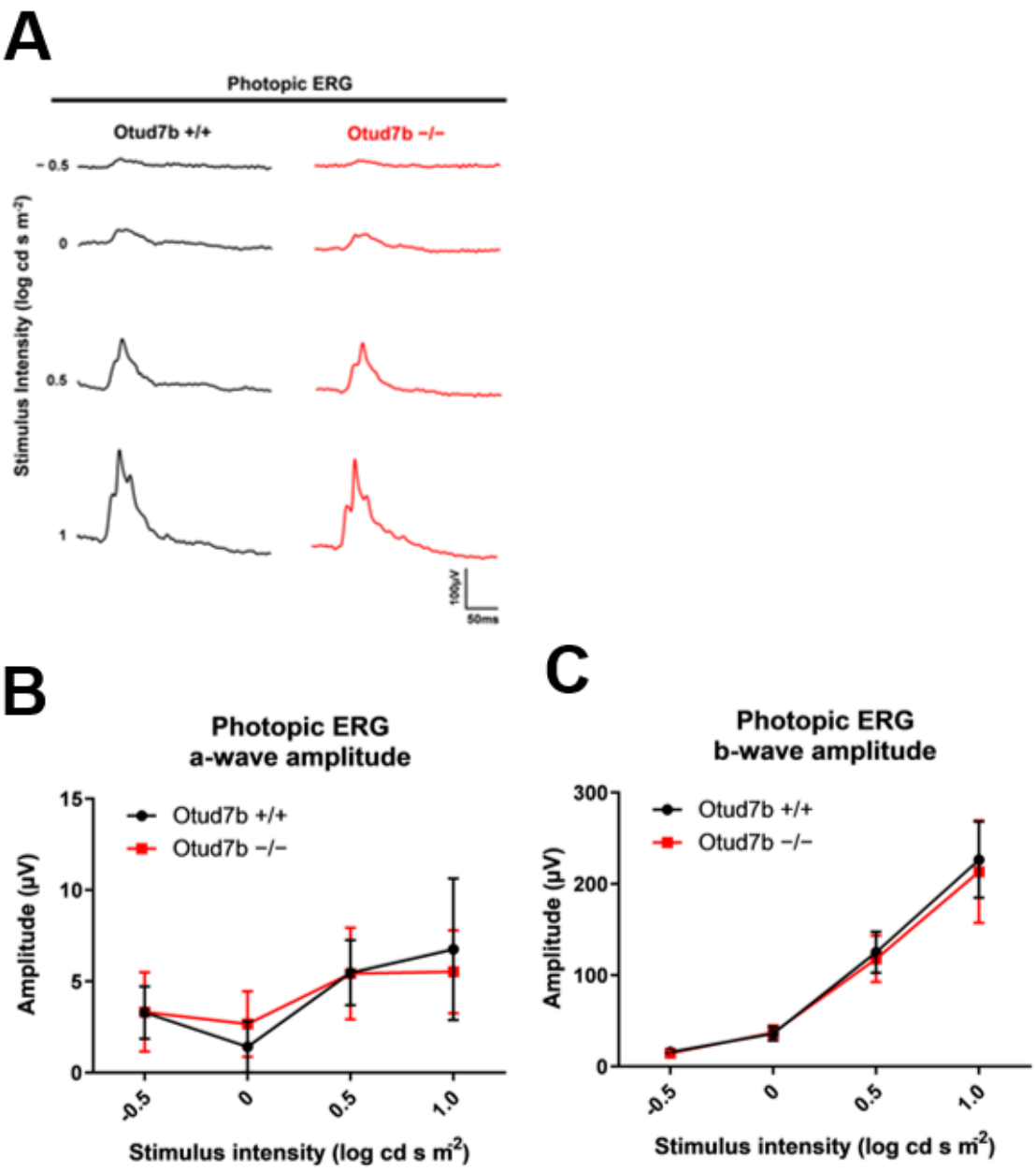

Figure 17. Photopic ERG analysis of *Otud7b*$^{+/+}$ and *Otud7b*$^{-/-}$ mice at 6 months.
(A) Representative photopic ERGs elicited by four stimulus intensities (−0.5 to 1.0 log cd s/m2). Photopic a-wave **(B)** and b-wave **(C)** amplitudes are shown as functions of stimulus intensity.Data are presented as the mean ± SD (unpaired t-test). n = 6 and 7 for *Otud7b*$^{+/+}$ and *Otud7b*$^{-/-}$ respectively.

Light-induced retinal damage to cone photoreceptor cells is augmented in *Otud7b*-deficient mice

Next, we investigated the effects of *Otud7b* deficiency on retinas under stress. *Otud7b*$^{-/-}$ mice were exposed to light-emitting diode (LED) light (Figure 18A). Exposure to LED light induces oxidative stress in the retina, which results in photoreceptor degeneration[48]. Immunofluorescence analysis using the anti-Otud7b antibody revealed the absence of Otud7b signal in the light-exposed *Otud7b*$^{-/-}$ retina (Figure 18B). To evaluate histological changes, we performed immunofluorescence analysis using antibodies against Rhodopsin, S-opsin, M-opsin, IbaI, and GFAP to observe the rod outer segments, S-cone outer segments, M-cone outer segments, microglia, and Müller glia, respectively (Figures 19 and 20). No obvious differences were observed in the microglia and Müller glia between light-exposed *Otud7b*$^{+/+}$ and *Otud7b*$^{-/-}$ retinas (Figure 20). We quantified ONL thickness of light-exposed *Otud7b*$^{+/+}$ and *Otud7b*$^{-/-}$ retinas. There were no significant differences between the *Otud7b*$^{+/+}$ and *Otud7b*$^{-/-}$ retinas (Figure 21A). There were no significant differences in the lengths of the rod and S-cone outer segments between the light-exposed *Otud7b*$^{+/+}$ and *Otud7b*$^{-/-}$ retinas (Figures 19A, 19B, 21B, and 21C). We also did not observe significant differences in the number of S-cones or M-cones between light-exposed *Otud7b*$^{+/+}$ and *Otud7b*$^{-/-}$ retinas (Figures 21D and 21E). However, M-cone outer segments were significantly shorter in the light-exposed *Otud7b*$^{-/-}$ retinas than in the *Otud7b*$^{+/+}$ retinas, suggesting that M-cone photoreceptor cells were more severely damaged in the light-exposed *Otud7b*$^{-/-}$mice (Figures 19C, 19D, and 21F). Previous studies have reported that outer segment shortening reflects photoreceptor degeneration[49,50]. Additionally, outer segment shortening has been observed in patients with RP[51,52]. Based on these reports, our observations suggest that Otud7b suppresses

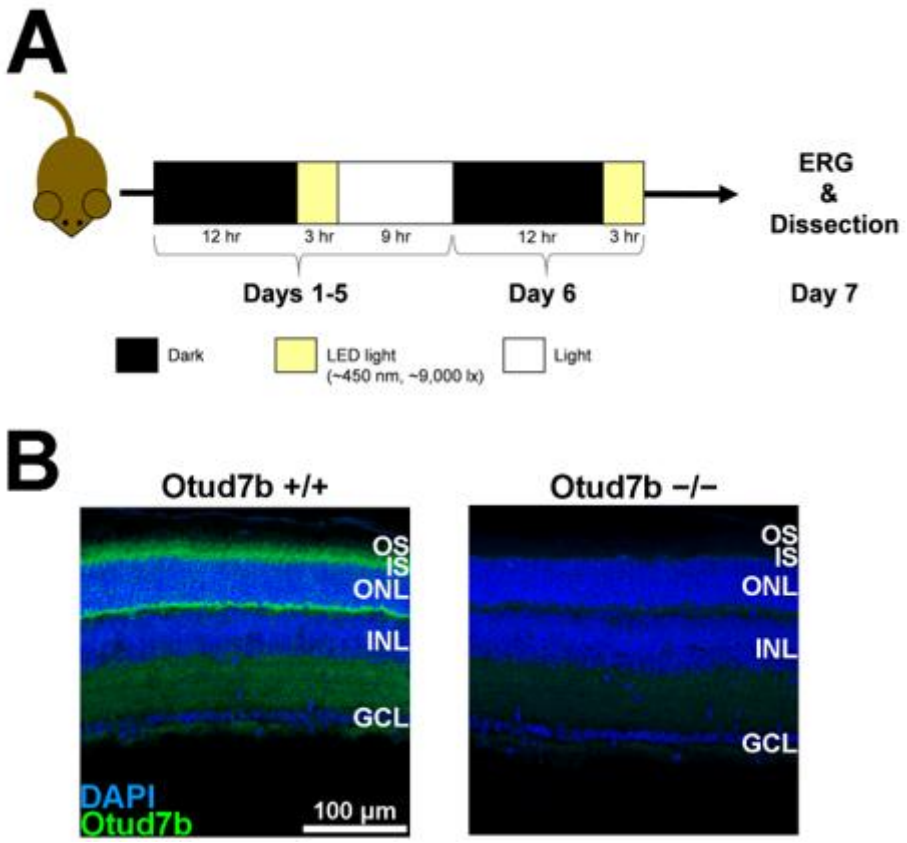

Figure 18. Light-induced damage protocol and *Otud7b* immunofluorescence.
(A) Schematic representation of the exposure of *Otud7b*$^{+/+}$ and *Otud7b*$^{-/-}$ mice to LED light. **(B)** Immunofluorescence analysis of retinal sections from *Otud7b*$^{+/+}$ and *Otud7b*$^{-/-}$ mice after light exposure using an anti-Otud7b antibody. Nuclei were stained with DAPI.

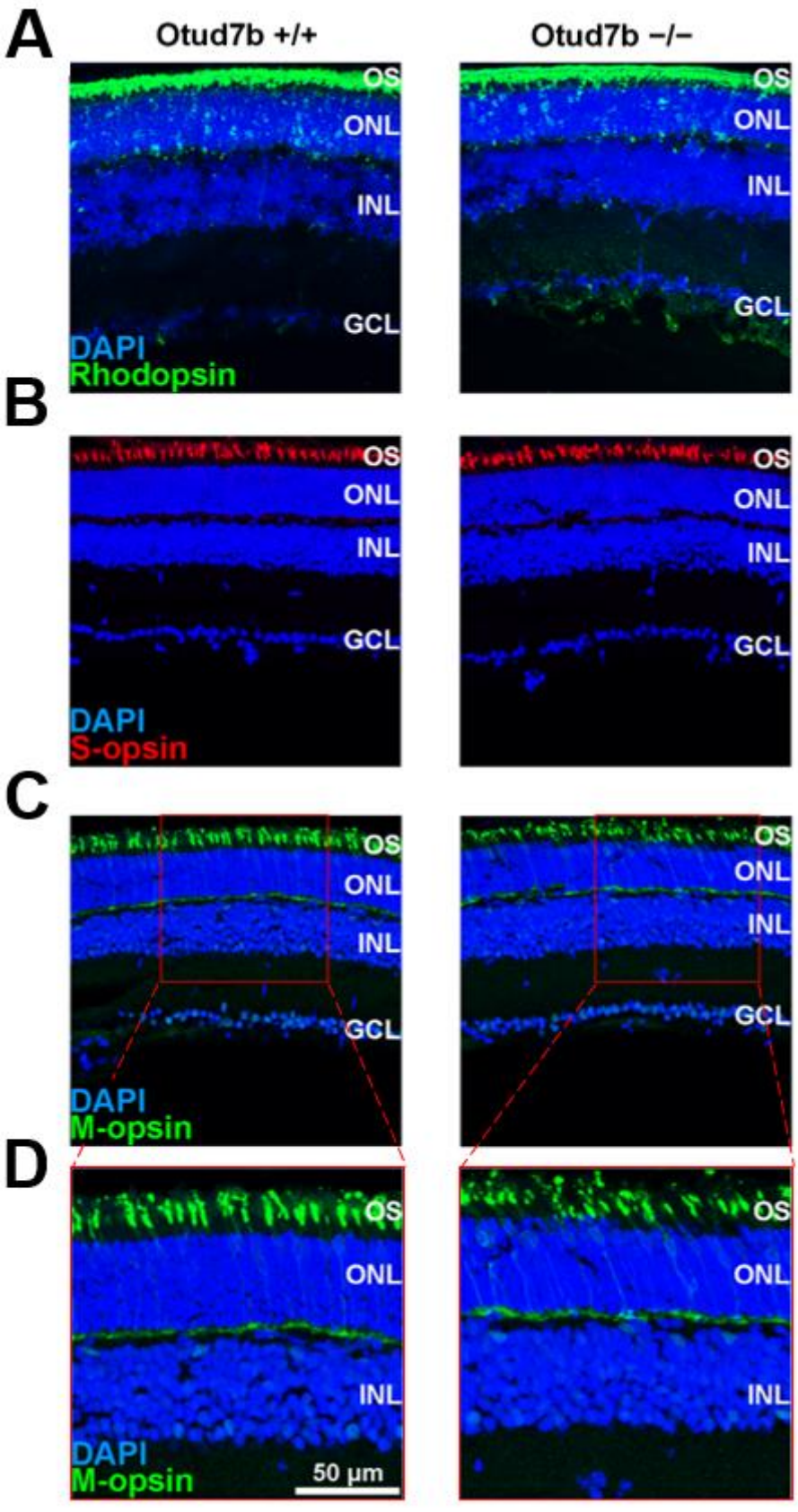
A
Otud7b +/+
Otud7b −/−
OS
ONL
INL
GCL
DAPI
Rhodopsin
B
DAPI
S-opsin
C
DAPI
M-opsin
D
50 µm

Figure 19. *Otud7b* deficiency exacerbates light-induced retinal damage to cone photoreceptor cells.

Immunofluorescence analysis of retinal sections from *Otud7b*$^{+/+}$ and *Otud7b*$^{-/-}$ mice after light exposure using antibodies as follows: Rhodopsin (a marker for rod outer segments **A**), S-opsin (a marker for S-cone outer segments **B**), and M-opsin (a marker for M-cone outer segments **C**). **(D)** Enlarged a section of M-opsin. Nuclei were stained with DAPI.

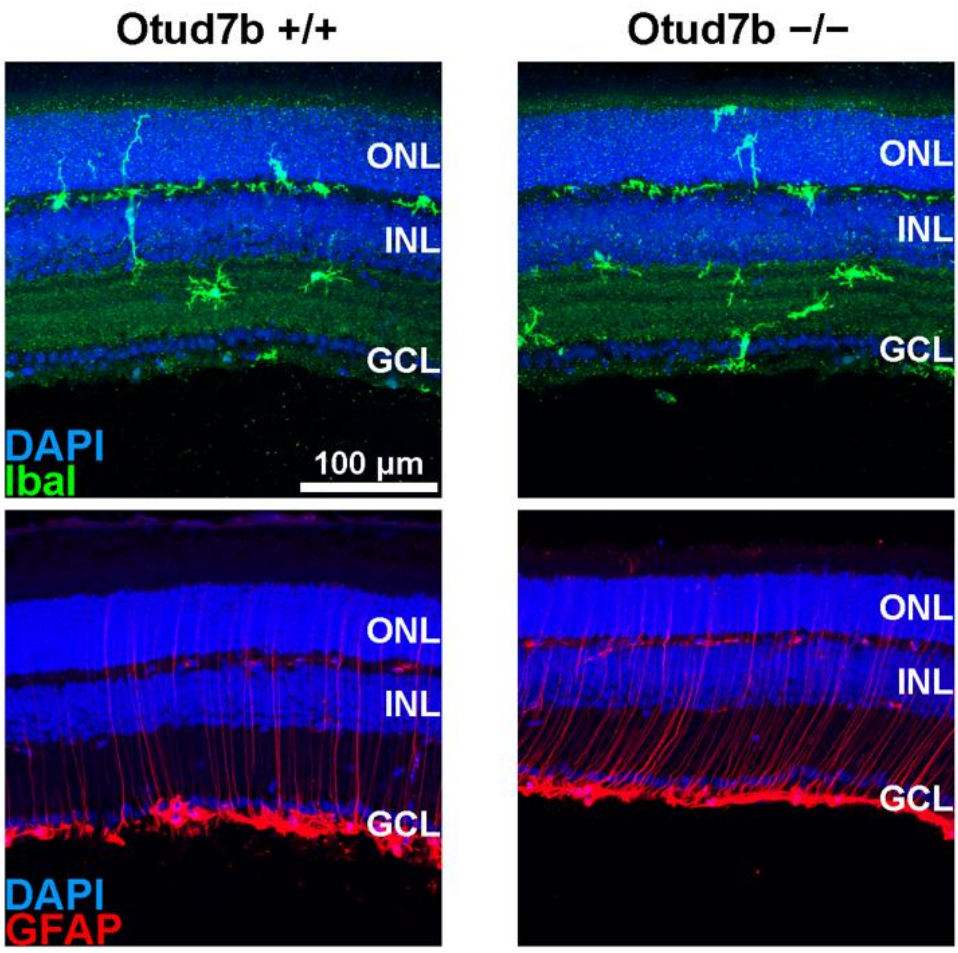

Figure 20. Microglial and Müller glial immunofluorescence.
Immunofluorescence analysis of retinal sections from *Otud7b*$^{+/+}$ and *Otud7b*$^{-/-}$ mice after light exposure using antibodies against: IbaI (a marker for microglia) and GFAP (a marker for reactive gliosis in Müller glia).

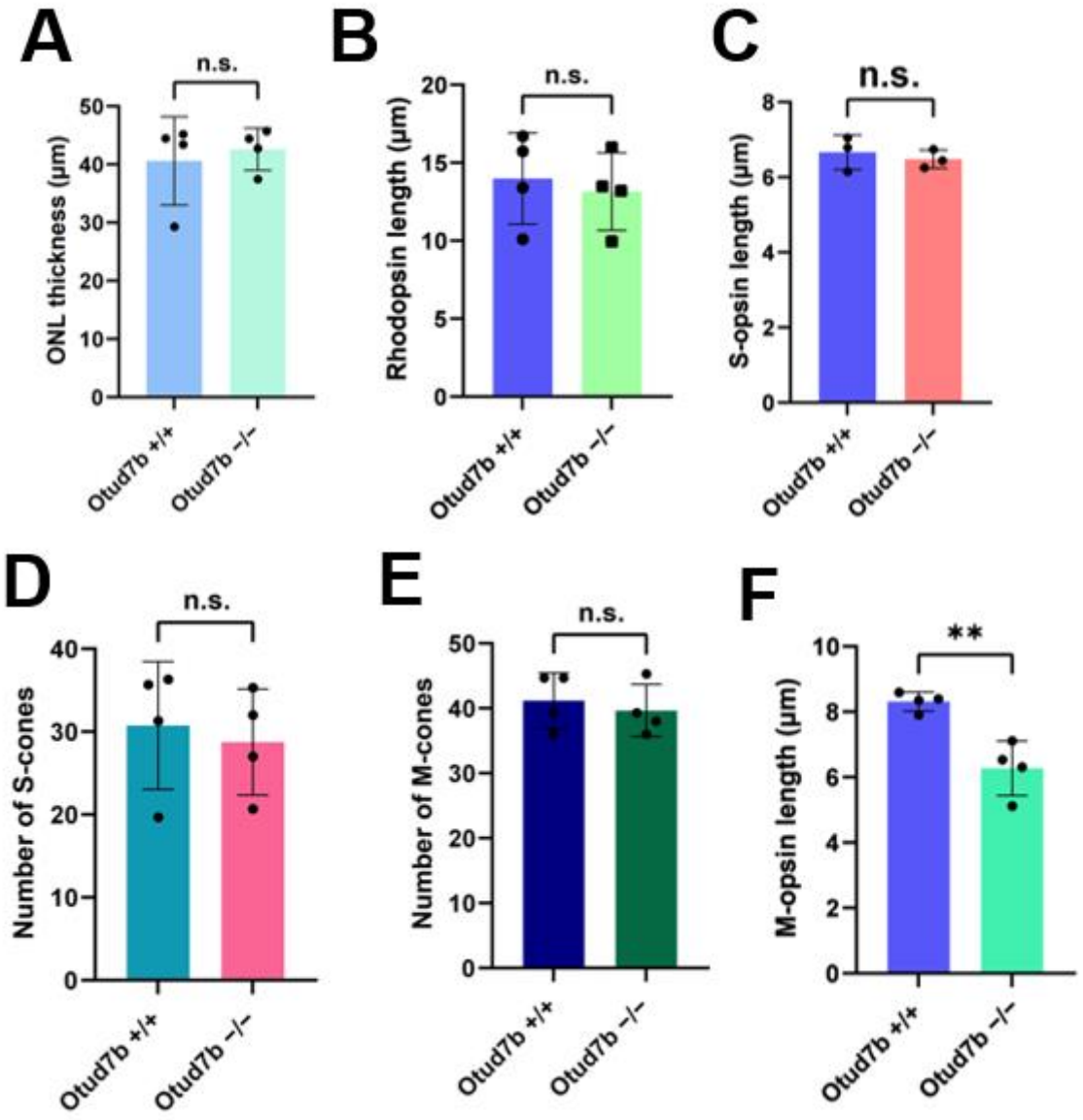

Figure 21. Quantification of photoreceptor cells of *Otud7b*$^{+/+}$ and *Otud7b*$^{-/-}$ mice after light exposure.

(A) The ONL thickness was measured. No significant difference in ONL thickness between the *Otud7b*$^{+/+}$ and *Otud7b*$^{-/-}$ retina. n = 3 retinal sections from 4 mice per genotype. **(B)** Rod outer segment lengths were measured. **(C)** S-cone outer segment lengths were measured. **(D, E)** The number of S-cones **(D)** and M-cones **(E)** were counted. **(F)** M-cone outer segment lengths were measured. M-cone outer segments were shorter in the *Otud7b*$^{-/-}$ retina than in the *Otud7b*$^{+/+}$ retina.

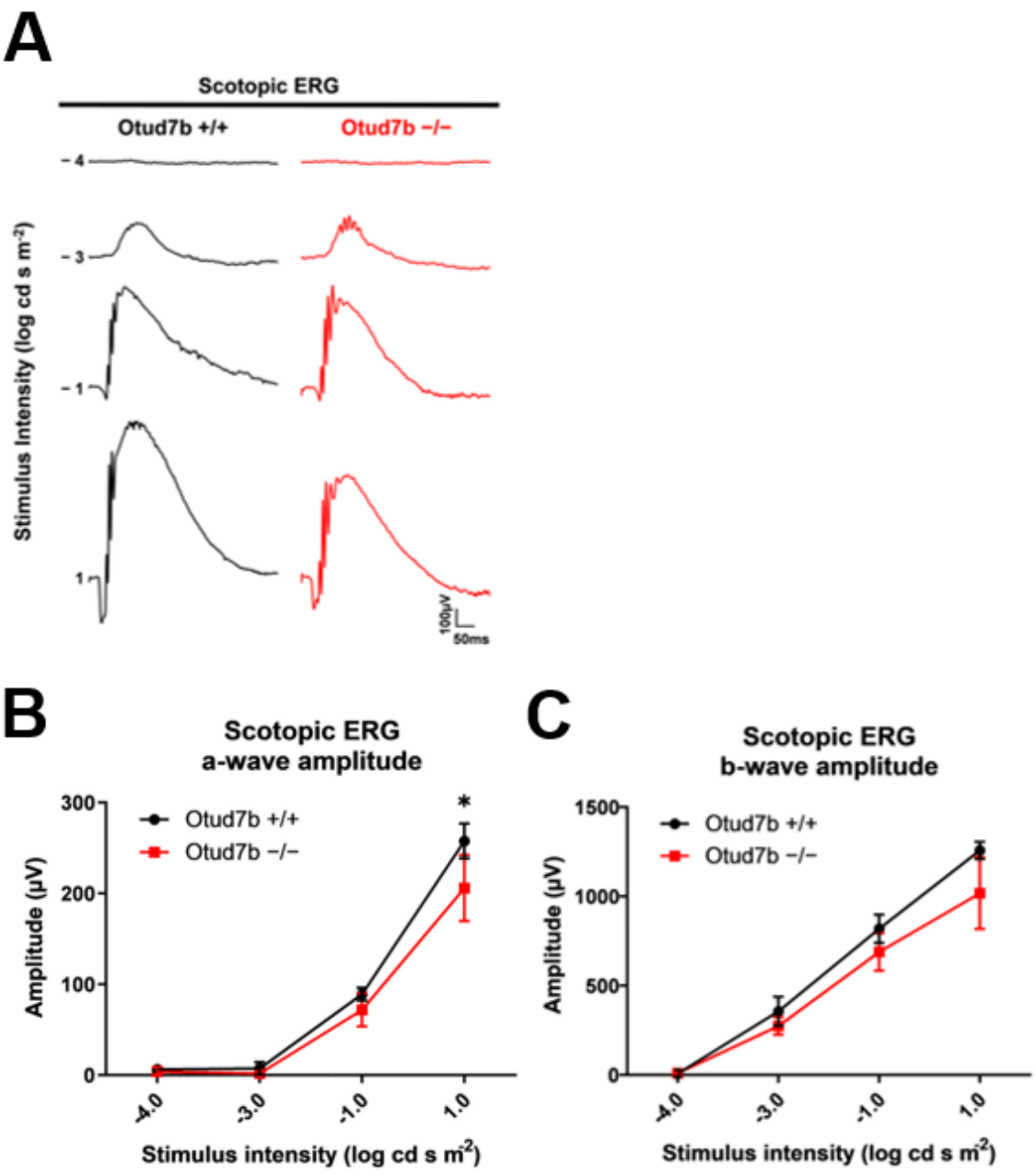

Figure 22. Scotopic ERG of *Otud7b*$^{+/+}$ and *Otud7b*$^{-/-}$ mice after light exposure.
(A) Representative scotopic ERGs elicited by four different stimulus intensities (−4.0 to 1.0 log cd s/m^2). Scotopic a-wave **(B)** and b-wave **(C)** amplitudes are shown as functions of stimulus intensity. Data are presented as the mean ± SD. n.s., not significant (unpaired t-test), *$p < 0.05$, **$p < 0.01$ (unpaired t-test), n = 4 per genotype.

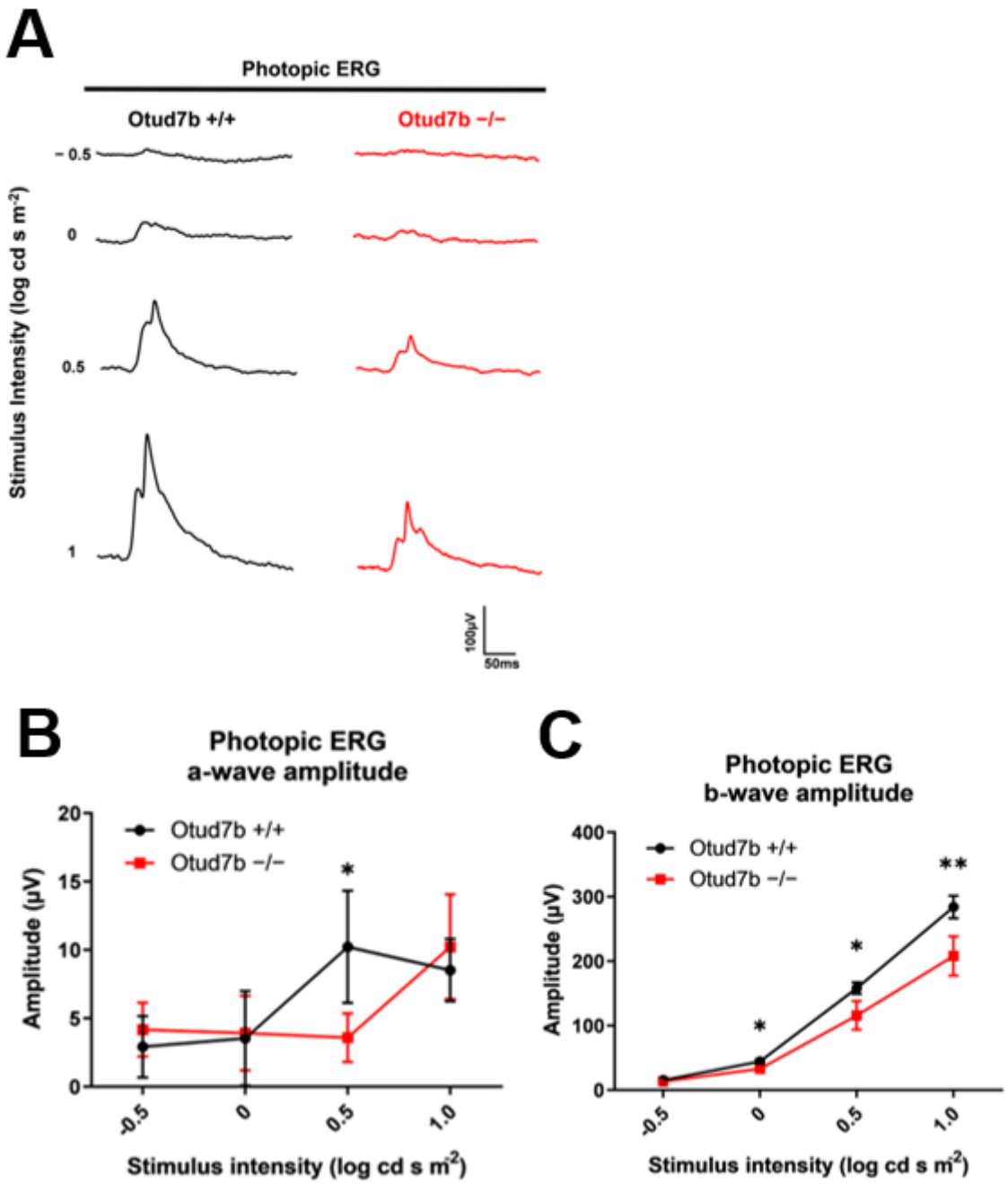

Figure 23. Photopic ERG analysis of *Otud7b*$^{+/+}$ and *Otud7b*$^{-/-}$ mice after light exposure.

(A) Representative photopic ERGs elicited by four different stimulus intensities (−0.5 to 1.0 log cd s/m^2). Photopic a-wave **(B)** and b-wave **(C)** amplitudes are shown as functions of stimulus intensity. Data are presented as the mean ± SD. n.s., not significant (unpaired t-test), *$p < 0.05$, **$p < 0.01$ (unpaired t-test), n = 4 per genotype.

cone photoreceptor damage under environmental stress. To evaluate physiological changes, we performed ERGs in light-exposed *Otud7b*$^{-/-}$ mice. In the scotopic ERG, the a-wave amplitude at the strongest stimulus showed a significant decrease in *Otud7b*$^{-/-}$ mice (Figure 22). Under the scotopic conditions, light stimuli below the threshold of -2 log cd s m^{-2} are purely derived from the rod photoreceptor cells; however, stronger light stimuli are derived from both the rod and cone photoreceptor cells[53]. In photopic ERG, *Otud7b*$^{-/-}$ mice had lower photopic amplitudes, which further supports that cone photoreceptor damage increases in light-exposed *Otud7b*$^{-/-}$ mice (Figure 23). These observations suggest that Otud7b protects cone photoreceptor cells from stress-induced degeneration.

Cone photoreceptor degeneration is intensified by *Otud7b* deficiency in the *Mak*$^{-/-}$ RP model mice

To determine the effects of *Otud7b* deficiency on progressive photoreceptor degeneration, we mated *Otud7b*$^{-/-}$ mice with male germ cell-associated kinase knockout (*Mak*$^{-/-}$) mice. We previously reported that *Mak* is highly expressed in retinal photoreceptor cells and that *Mak*$^{-/-}$ mice exhibit progressive photoreceptor degeneration[54,55]. Subsequent analyses have shown that mutations in the human *MAK* gene are associated with RP[56,57]. Immunofluorescence analysis was performed using antibodies against Rhodopsin, S-opsin, M-opsin, and Gnat2 (a marker for cone outer segments) in *Otud7b*$^{-/-}$; *Mak*$^{-/-}$ retinas (Figure 24). Although there were no obvious differences in rod outer segments between the *Otud7b*$^{+/+}$; *Mak*$^{-/-}$ and *Otud7b*$^{-/-}$; *Mak*$^{-/-}$ retinas, the *Otud7b*$^{-/-}$; *Mak*$^{-/-}$ retinas had shorter cone outer segments than the *Otud7b*$^{+/+}$; *Mak*$^{-/-}$ retinas (Figure 25A). In addition, we observed that ONL thickness decreased in

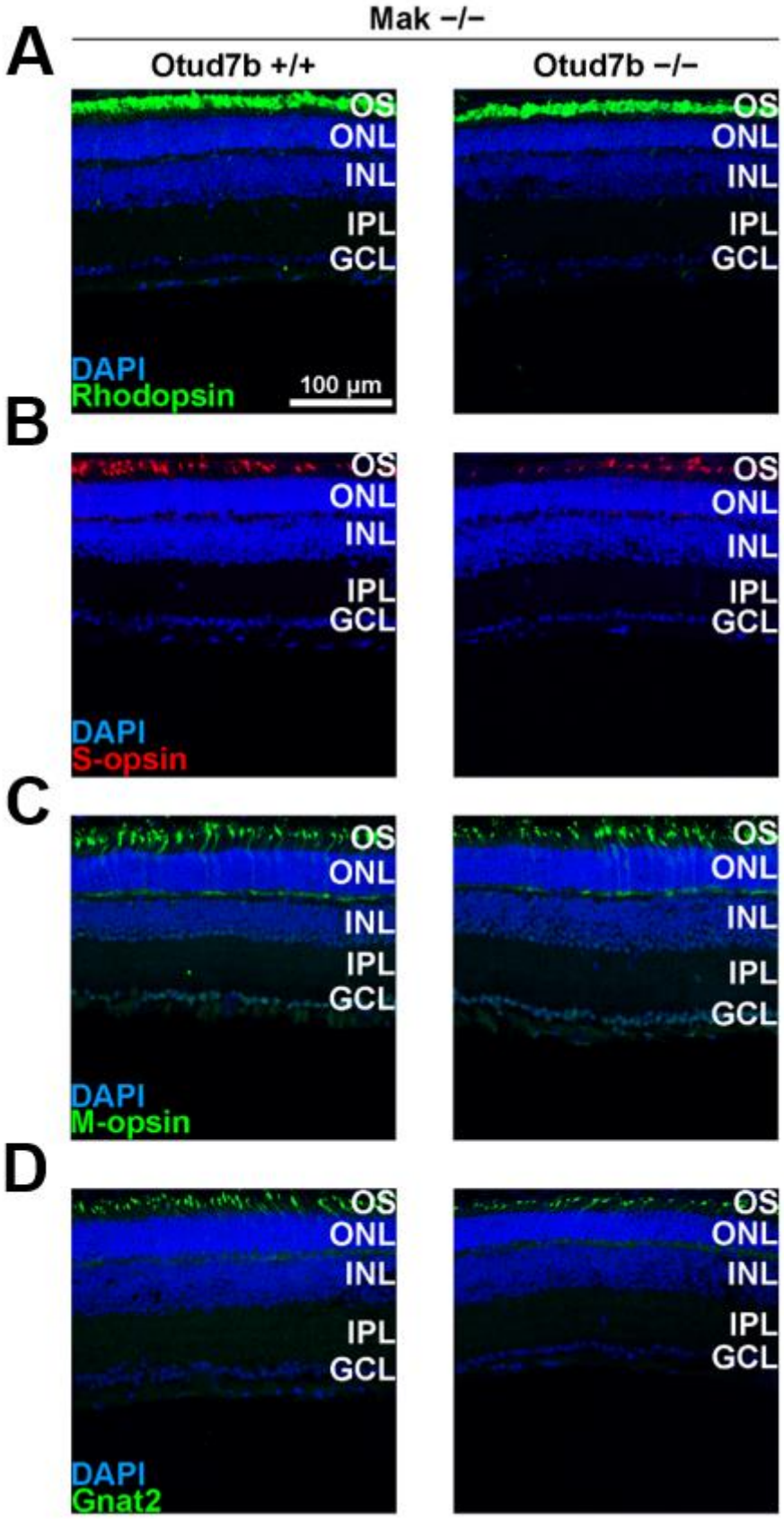
A
Mak −/−
Otud7b +/+
Otud7b −/−
OS
ONL
INL
IPL
GCL
DAPI
Rhodopsin
100 µm
B
DAPI
S-opsin
C
DAPI
M-opsin
D
DAPI
Gnat2

Figure 24. Immunofluorescence of photoreceptor cells.
Immunofluorescence analysis of retinal sections from *Otud7b*$^{+/+}$; *Mak*$^{-/-}$ and *Otud7b*$^{-/-}$; *Mak*$^{-/-}$ at 2 months using antibodies against Rhodopsin (a marker for rod outer segments **A**), S-opsin (a marker for S-cone outer segments **B**), M-opsin (a marker for M-cone outer segments **C**), and Gnat2 (a marker for cone outer segments **D**). Nuclei were stained with DAPI.

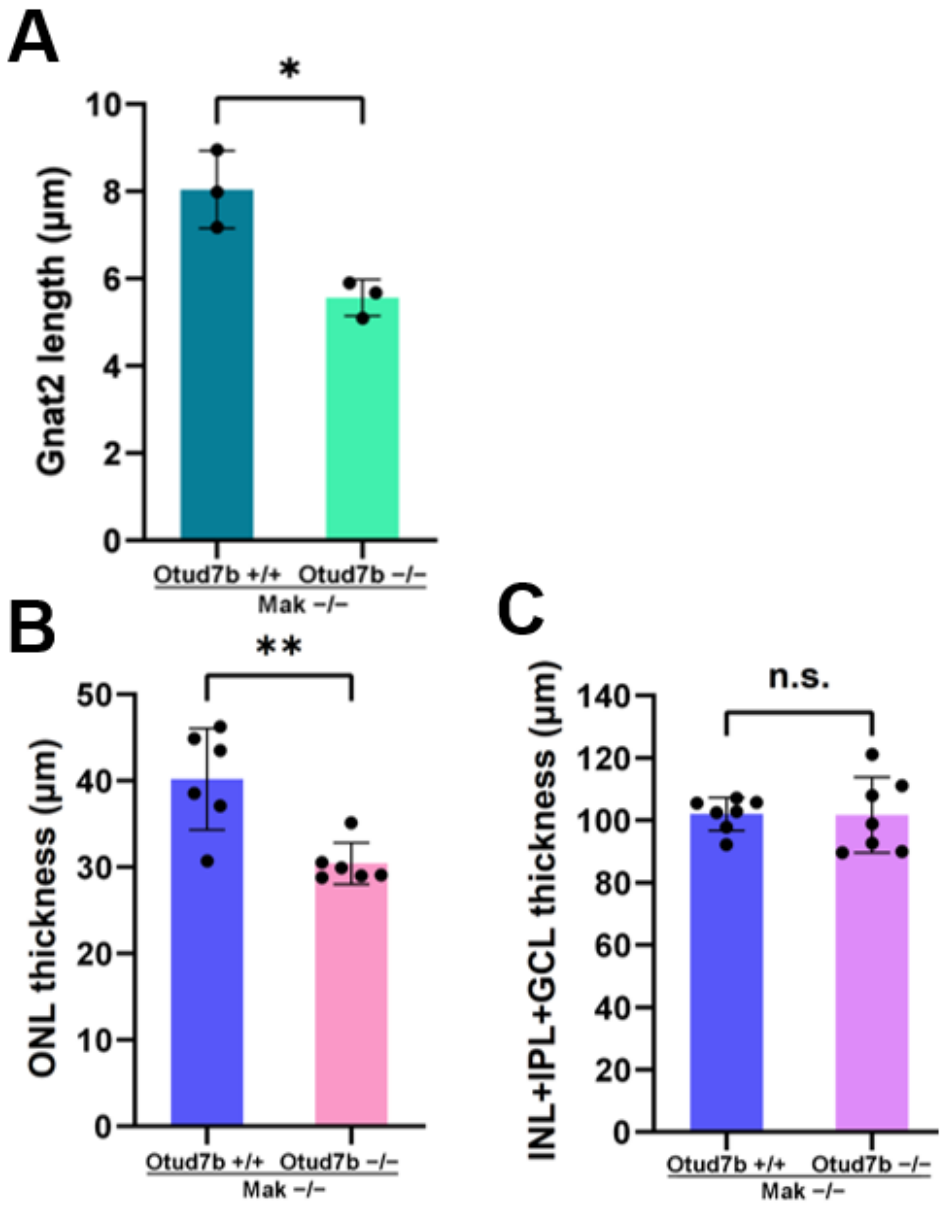

Figure 25. *Otud7b* deficiency exacerbates retinal degeneration in *Mak*$^{-/-}$ mice. **(A)** Cone outer segment length was measured in *Otud7b*$^{+/+}$; *Mak*$^{-/-}$ and *Otud7b*$^{-/-}$; *Mak*$^{-/-}$ retinas at 2 months. *Otud7b*$^{-/-}$; *Mak*$^{-/-}$ retinas had significantly shorter cone outer segments. Data are presented as the mean ± SD. *$p < 0.05$ (unpaired t-test), n = 3 per genotype. **(B)** The ONL thickness was measured. The ONL thickness in the *Otud7b*$^{-/-}$; *Mak*$^{-/-}$ retina was significantly thinner than that in the *Otud7b*$^{+/+}$; *Mak*$^{-/-}$ retina. Data are presented as the mean ± SD. **$p < 0.01$ (unpaired t-test), n = 6 retinal sections from 3 mice per genotype. **(C)** The INL+IPL+GCL thickness was measured. Data are presented as the mean ± SD. n.s., not significant (unpaired t-test). n = 6 retinal sections from 3 mice per genotype.

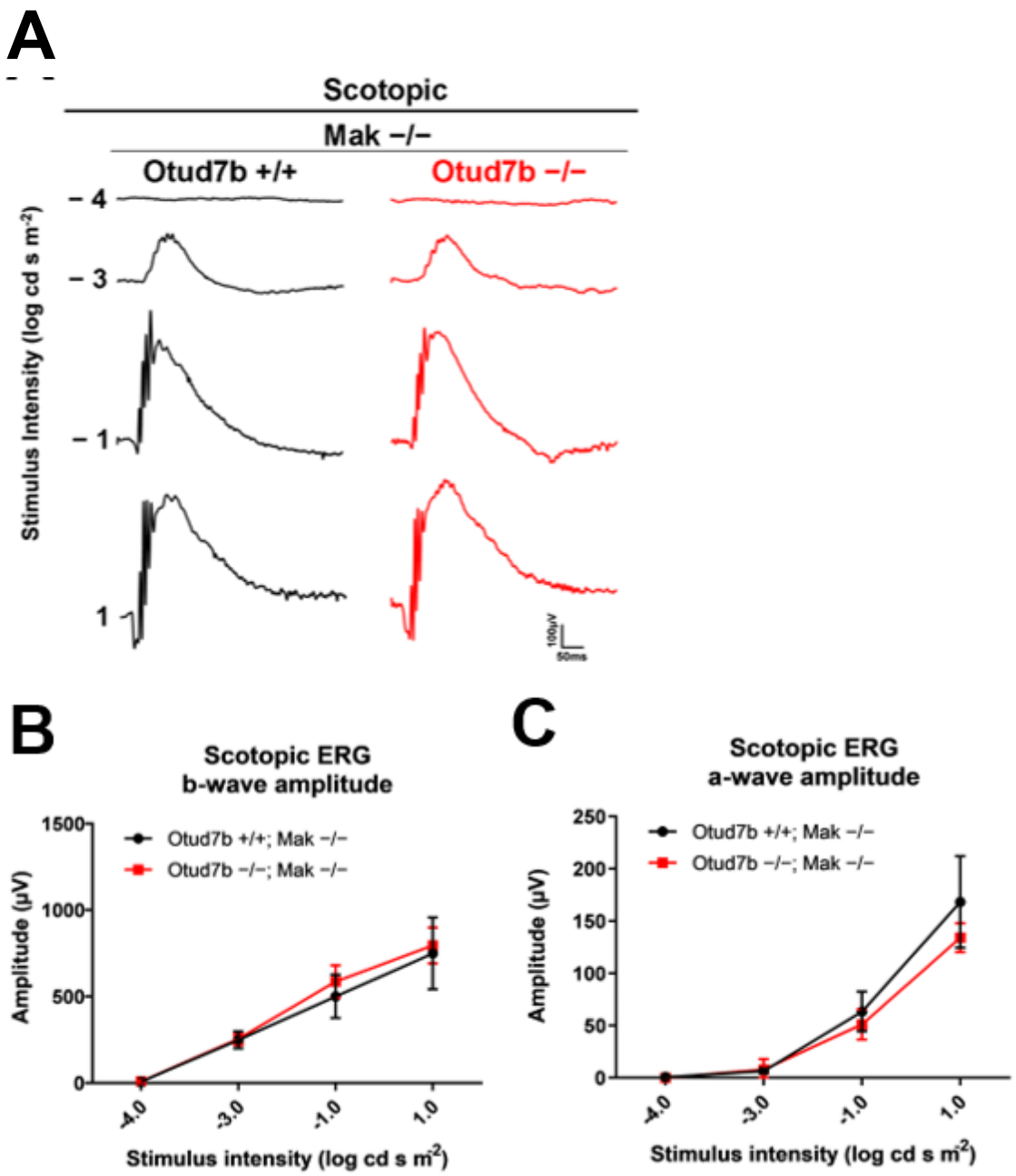

Figure 26. Scotopic ERG analysis of *Otud7b*$^{+/+}$; *Mak*$^{-/-}$ and *Otud7b*$^{-/-}$; *Mak*$^{-/-}$ mice at 2 months.

(A) Representative scotopic ERGs elicited by four different stimulus intensities (−4.0 to 1.0 log cd s/m^2). Scotopic a-wave **(B)** and b-wave **(C)** amplitudes are shown as functions of stimulus intensity. Data are presented as the mean ± SD (unpaired t-test). n = 3 per genotype.

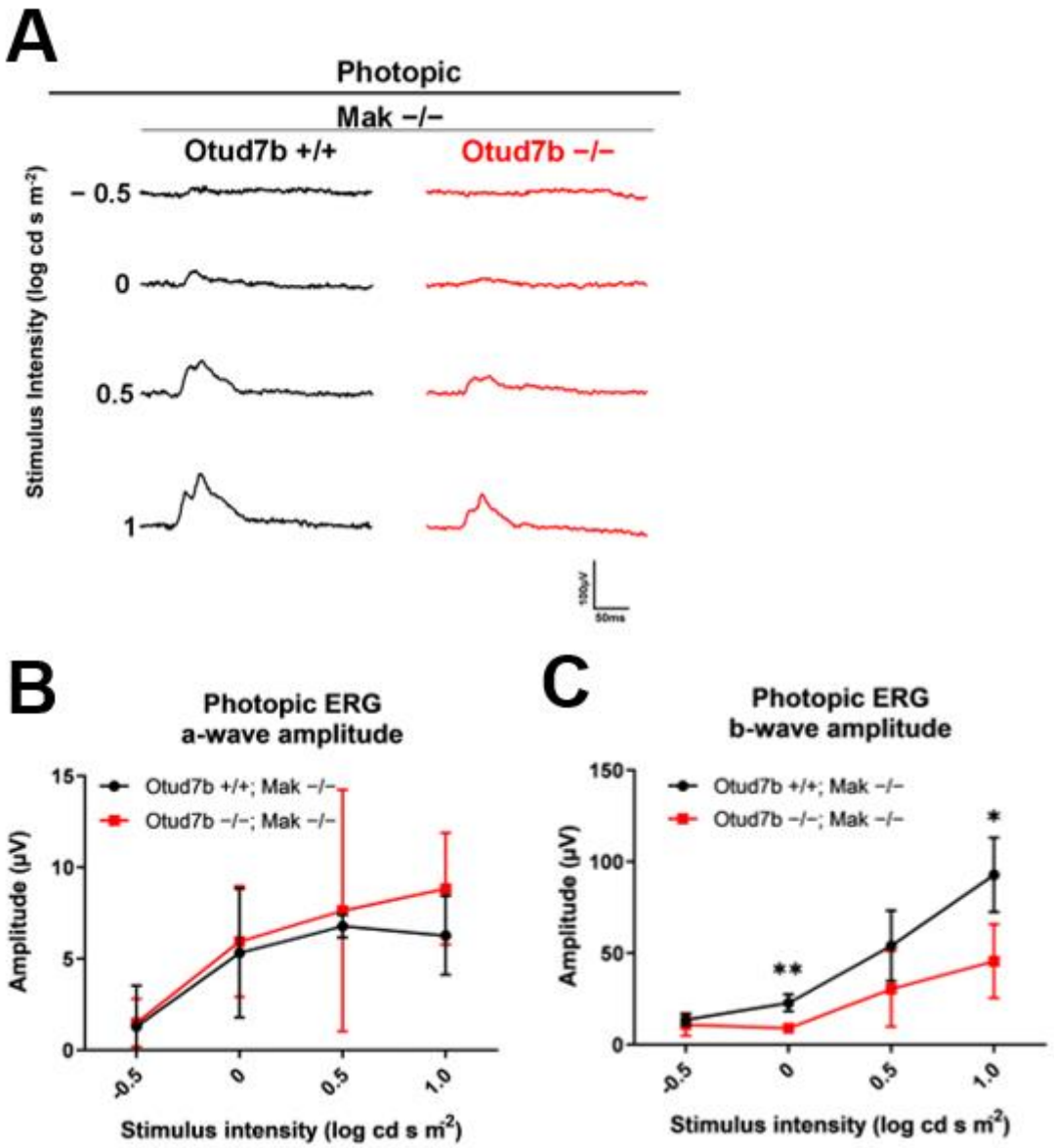

Figure 27. Photopic ERG analysis of *Otud7b*$^{+/+}$; *Mak*$^{-/-}$ and *Otud7b*$^{-/-}$; *Mak*$^{-/-}$ mice at 2 months.

(A) Representative photopic ERGs elicited by four stimulus intensities (−0.5 to 1.0 log cd s/m^2). Photopic a-wave **(B)** and b-wave **(C)** amplitudes are shown as functions of stimulus intensity. Data are presented as the mean ± SD. *$p < 0.05$, **$p < 0.01$ (unpaired t-test). n = 3 per genotype.

the *Otud7b*$^{-/-}$; *Mak*$^{-/-}$ retina (Figure 25B). In contrast, the thickness of the other retinal layers did not differ significantly between *Otud7b*$^{+/+}$; *Mak*$^{-/-}$ and *Otud7b*$^{-/-}$; *Mak*$^{-/-}$ mice (Figure 25C). Next, we examined the electrophysiological properties of *Otud7b*$^{-/-}$; *Mak*$^{-/-}$ mice by ERG analysis. While we did not observe a significant difference in the scotopic ERGs (Figure 26), the photopic ERG b-wave amplitudes were significantly lower in *Otud7b*$^{-/-}$; *Mak*$^{-/-}$ mice than in *Otud7b*$^{+/+}$; *Mak*$^{-/-}$ mice (Figure 27). Consistent with the results obtained from the light exposure experiments (Figures 18–23), these results suggest that Otud7b suppresses cone photoreceptor degeneration under stress conditions.

Otud7b-deficient neuronal cells are susceptible to cell death under stress

We investigated the role of Otud7b in neuronal cells cultured under stress from serum starvation, an environmental stress that has been shown to induce oxidative stress[58,59]. We constructed plasmids expressing a short hairpin RNA (shRNA) to knockdown *Otud7b* and confirmed by western blotting that Otud7b-shRNA1 was able to suppress Otud7b expression (Figure 28A). Plasmids encoding shRNA-control or Otud7b-shRNA1 were transfected into the murine neuronal cell line, Neuro2A. These cells were starved of serum for 14 h before immunofluorescence analysis using an antibody against Otud7b or cleaved caspase 3 (a marker of apoptosis) (Figures 28B and 29A). We observed that Otud7b signals markedly decreased in the cells expressing Otud7b-shRNA1 but not in those expressing shRNA-control, indicating that *Otud7b* was knocked down in Neuro2A cells by Otud7b-shRNA1 (Figure 28B). We quantified cleaved caspase 3 and GFP double-positive cells and normalized them to GFP-positive cells. Neuro2A cells transfected with Otud7b-shRNA1 had more double-positive cells than those transfected with shRNA-control (Figure 29B). In addition, a cell viability assay was performed to compare the

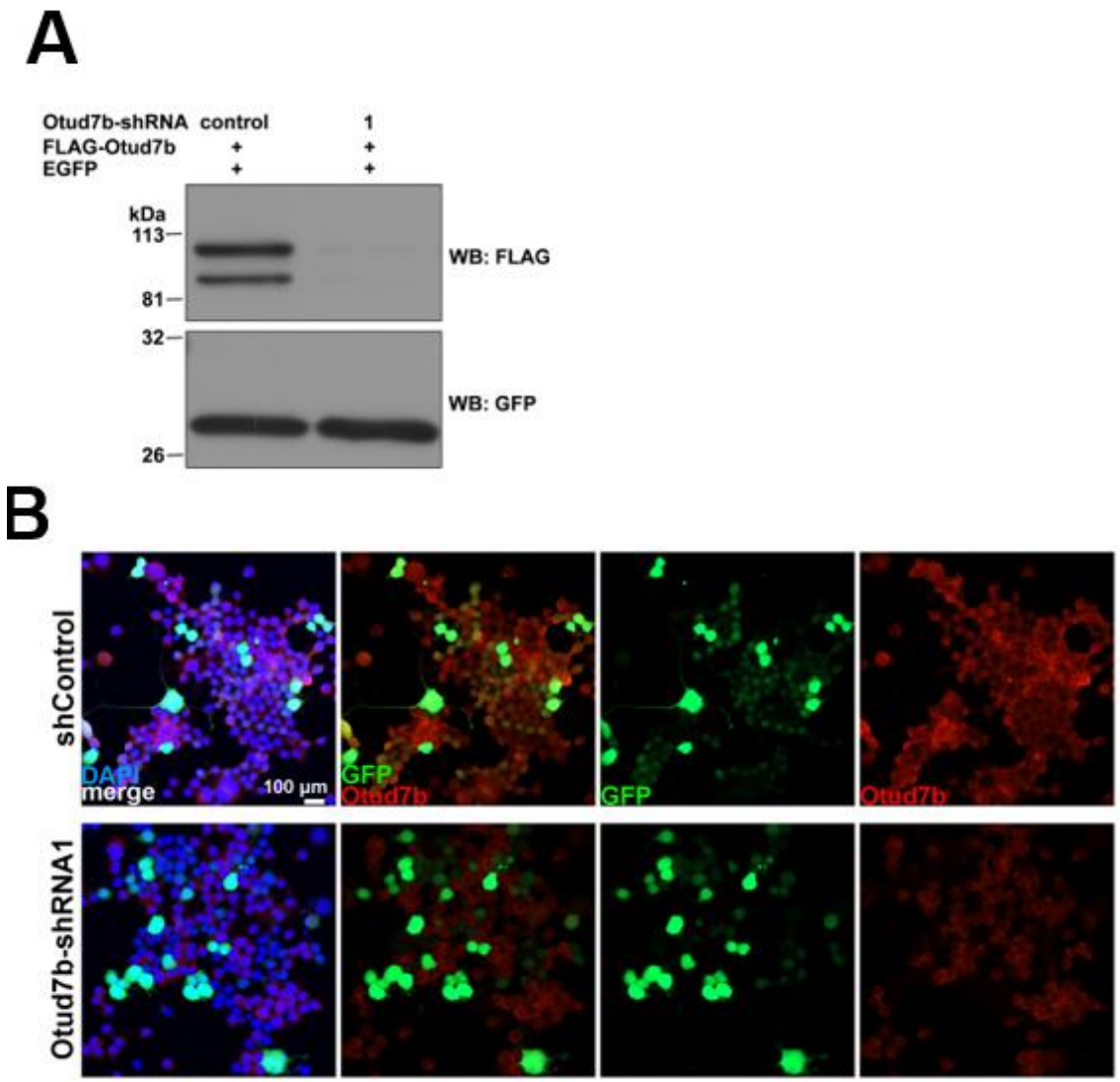

Figure 28. Efficiency of *Otud7b* knockdown using shRNA.

(A) Inhibition efficacy of shRNA expression constructs for *Otud7b* knockdown. ShRNA-control or Otud7b-shRNA1 expression plasmids were co-transfected with plasmids expressing a FLAG-tagged Otud7b and a GFP into HEK293T cells. Western blotting was performed using anti-FLAG and anti-GFP antibodies. GFP was used as an internal transfection control. Otud7b-shRNA1 effectively suppressed Otud7b expression. **(B)** Inhibition efficacy of shRNA expression constructs for *Otud7b* knockdown. ShRNAcontrol or Otud7b-shRNA1 expression plasmids were co-transfected with plasmids expressing a FLAG-tagged Otud7b and a GFP into Neuro2A cells. The cells were serum starved for 14 h. Immunofluorescence analysis was performed using anti-Otud7b antibody. Nuclei were stained with DAPI.

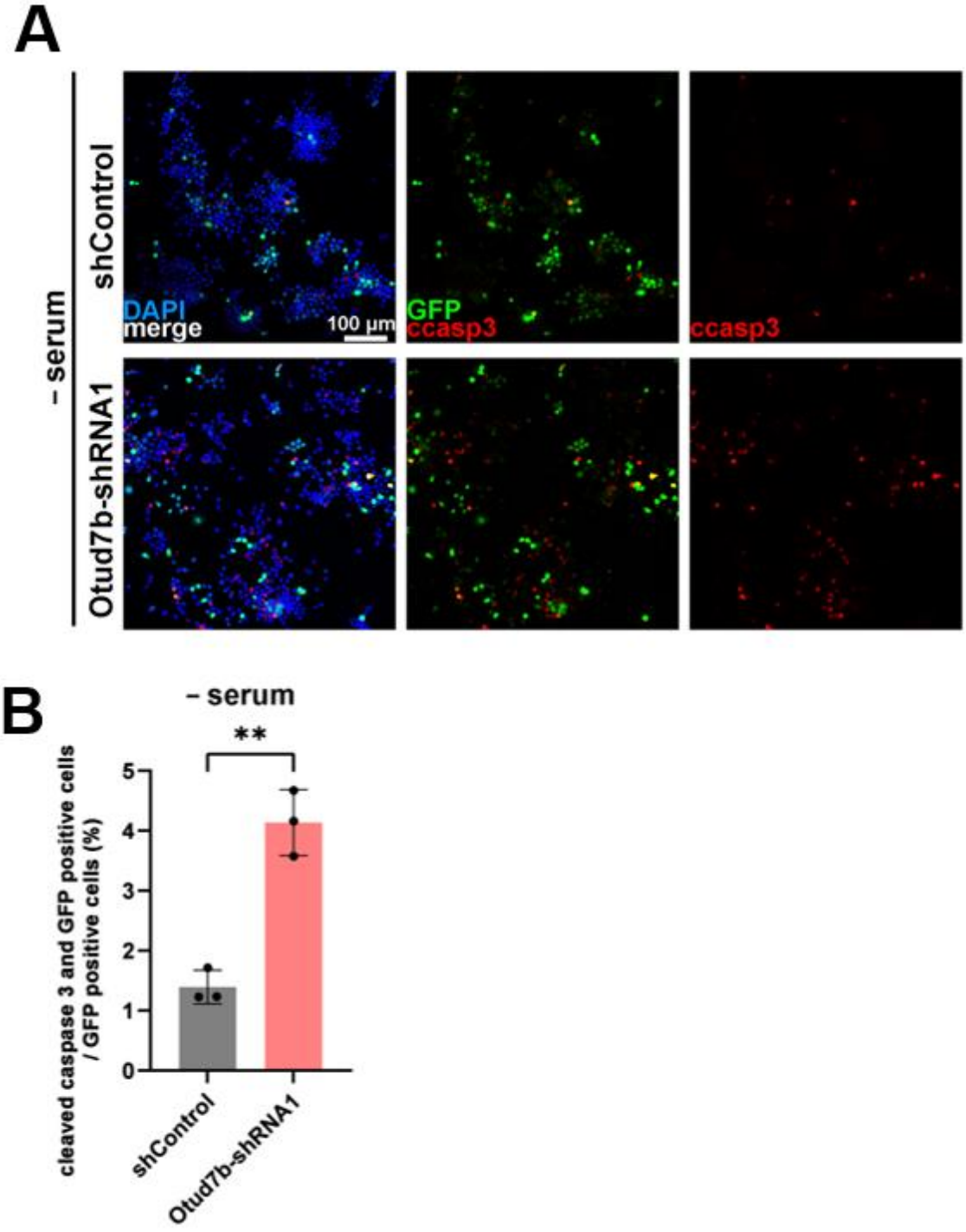
A
– serum
shControl
Otud7b-shRNA1
DAPI
merge
100 μm
GFP
ccasp3
ccasp3
B
– serum
**
cleaved caspase 3 and GFP positive cells / GFP positive cells (%)
0
1
2
3
4
5
shControl
Otud7b-shRNA1

Figure 29. Knockdown of *Otud7b* with shRNA in neuronal cells increases susceptibility to cell death under stress.

(A, B) ShRNA-control or Otud7b-shRNA1 expression plasmids were co-transfected with a plasmid expressing EGFP into Neuro2A cells. The cells were serum starved for 14 h. **(A)** Immunofluorescence analysis was performed using an anti-cleaved caspase 3 antibody. Nuclei were stained with DAPI. Increased number of cleaved caspase 3 and GFP double-positive cells was observed in the Otud7b-shRNA1 transfected cells. **(C)** The number of cleaved caspase 3 and GFP double-positive cells per GFP-positive cells was measured. Data are presented as the mean ± SD. $^{**}p < 0.01$ (unpaired t-test). n = 3 experiments.

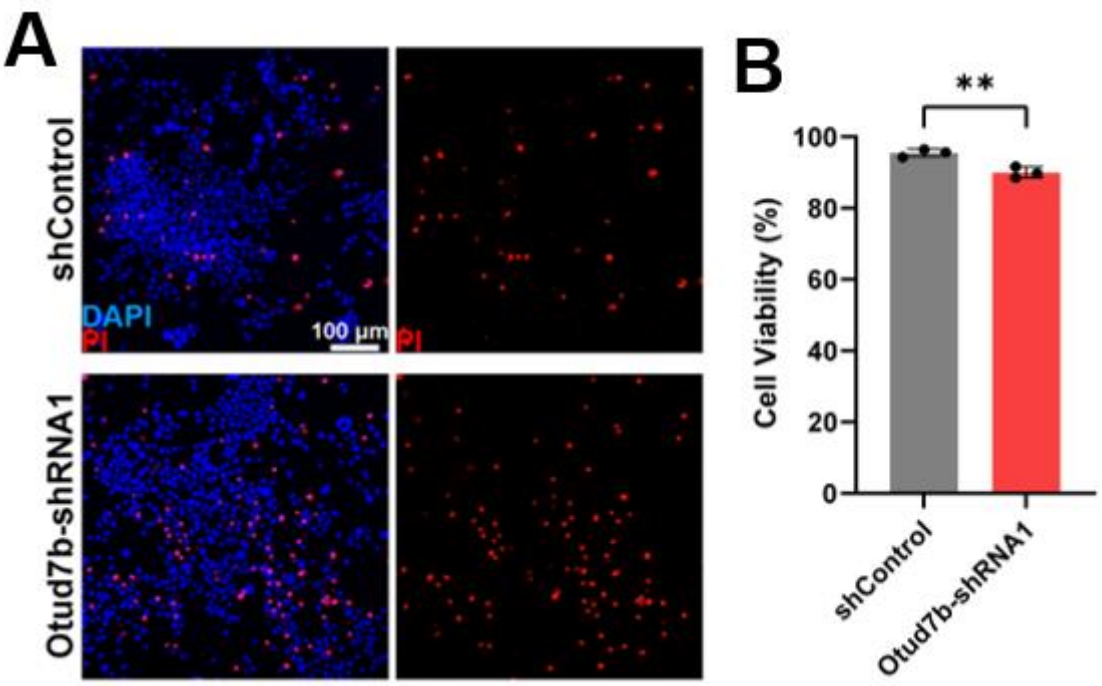

Figure 30. Cell viability assay was performed on Neuro2A cells transfected with shRNA.

(A) Fluorescent imaging of cell viability assay after 14 h serum starvation performed by ReadyProbes™ cell viability imaging kit. Neuro2A cells were stained with NucBlue™ (total cells) and propidium iodide (non-viable cells). **(B)** Cell viabilities are shown as percentage. Otud7b-shRNA1 transfected cells showed a decrease in cell viability compared to the shRNA-control. Data are presented as the mean ± SD. $^{**}p < 0.01$ (unpaired t-test). n = 3 experiments.

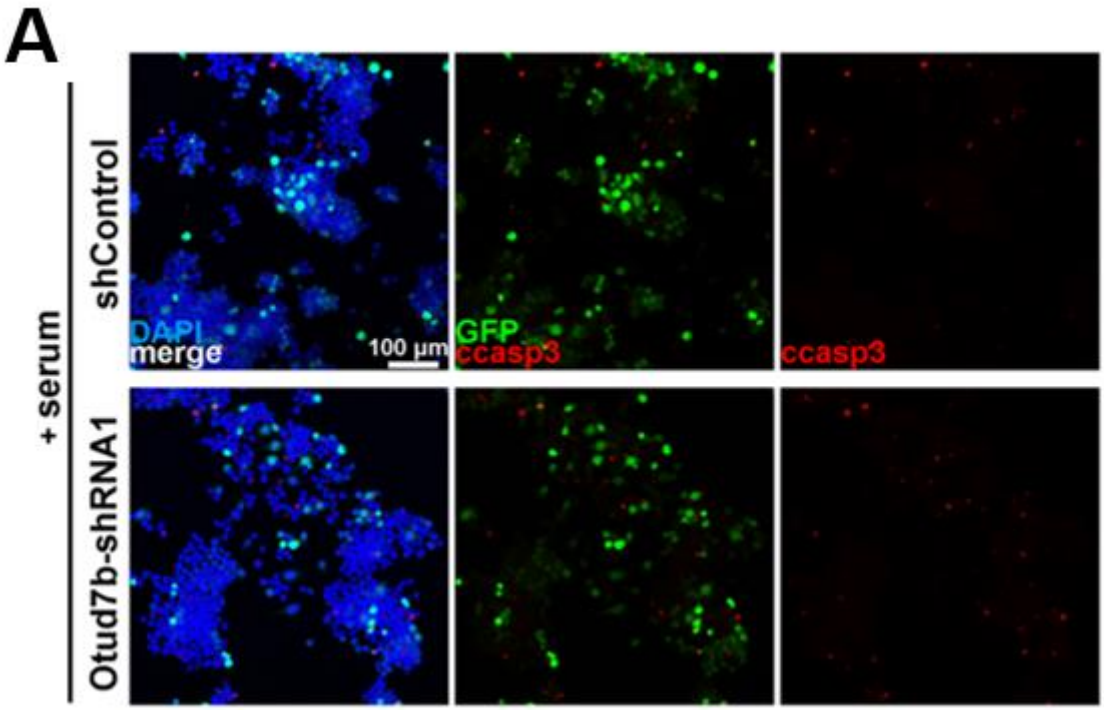
A
+ serum
shControl
Otud7b-shRNA1
DAPI
merge
100 μm
GFP
ccasp3
ccasp3

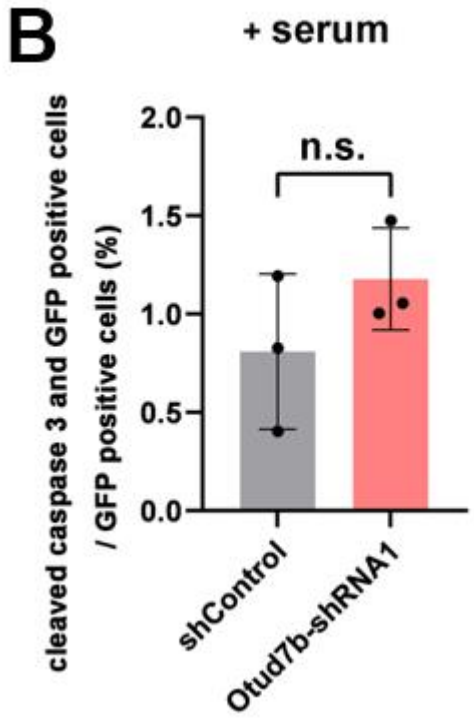
B
+ serum
cleaved caspase 3 and GFP positive cells
/ GFP positive cells (%)
2.0
1.5
1.0
0.5
0.0
n.s.
shControl
Otud7b-shRNA1

Figure 31. Knockdown of *Otud7b* with shRNA in neuronal cells increases susceptibility to cell death under stress.

(A, B) ShRNA control or Otud7b-shRNA1 expression plasmids were co-transfected with a plasmid expressing EGFP into Neuro2A cells. Cells were cultured with serum. **(A)** Immunofluorescence analysis was performed using an anti-cleaved caspase 3 antibody. Nuclei were stained with DAPI. **(B)** Number of cleaved caspase 3 and GFP double-positive cells per GFP-positive cell was determined. Data are presented as the mean ± SD. n.s., not significant (unpaired t-test). n = 3 experiments.

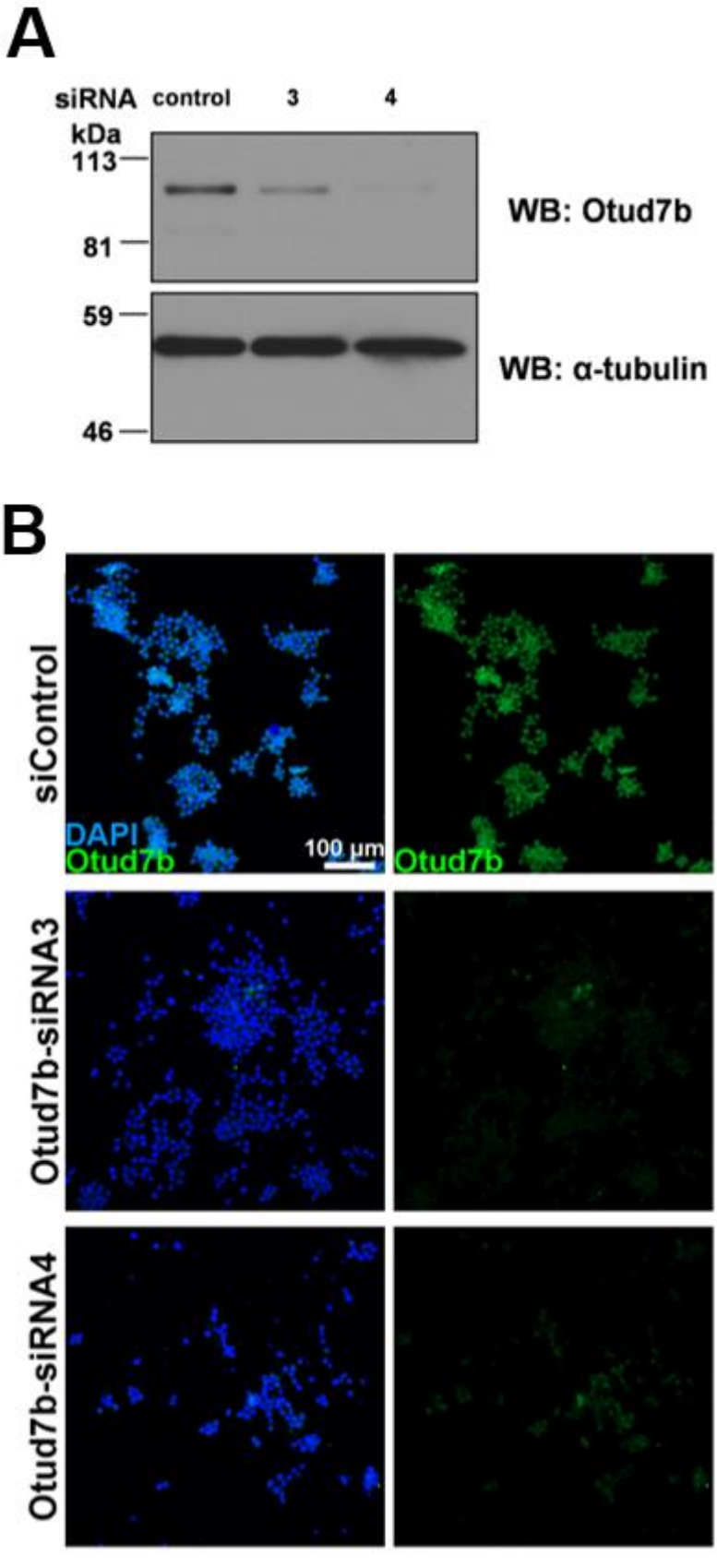
A
siRNA control 3 4
kDa
113
81
59
46
WB: Otud7b
WB: α-tubulin
B
siControl
Otud7b-siRNA3
Otud7b-siRNA4
DAPI
Otud7b
100 μm
Otud7b

Figure 32. Efficiency of *Otud7b* knockdown using shRNA.
(A) Inhibition efficacy of siRNAs for *Otud7b* knockdown. SiRNA-control, Otud7b-siRNA3, or Otud7b-siRNA4 was transfected into Neuro2A cells. Western blotting was performed using antibodies against Otud7b and α-tubulin. α-tubulin was used as a loading control. Otud7b-siRNA3 and Otud7b-siRNA4 effectively suppressed Otud7b expression. **(B)** Inhibition efficacy of siRNA for *Otud7b* knockdown. SiRNA-control, Otud7bsiRNA3, or Otud7b-siRNA4 was transfected into Neuro2A cells. The cells were serum starved for 14 h. Immunofluorescence analysis was performed using anti-Otud7b antibody. Nuclei were stained with DAPI.

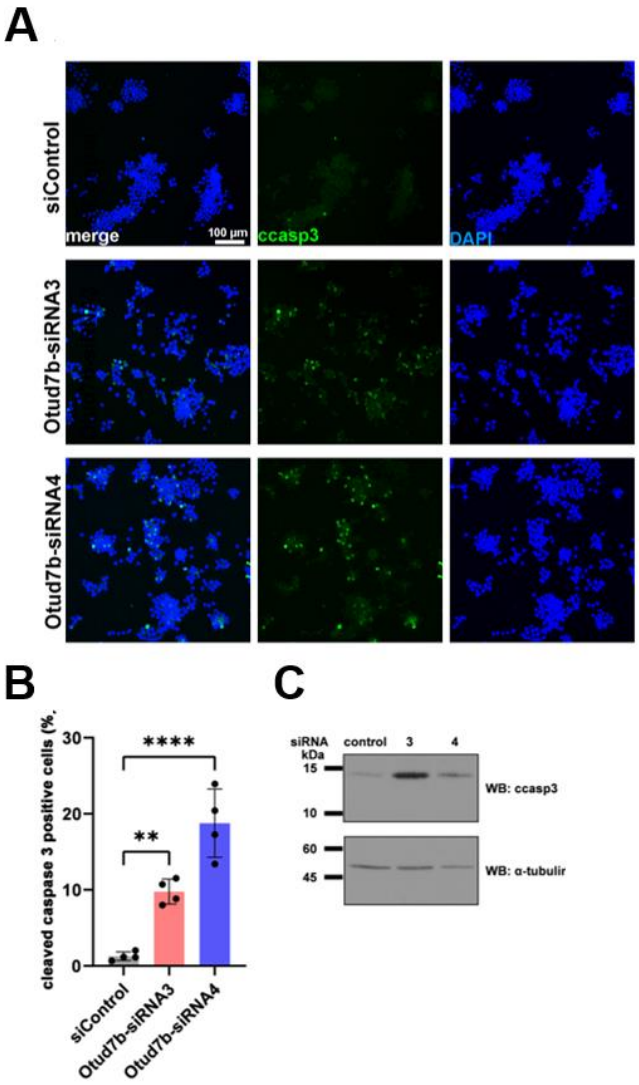

Figure 33. *Otud7b* knockdown using siRNA reduces cell survival in neuronal cells. **(A, B)** Neuro2A cells were transfected with siRNA-control, Otud7b-siRNA3, or Otud7b-siRNA4. The cells were serum starved for 14 h. **(A)** Immunofluorescence analysis was performed with an anti-cleaved caspase 3 antibody. Nuclei were stained with DAPI. Increased number of cleaved caspase 3-positive cells was observed in the cells transfected with Otud7b-siRNA3 and Otud7b-siRNA4. **(B)** The number of cleaved caspase 3-positive cells was measured. Data are presented as the mean ± SD. $^{**}p < 0.01$, $^{****}p < 0.0001$ (one-way ANOVA followed by Tukey's multiple comparisons test). n = 4 experiments. **(C)** Western blot analysis using an anti-cleaved caspase 3 was performed on Neuro2A cells that were transfected with siRNA-control, Otud7b-siRNA3, or Otud7bsiRNA4 and serum starved for 14 h.

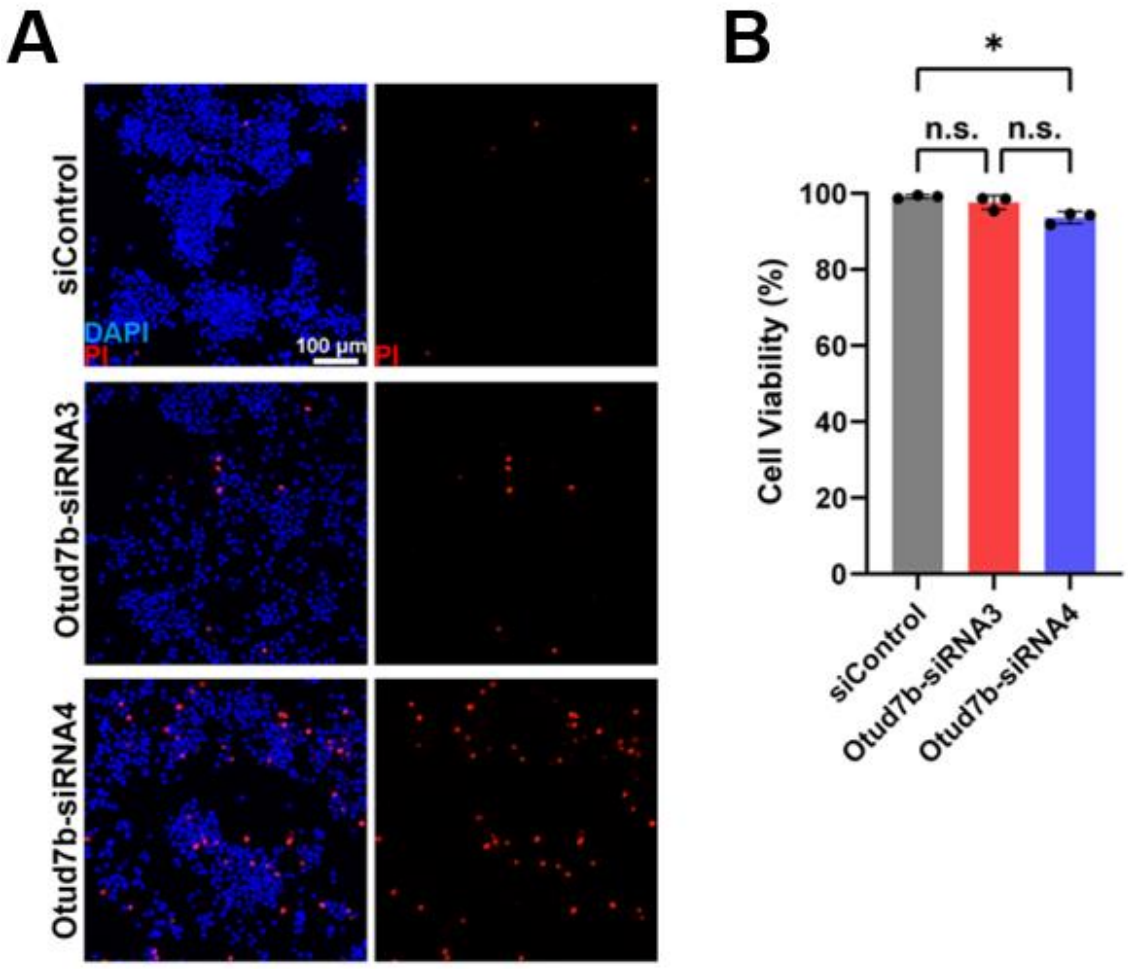

Figure 34. Cell viability of *Otud7b* knockdown using siRNA.

(A, B) Cell viability assay was performed on Neuro2A cells transfected with siRNA-control, Otud7b-siRNA3, or Otud7b-siRNA4. **(A)** Fluorescent imaging of cell viability assay after 14 h serum starvation performed by ReadyProbes™ cell viability imaging kit. Neuro2A cells were stained with NucBlue™ (total cells) and propidium iodide (non-viable cells). **(B)** Cell viabilities are shown as percentages. Otud7b-siRNA4 transfected cells showed a decrease in cell viability compared to the siRNA-control. Data are presented as the mean ± SD. *$p < 0.05$ (two-way ANOVA followed by Tukey's multiple comparisons test). n = 3 experiments.

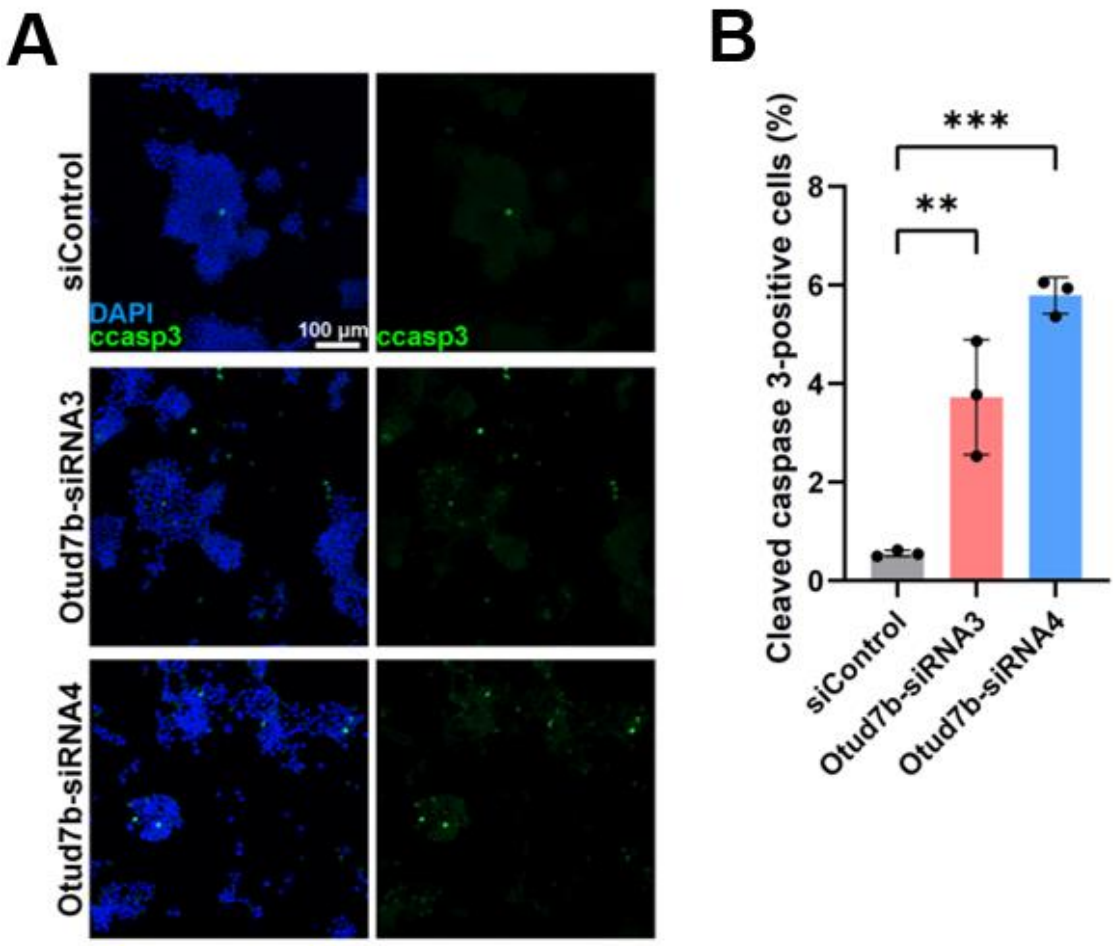

Figure 35. *Otud7b* knockdown with siRNA increases cell death after H_2O_2.
(A, B) Neuro2A cells were transfected with siRNA-control, Otud7b-siRNA3, or Otud7b-siRNA4. The cells were treated with 10 µM H_2O_2 for 20 h. **(A)** Immunofluorescence analysis was performed with an anti-cleaved caspase 3 antibody. Nuclei were stained with DAPI. Increased number of cleaved caspase 3-positive cells was observed in the cells transfected with Otud7b-siRNA3 and Otud7b-siRNA4. **(B)** The number of cleaved caspase 3-positive cells was measured. Data are presented as the mean ± SD. $^{**}p < 0.01$, $^{***}p < 0.001$ (two-way ANOVA followed by Tukey's multiple comparisons test). n = 3 experiments.

Neuro2A cells expressing shRNA-control with those expressing Otud7b-shRNA1 (Figure 30A and 30B). Neuro2A cells expressing the Otud7b-shRNA1 showed a decrease in cell viability compared to those expressing the shRNA-control (Figure 30B). However, no significant difference in the number of double-positive cells was observed between the shRNA-control and Otud7b-shRNA1-expressing cells without serum starvation (Figure 31). To confirm these results, we used small interfering RNAs (siRNAs) to knock down *Otud7b* in Neuro2A cells. After confirming the knockdown efficiency of the siRNAs (Figure 32A), we transfected Otud7b-siRNAs into Neuro2A cells that were then cultured in serum-free medium. We performed immunofluorescence analysis using an anti-Otud7b antibody and observed that Otud7b-positive cells markedly decreased in the cells transfected with Otud7b-siRNA3 or Otud7b-siRNA4 compared with the cells transfected with the siRNA-control (Figure 32B). Immunofluorescence analysis of serum-starved cells revealed an increase in cleaved caspase 3-positive cells among cells transfected with Otud7b-siRNAs (Figures 33A and 33B). We performed western blot analysis and observed an increase in cleaved caspase 3 in Neuro2A cells transfected with Otud7b-siRNA3 or Otud7b-siRNA4 after serum starvation (Figure 33C). Furthermore, a significant reduction in cell viability was observed in the serum-starved cells transfected with the Otud7b-siRNA4, while the serum-starved cells transfected with the Otud7b-siRNA3 showed a tendency to decrease cell viability (Figure 34). Additionally, we treated Neuro2A cells with 10 μM H_2O_2 for 20 h to induce oxidative stress and performed immunofluorescence analysis using an anti-cleaved caspase 3 antibody (Figure 35A). The percentage of cleaved caspase 3-positive cells significantly increased in the H_2O_2-treated cells transfected with Otud7b-siRNA3 and Otud7b-siRNA4 compared to those transfected with the siRNA-control (Figure 35B). These results suggest that Otud7b

protects neuronal cells from stress-induced damage.

NF-κB is activated by *Otud7b* deficiency

To gain insights into how neuronal cell damage is enhanced by *Otud7b* deficiency in cultured cells and *in vivo*, we performed RNA-seq analysis using retinal RNAs from *Otud7b*$^{+/+}$ and *Otud7b*$^{-/-}$ mice exposed to light. Ingenuity pathway analysis (IPA) revealed that the genes encoding transcription regulators of Cebpa, Rela, Ebf1, Cebpd, Spi1, Ncoa1, Id3, and Srebf1 were upregulated in light-exposed *Otud7b*$^{-/-}$ retina (Z scores > 2) (Figure 36). The IPA networks showed that the transcription factor RelA was an upstream regulator (Figure 37). RelA is one of the five NF-κB proteins known to form dimers with four other proteins that regulate NF-κB activity[60,61]. Activation of NF-κB has been associated with retinal degeneration[62]. We performed immunofluorescence analysis of RelA in light-exposed *Otud7b*$^{+/+}$ and *Otud7b*$^{-/-}$ retinas (Figure 38A). We detected a significant increase in RelA signals in the ONL of light-exposed *Otud7b*$^{-/-}$ retinas, suggesting that NF-κB is activated in photoreceptor cells of the light-exposed *Otud7b*$^{-/-}$ retina compared to that in the light-exposed *Otud7b*$^{+/+}$ retina (Figure 38B). We next analyzed NF-κB activation in the serum-starved Neuro2A cell lysates using a NanoLuc luciferase reporter construct driven by a NF-κB response element and minimal promoter and observed that luciferase activity increased in the *Otud7b* knockdown cells (Figure 39). These results suggest that Otud7b suppresses aberrant NF-κB activation.

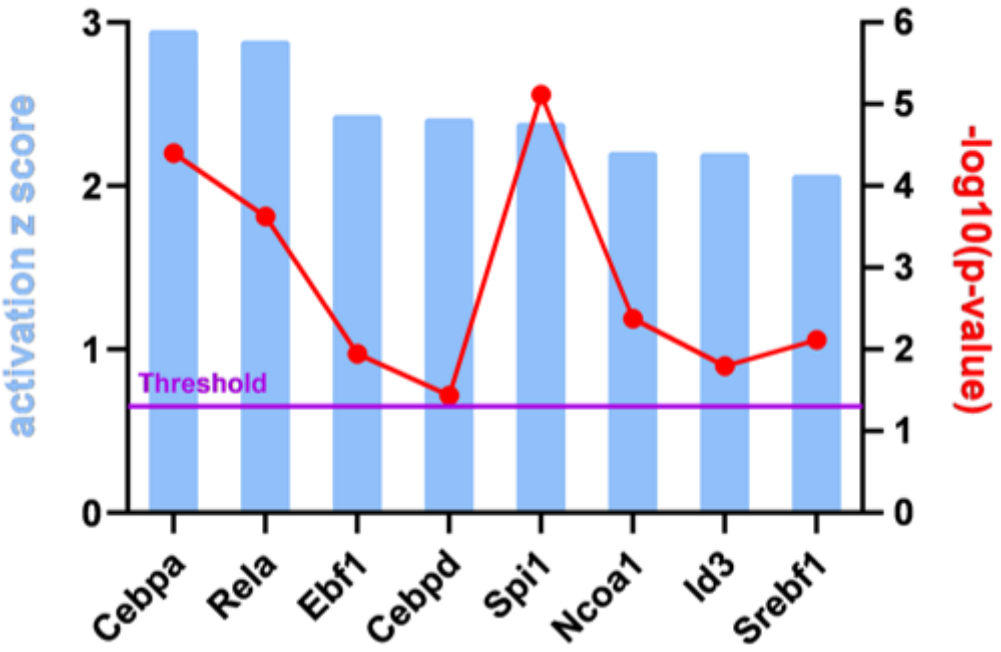

Figure 36. NF-κB is activated by *Otud7b* deficiency.
IPA to predict the upstream transcription regulators affecting gene expression changes (fold change > 1.5 or < –1.5; FPKM > 0.2) in the *Otud7b*$^{-/-}$ retina after light exposure. The transcription regulators with activation Z scores > 2 and $p <$ 0.05 are shown.

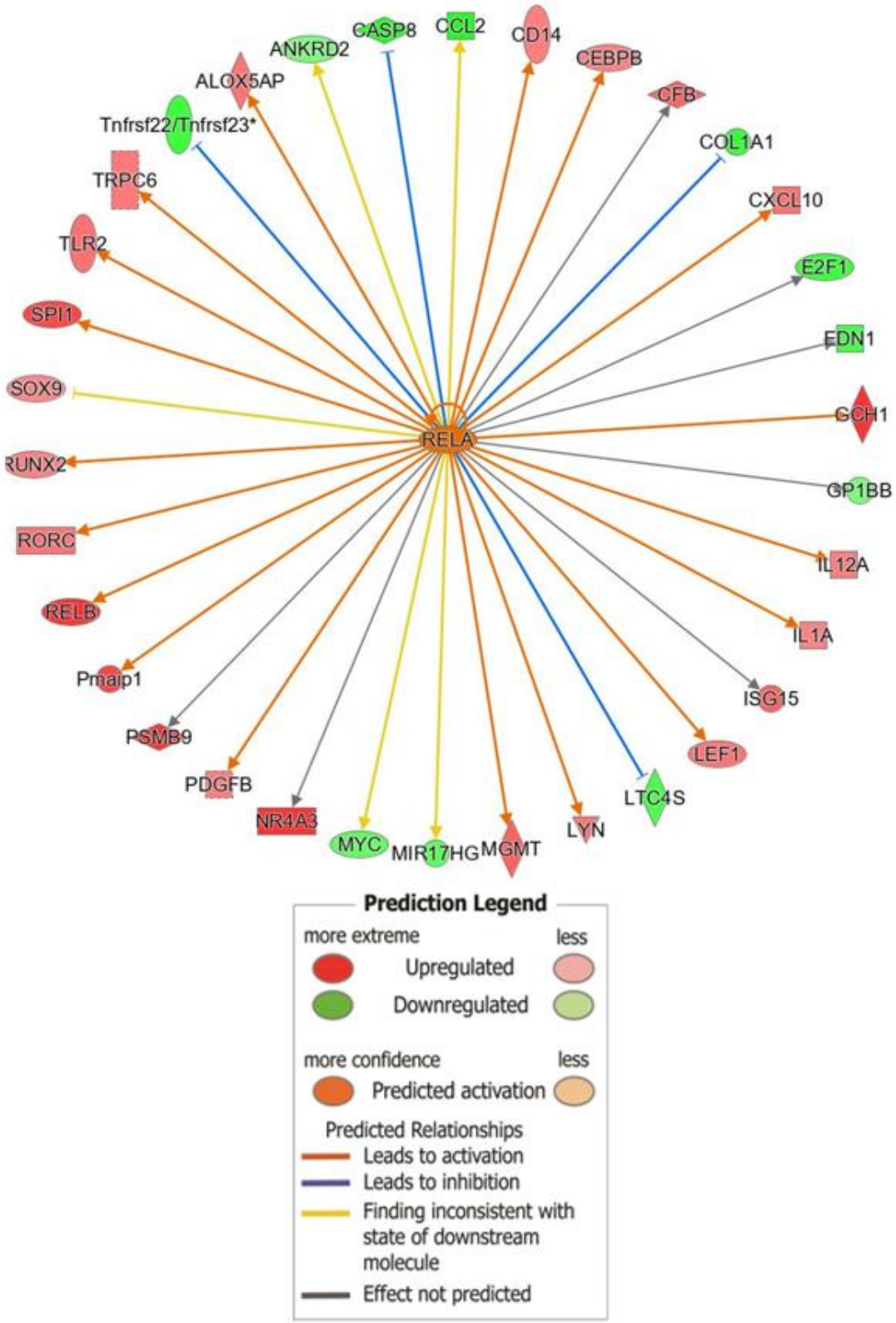
CASP8
CCL2
CD14
ANKRD2
CEBPB
ALOX5AP
CFB
Tnfrsf22/Tnfrsf23*
COL1A1
TRPC6
CXCL10
TLR2
E2F1
SPI1
EDN1
SOX9
GCH1
RELA
RUNX2
GP1BB
RORC
IL12A
RELB
IL1A
Pmaip1
ISG15
PSMB9
LEF1
PDGFB
LTC4S
NR4A3
LYN
MYC
MIR17HG
MGMT
Prediction Legend
more extreme
less
Upregulated
Downregulated
more confidence
less
Predicted activation
Predicted Relationships
Leads to activation
Leads to inhibition
Finding inconsistent with state of downstream molecule
Effect not predicted

Figure 37. NF-κB is activated by *Otud7b*$^{-/-}$ mouse retina after light exposure.
(A) The IPA networks showing the transcription factor RelA as an upstream regulator. RelA is predicted to be activated in *Otud7b*$^{-/-}$ mouse retina after light exposure. IPA, ingenuity pathway analysis.

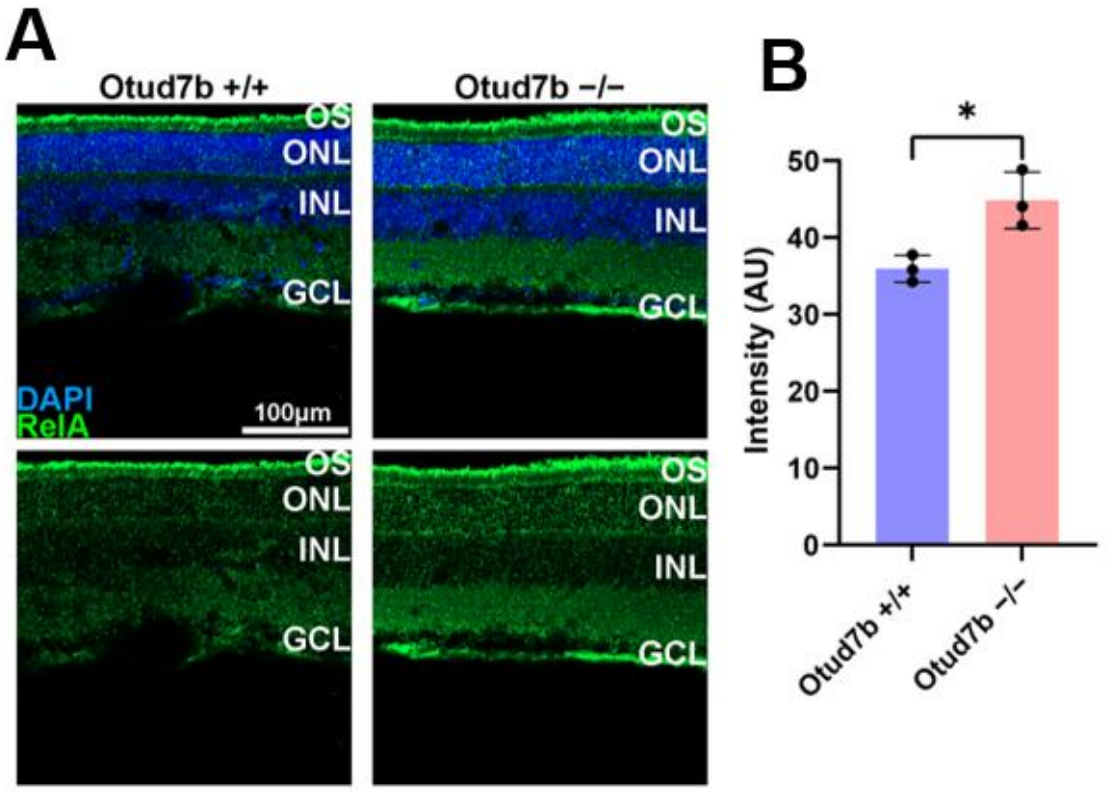

Figure 38. Higher RelA intensity in the ONL of *Otud7b*$^{-/-}$

(A) Immunofluorescence analysis of retinal sections from *Otud7b*$^{+/+}$ and *Otud7b*$^{-/-}$ mice after light exposure using an anti-RelA antibody. Nuclei were stained with DAPI. **(B)** RelA signal intensity in the ONL of *Otud7b*$^{+/+}$ and *Otud7b*$^{-/-}$ retinas after light exposure was measured. RelA signal intensity in the ONL increased in the *Otud7b*$^{-/-}$ retina. Data are presented as the mean ± SD. **p* < 0.05 (unpaired t-test). n = 3 experiments

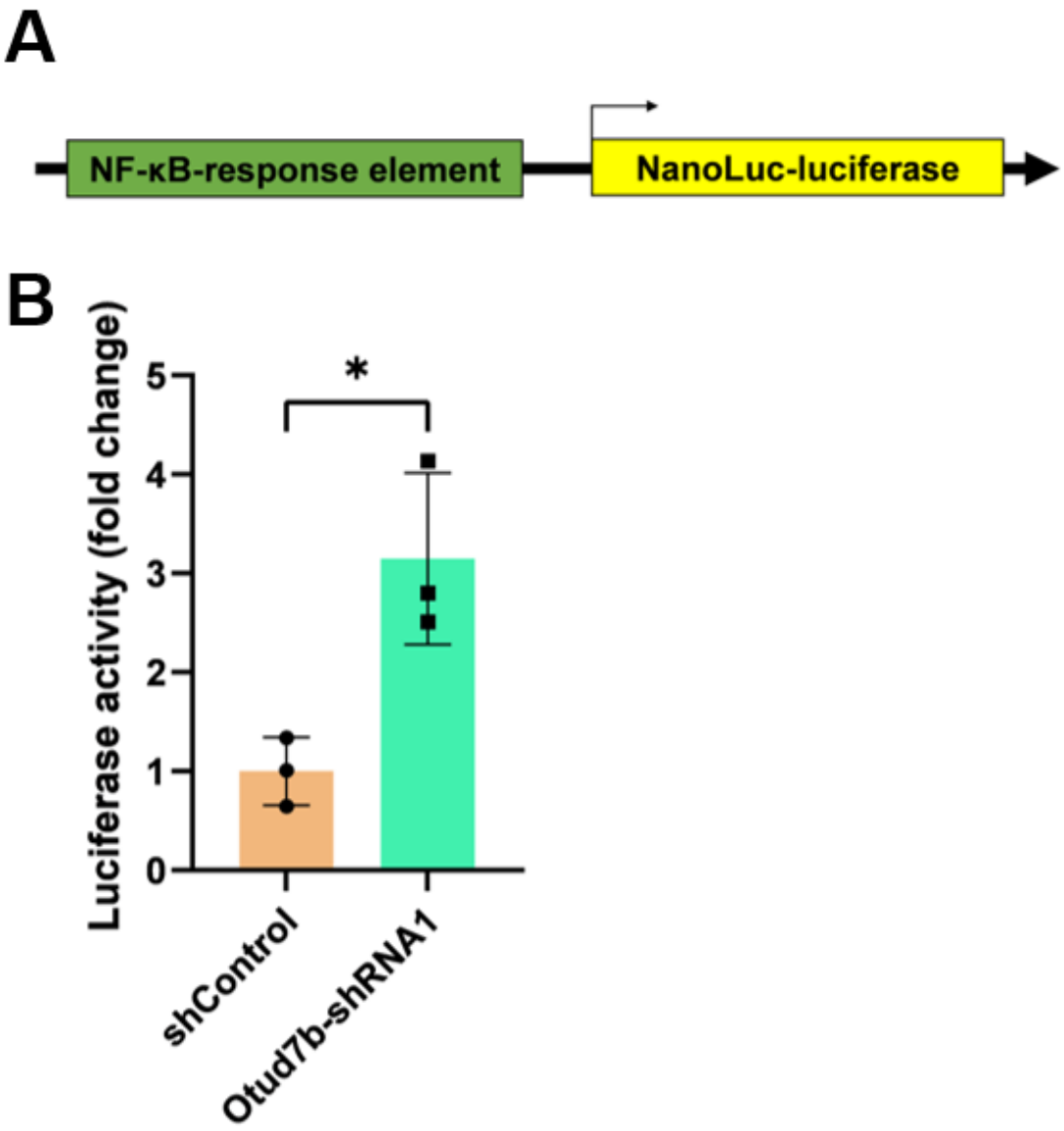

Figure 39. NF-κB is activated by *Otud7b* deficient Neuro2A cells.
(A) Schematic diagram of the NF-κB response element and minimal promoter. **(F)** ShRNA-control or Otud7b-shRNA1 expression plasmids were co-transfected into Neuro2A cells with a *NanoLuc luciferase* reporter construct driven by a NF-κB response element and minimal promoter as well as a *Firefly luciferase*-expressing construct driven by a minimal promoter. Luciferase activity of the cell lysates was measured 14 h after serum starvation. NanoLuc luciferase activity was normalized to Firefly luciferase activity. Data are presented as the mean ± SD. *$p < 0.05$ (unpaired t-test). n = 3 experiments.

Neuronal cell death resulting from *Otud7b* knockdown is suppressed by NF-κB pathway inhibition

Based on the results of the IPA analysis and NanoLuc-luciferase (Figure 37 and 39), we hypothesized NF-κB as a factor for Neuro2A cell death and photoreceptor degeneration caused by *Otud7b* deficiency. To test this hypothesis, we examined the effects of curcumin, an inhibitor of the NF-κB pathway, on neuronal cell death induced by *Otud7b* knockdown under stress conditions. Neuro2A cells expressing Otud7b-siRNAs were treated with curcumin, and immunofluorescence analysis was performed to observe apoptotic cells (Figure 40). We observed no significant difference in the number of cleaved caspase 3-positive cells between cells expressing siRNA-control treated with DMSO and those treated with curcumin; however, the increase in cleaved caspase 3-positive cells induced by Otud7b-siRNAs was suppressed by curcumin treatment (Figure 40). In addition, immunofluorescence analysis of RelA revealed that curcumin repressed the increased nuclear localization of RelA in the cells transfected with Otud7b-siRNAs (Figure 41A). In addition, immunofluorescence analysis of RelA revealed that curcumin repressed the increased nuclear-to-cytoplasmic ratio of RelA in the cells transfected with Otud7b-siRNAs (Figures 41B). To confirm these results, we performed similar experiments using another NF-κB inhibitor, BMS-345541 (Figures 42A). *Otud7b* knockdown cells treated with BMS-345541 also showed significantly decreased numbers of cleaved caspase 3-positive cells compared to those treated with DMSO (Figure 42B). Similar to the results for curcumin, BMS-345541 also repressed the increased nuclear localization of RelA in the cells transfected with Otud7b-siRNAs (Figure 43). These results suggest that Otud7b protects neuronal cells from cell damage by downregulating NF-κB activation under stress conditions.

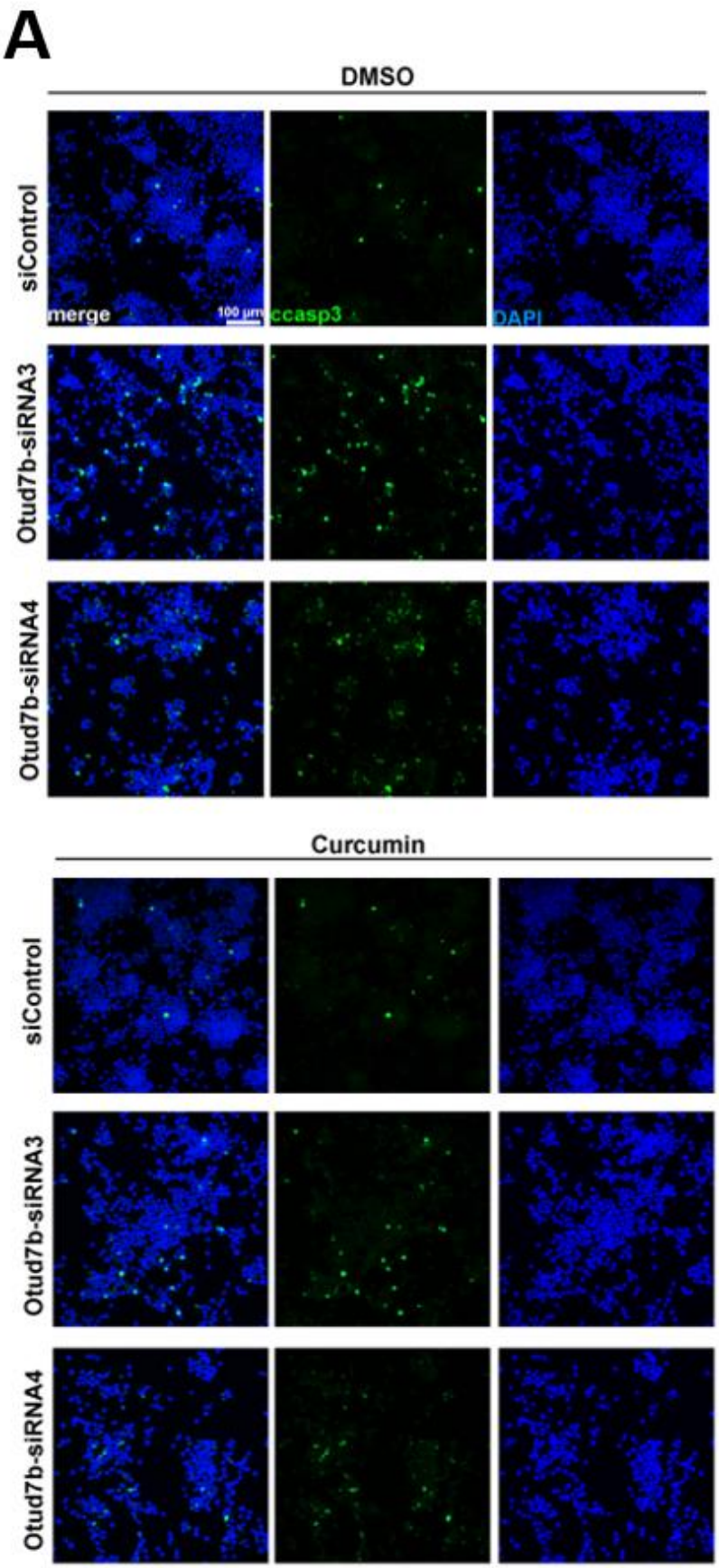
A
DMSO
siControl
merge
100 μm
ccasp3
DAPI
Otud7b-siRNA3
Otud7b-siRNA4
Curcumin
siControl
Otud7b-siRNA3
Otud7b-siRNA4

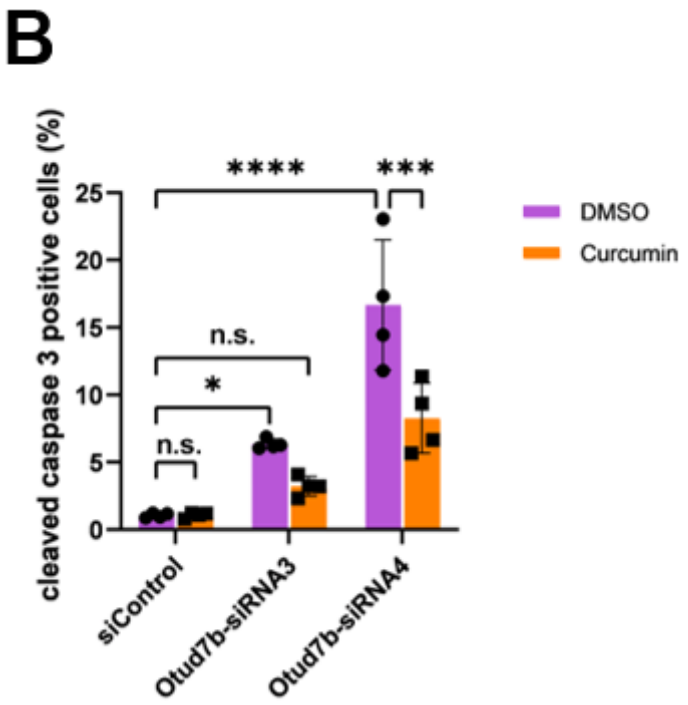

Figure 40. NF-κB pathway inhibition using curcumin reduces cell death induced by *Otud7b* knockdown.

(A) Neuro2A cells treated with curcumin were transfected with siRNA-control, Otud7b- siRNA3, or Otud7b-siRNA4. The cells were serum starved for 24 h in a medium containing curcumin. Cells were immunostained with an anti-cleaved caspase 3 antibody. Nuclei were stained with DAPI. **(B)** The number of cleaved caspase 3-positive cells was counted. Curcumin treatment suppressed the increase of cleaved caspase 3-positive cells caused by *Otud7b* knockdown. Data are presented as the mean ± SD. *$p < 0.05$, ***$p < 0.001$ ****$p < 0.0001$, n.s. not significant (two-way ANOVA followed by Tukey's multiple comparisons test). n = 4 experiments.

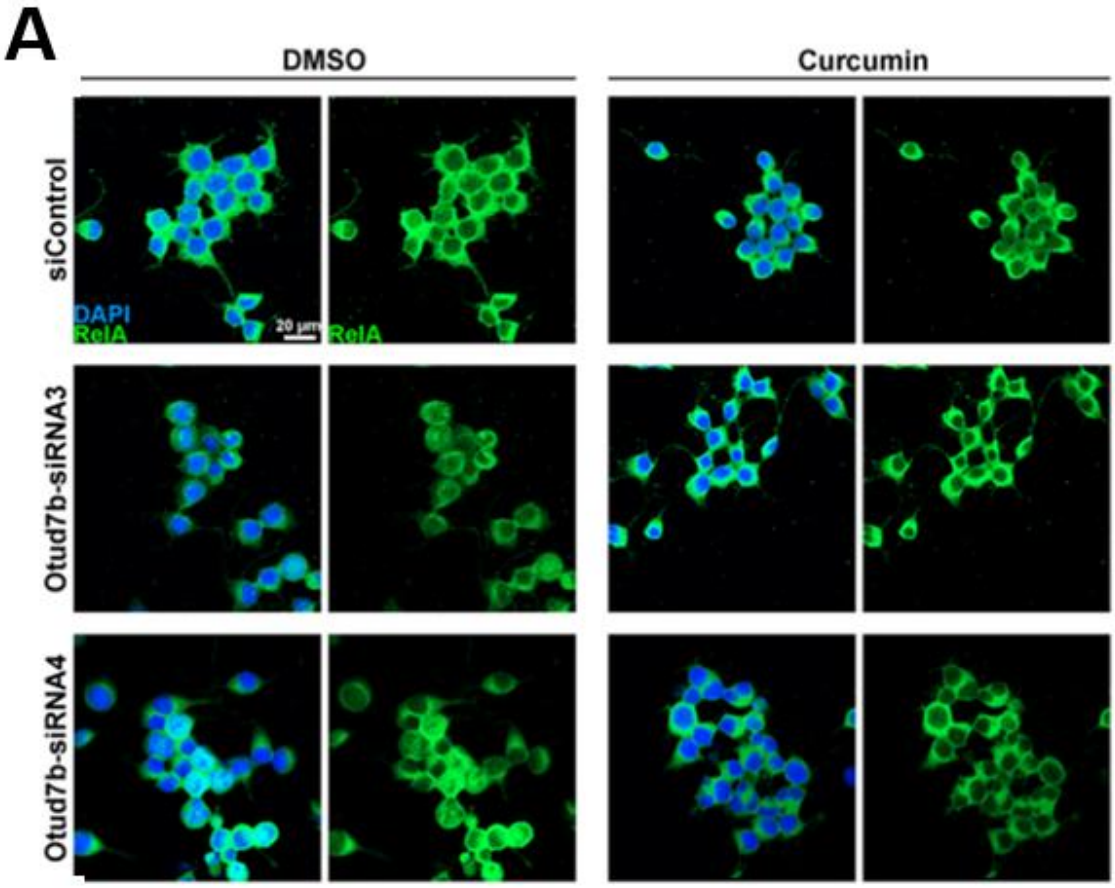
A
DMSO
Curcumin
siControl
Otud7b-siRNA3
Otud7b-siRNA4
DAPI
RelA
20 μm
RelA

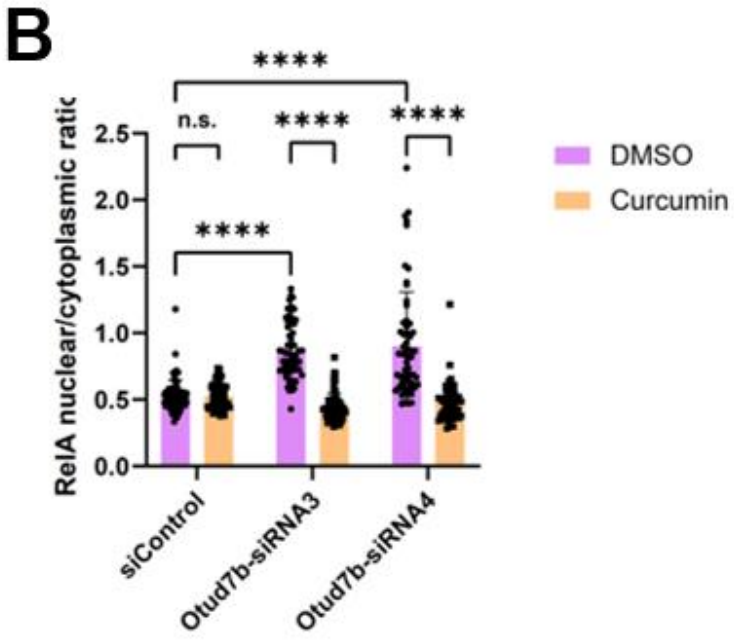
B
****
n.s.
****
****
****
RelA nuclear/cytoplasmic ratio
2.5
2.0
1.5
1.0
0.5
0.0
siControl
Otud7b-siRNA3
Otud7b-siRNA4
DMSO
Curcumin

Figure 41. RelA nuclear localization inhibited by curcumin treatment.
(A) Immunofluorescence analysis of serum starved Neuro2A cells using an anti-RelA antibody. Curcumin suppressed the nuclear localization of RelA. Nuclei were stained with DAPI. **(B)** RelA nuclear-to-cytoplasmic ratio was measured in curcumin-treated Neuro2A cells transfected with siRNA-control, Otud7b-siRNA3, or Otud7b-siRNA4. Data are presented as the mean ± SD. **** $p < 0.0001$, n.s. not significant (two-way ANOVA followed by Tukey's multiple comparisons test). n = 50-70 cells per treatment.

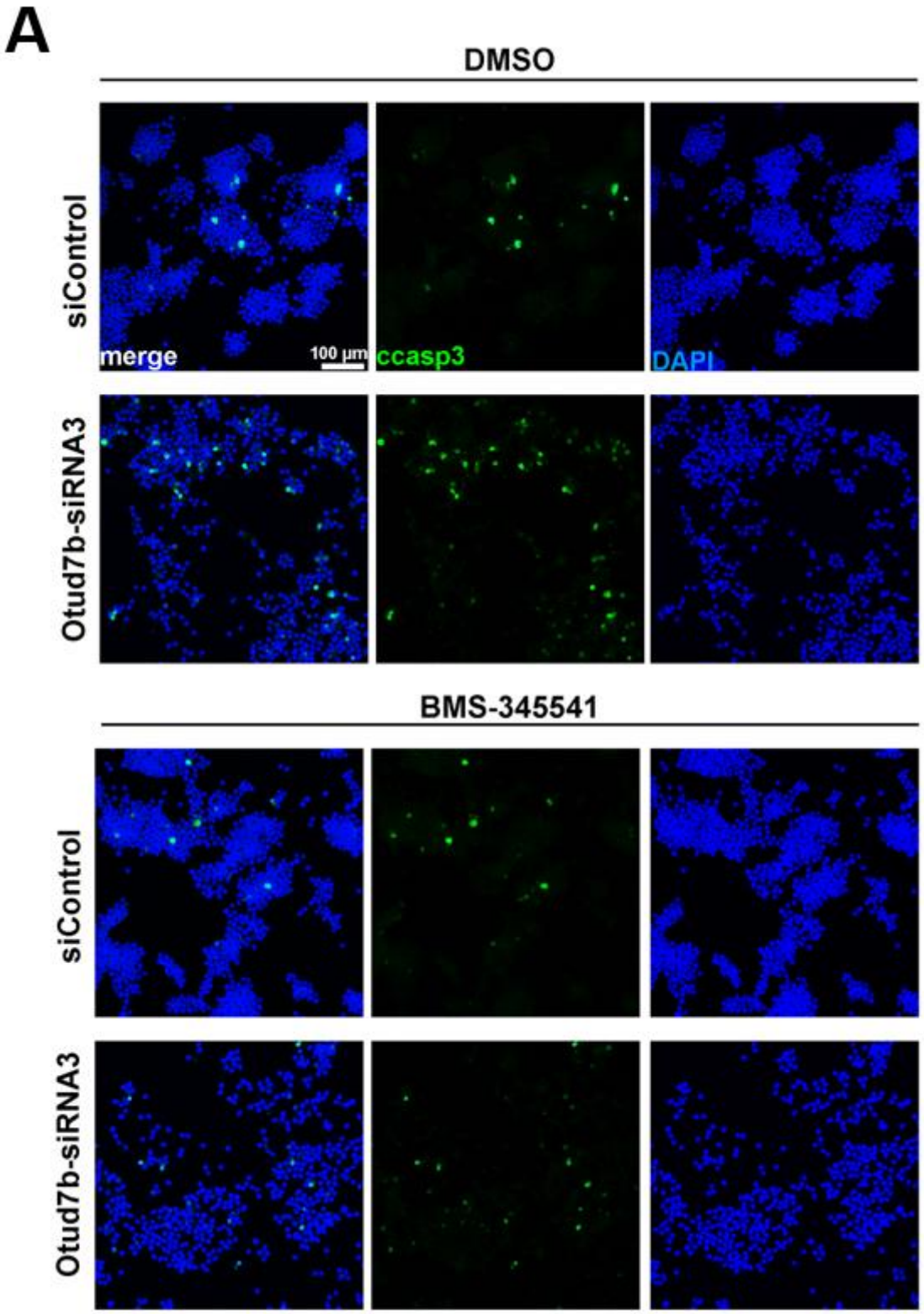
A
DMSO
siControl
merge
100 μm
ccasp3
DAPI
Otud7b-siRNA3
BMS-345541
siControl
Otud7b-siRNA3

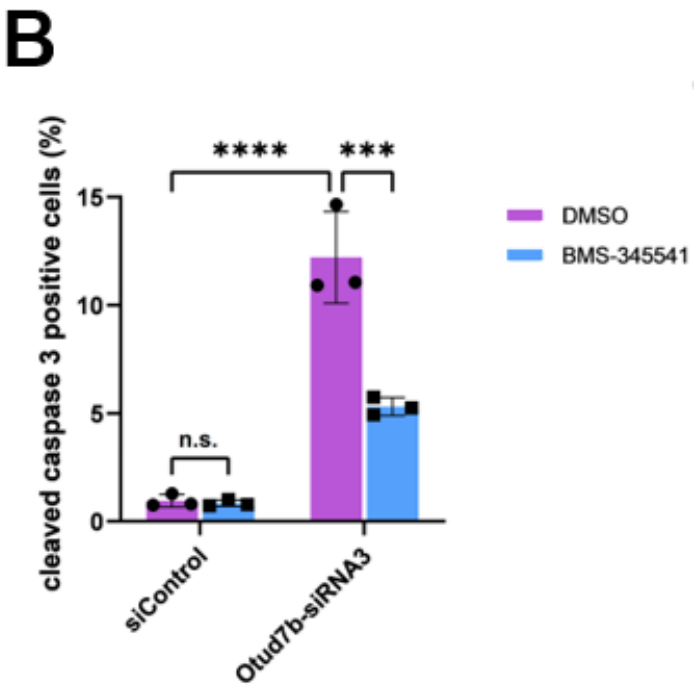

Figure 42. NF-κB pathway inhibition using BMS-345541 reduces cell death induced by *Otud7b* knockdown.

(A) Neuro2A cells treated with BMS-345541 were transfected with siRNA-control or Otud7b- siRNA3. The cells were serum starved for 24 h in the medium containing BMS-345541. Cells were immunostained with an anti-cleaved caspase 3 antibody. Nuclei were stained with DAPI. **(B)** The number of cleaved caspase 3-positive cells was counted. BMS-345541 treatment suppressed the increase of cleaved caspase 3-positive cells caused by *Otud7b* knockdown. Data are presented as the mean ± SD. ***$p < 0.001$ ****$p < 0.0001$, n.s. not significant (two-way ANOVA followed by Tukey's multiple comparisons test). n = 3 experiments. **(C)** Immunofluorescence analysis of serum starved Neuro2A cells using an anti-RelA antibody. BMS-345541 suppressed the nuclear localization of RelA. Nuclei were stained with DAPI.

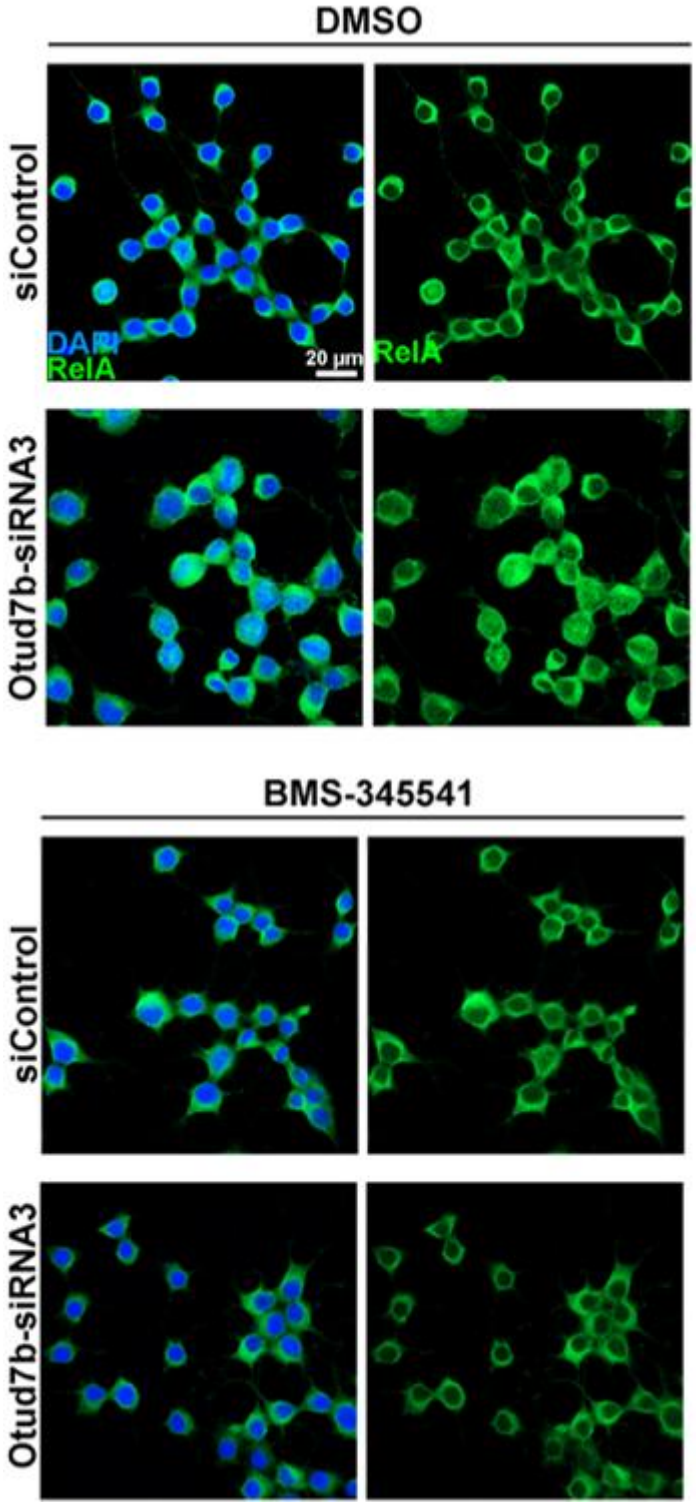

Figure 43. RelA nuclear localization inhibited by BMS-345541 treatment. Immunofluorescence analysis of serum starved Neuro2A cells using an anti-RelA antibody. BMS-345541 suppressed the nuclear localization of RelA. Nuclei were stained with DAPI.

Light-induced retinal damage augmented by *Otud7b* deficiency is repressed by NF-κB pathway inhibition

We stained both retinal flat mounts and sections using PNA, assessed the number of cones, and found that there were no significant differences between the light-exposed *Otud7b*$^{+/+}$ and *Otud7b*$^{-/-}$ retinas treated with DMSO (Figures 44A–D). We then examined the cone outer segment length from the retinal sections and found that the cone outer segment lengths of *Otud7b*$^{-/-}$ retinas were significantly shorter than those of *Otud7b*$^{+/+}$ retinas (Figures 44C and 44E). To examine whether the inhibition of NF-κB would rescue the phenotypes observed in *Otud7b*$^{-/-}$ mouse retinas under stress conditions, we exposed *Otud7b*$^{-/-}$ mice injected with curcumin to LED light (Figure 45A). We analyzed the histological changes by immunofluorescence using antibodies against Rhodopsin, S-opsin-, and M-opsin (Figures 45B–45D). No significant differences were observed in the outer segments of the rod and S-cones between *Otud7b*$^{+/+}$ and *Otud7b*$^{-/-}$ mice treated with or without curcumin (Figures 45B, 45C, 46A, and 46B). The numbers of S-cones and M-cones also did not show a significant difference (Figures 46C and 46D). However, the decrease in the M-cone outer segment length in the *Otud7b*$^{-/-}$ retina was suppressed by curcumin (Figures 45B and 46E). We observed a significant increase in cells that express cleaved caspase 3 in the ONL of the retina from *Otud7b*$^{-/-}$ mice treated with DMSO compared to those from *Otud7b*$^{+/+}$ mice treated with DMSO, whereas curcumin treatment reduced the number of cleaved caspase 3 in the ONL of *Otud7b*$^{-/-}$ retinas (Figure 47). These results suggest that Otud7b suppresses light-induced retinal damage by downregulating NF-κB activation. In addition, we performed immunofluorescence analysis using an anti-RelA antibody and measured the RelA signal intensity in the ONL of light-exposed DMSO-treated and curcumin-treated *Otud7b*$^{-/-}$ retinas (Figure 48A).

The RelA signal intensity in the ONL decreased significantly in the curcumin-treated *Otud7b*$^{-/-}$ mice compared to that in the DMSO-treated *Otud7b*$^{-/-}$ mice, suggesting that the increased NF-κB activity in photoreceptor cells of the *Otud7b*$^{-/-}$ retina is suppressed by curcumin (Figure 48B). To confirm these results, we exposed *Otud7b*$^{+/+}$ and *Otud7b*$^{-/-}$ mice injected with BMS-345541 to LED light (Figure 49A). Immunofluorescence analysis using antibodies against Rhodopsin, S-opsin, and M-opsin were used to observe the histological changes (Figures 49B–49D). Similar to the curcumin-treated mice, rod and S-cone outer segment lengths did not show a significant difference (Figures 50A and 50B). There was no significant difference in the number of S-cones or M-cones between *Otud7b*$^{+/+}$ and *Otud7b*$^{-/-}$ mice treated with either DMSO or BMS-345541 (Figures 50C and 50D). In contrast, the decrease in the M-cone outer segment lengths of the *Otud7b*$^{-/-}$ retina was suppressed by BMS-345541 (Figure 50E). In addition, the increased number of cleaved caspase 3-positive cells in the ONL of the light-exposed *Otud7b*$^{-/-}$ retina was reduced by BMS-345541 treatment (Figure 51). Furthermore, we performed immunofluorescence analysis of RelA and measured RelA signal intensity in the ONL of the retina from light-exposed *Otud7b*$^{-/-}$ mice treated with either DMSO or BMS-345541 (Figure 52A). The RelA signal intensity in the ONL decreased significantly in BMS-345541-treated *Otud7b*$^{-/-}$ mice compared to that in DMSO-treated *Otud7b*$^{-/-}$ mice (Figure 52B). These results further support the idea that Otud7b suppresses light-induced retinal damage by downregulating NF-κB activation.

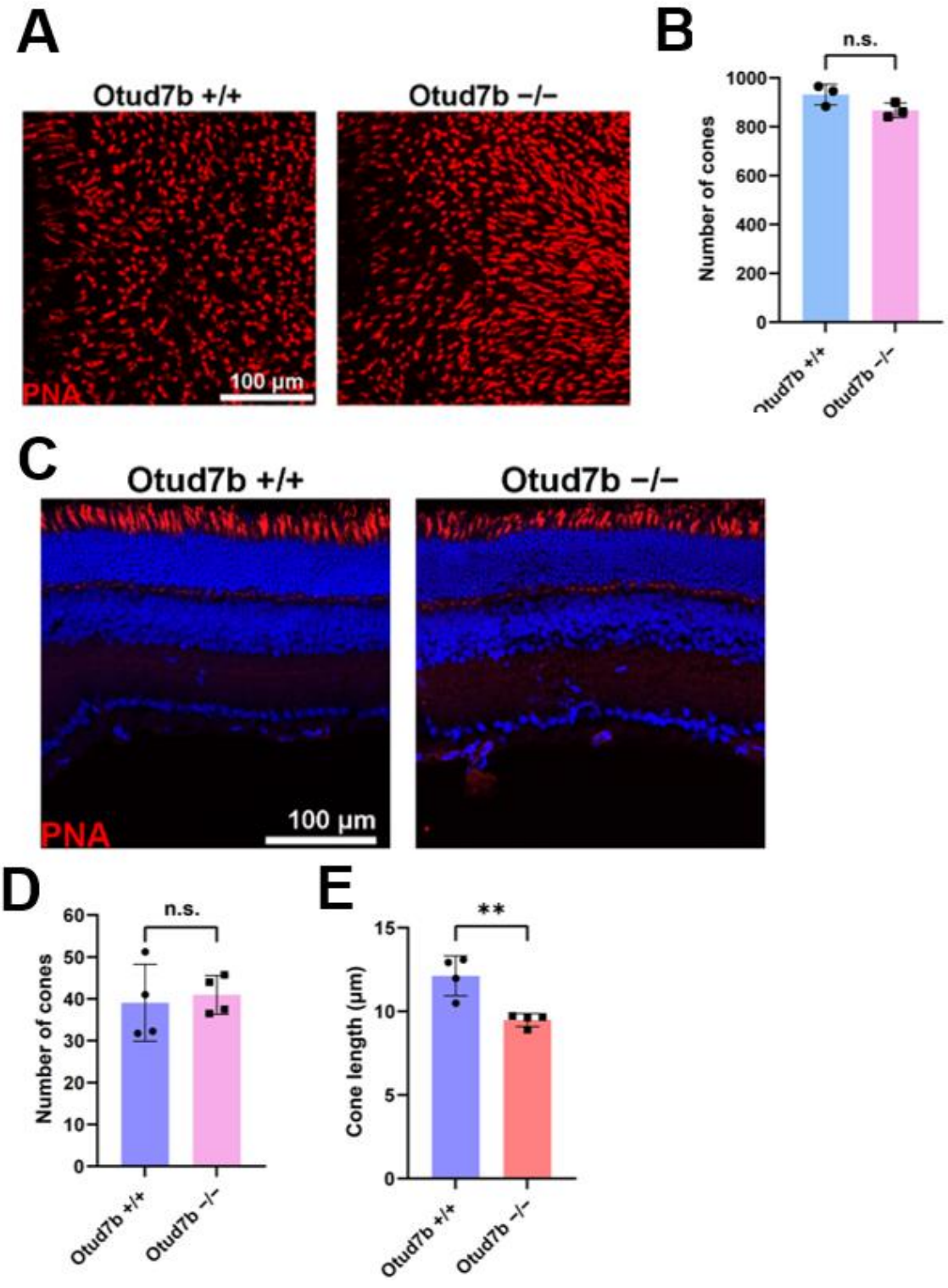
A
Otud7b +/+
Otud7b −/−
PNA
100 µm
B
n.s.
Number of cones
1000
800
600
400
200
0
Otud7b +/+
Otud7b −/−
C
Otud7b +/+
Otud7b −/−
PNA
100 µm
D
n.s.
Number of cones
60
50
40
30
20
10
0
Otud7b +/+
Otud7b −/−
E
**
Cone length (µm)
15
10
5
0
Otud7b +/+
Otud7b −/−

Figure 44. Flat-mount of *Otud7b*$^{+/+}$ and *Otud7b*$^{-/-}$ retinas after light-exposure.
(A) Retinal flat-mount fluorescent staining with PNA of *Otud7b*$^{+/+}$ and *Otud7b*$^{-/-}$ retinas after light-exposure. No significant difference observed in the *Otud7b*$^{-/-}$ retina. **(B)** The number of cones was counted. Data are presented as the mean ± SD. n.s., not significant (unpaired t-test). n = 3 per genotype. **(C)** Immunofluorescence analysis of retinal sections from DMSO-treated *Otud7b*$^{+/+}$ and *Otud7b*$^{-/-}$ mice after light exposure using PNA. Nuclei were stained with DAPI. **(D, E)** The number of cones **(D)** and the length of PNA **(E)** was measured. Cone outer segments were shorter in the DMSO-treated *Otud7b*$^{-/-}$ retina than in the *Otud7b*$^{+/+}$ retina. Data are presented as the mean ± SD. $^{**}p < 0.01$, n.s., not significant (unpaired t-test), n = 4 per genotype.

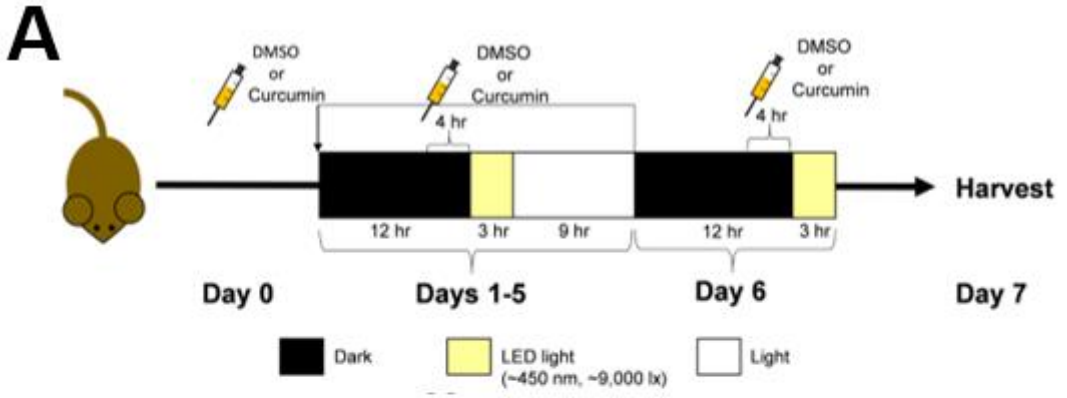
A
DMSO or Curcumin
DMSO or Curcumin
4 hr
DMSO or Curcumin
4 hr
Harvest
12 hr
3 hr
9 hr
12 hr
3 hr
Day 0
Days 1-5
Day 6
Day 7
Dark
LED light (~450 nm, ~9,000 lx)
Light

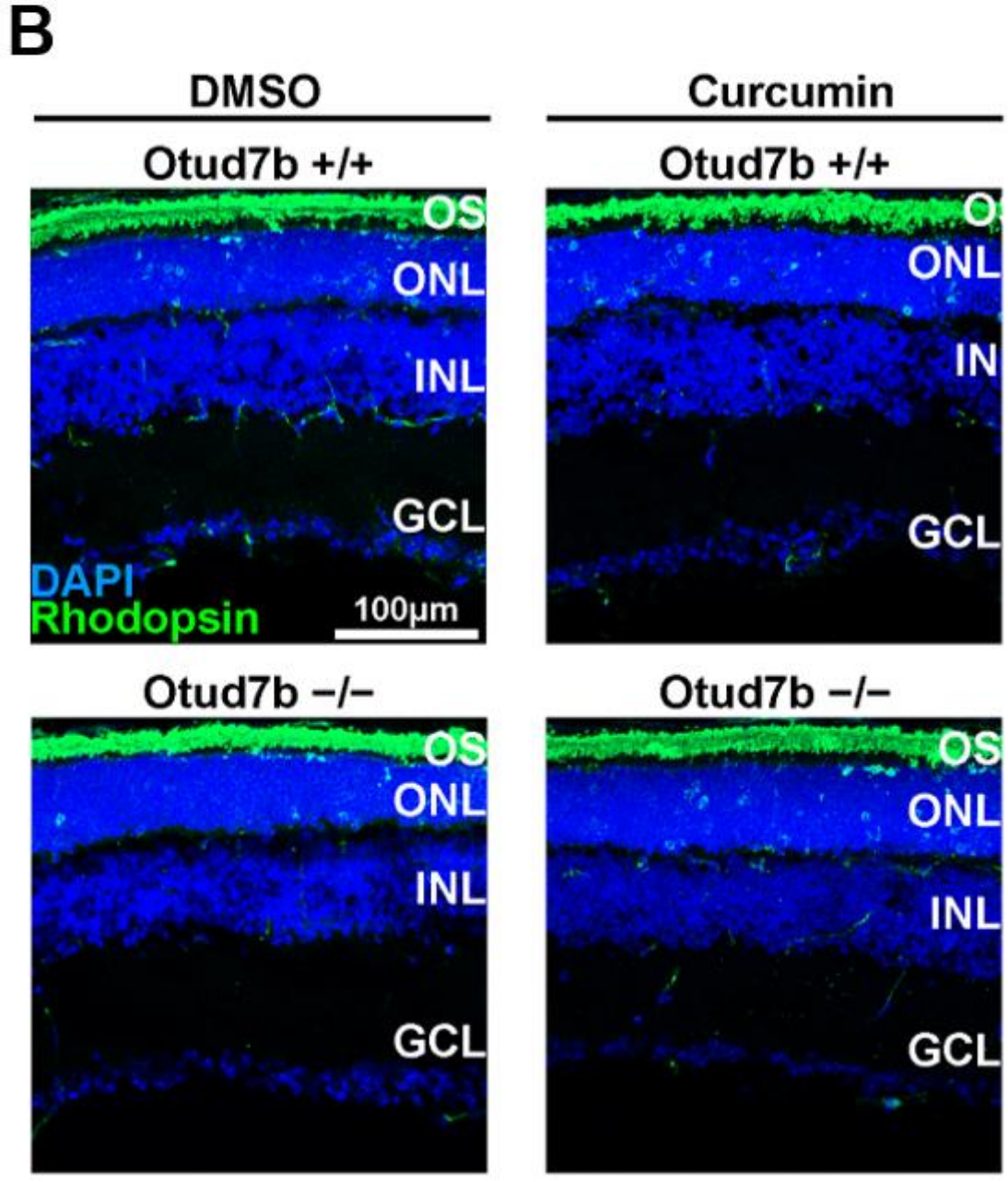
B
DMSO
Curcumin
Otud7b +/+
Otud7b +/+
OS
ONL
INL
GCL
DAPI
Rhodopsin
100µm
ONL
IN
GCL
Otud7b −/−
Otud7b −/−
OS
ONL
INL
GCL
OS
ONL
INL
GCL

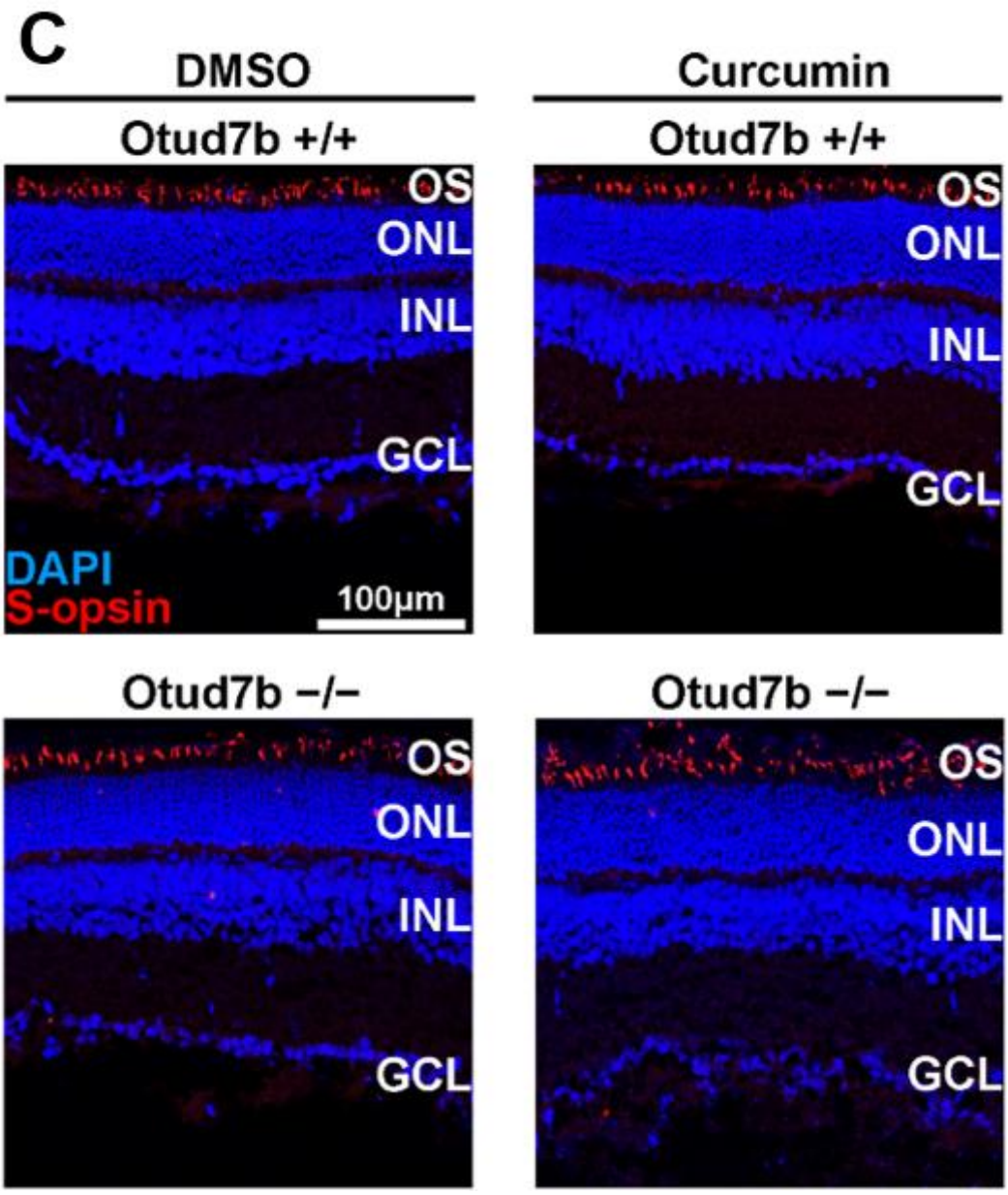
C
DMSO
Curcumin
Otud7b +/+
Otud7b +/+
OS
ONL
INL
GCL
DAPI
S-opsin
100μm
Otud7b −/−
Otud7b −/−
OS
ONL
INL
GCL

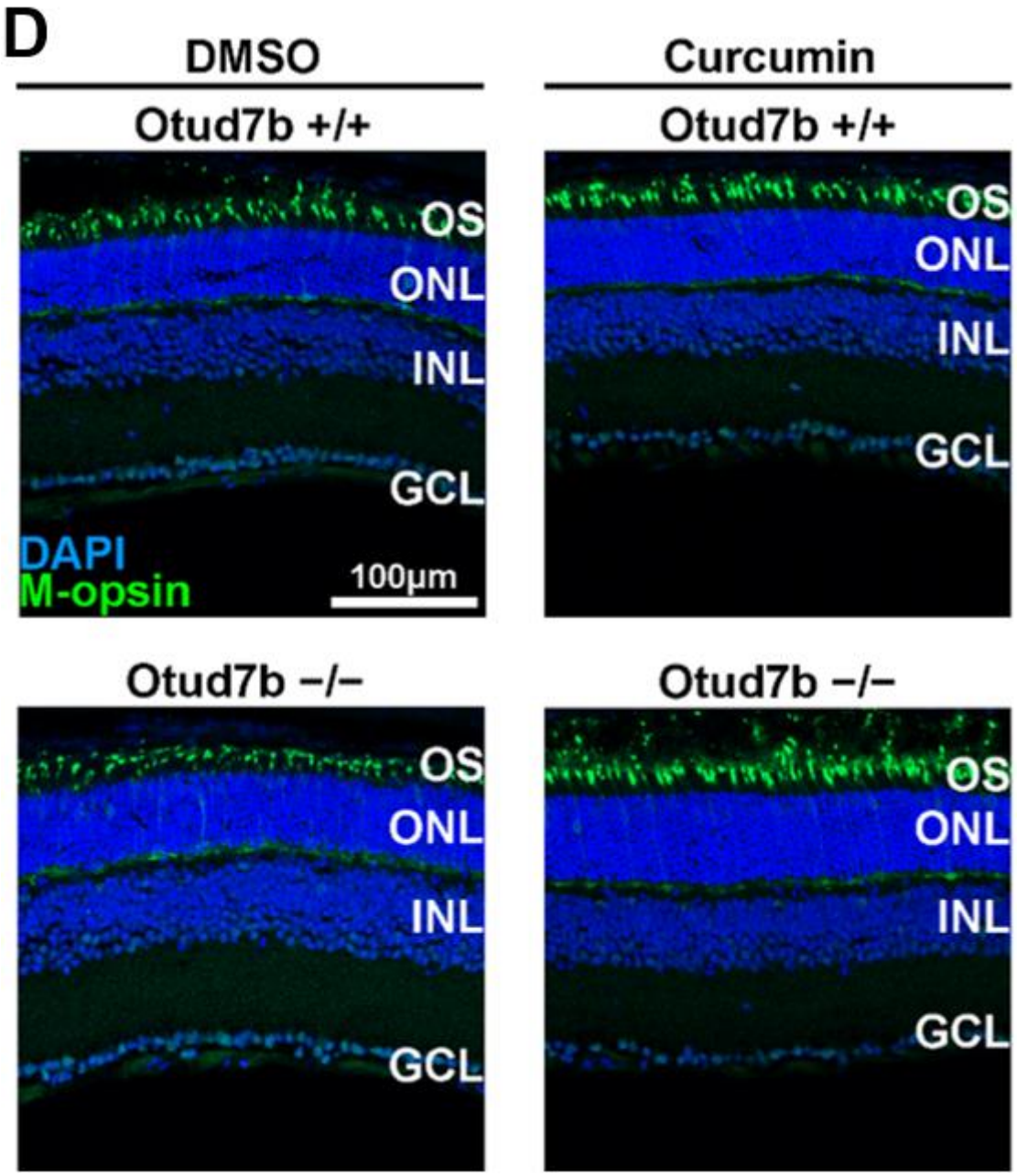

Figure 45 NF-κB pathway inhibition suppresses light-induced retinal damage in *Otud7b*$^{-/-}$ mice.

(A) Schematic representation of LED light exposure to mice treated with curcumin. Curcumin was injected into mice every treated *Otud7b*$^{+/+}$ and *Otud7b*$^{-/-}$ mice after light exposure using the following antibodies: Rhodopsin (a marker for rod outer segments, **B**), S-opsin (a marker for S-cone outer segments, **C**), and M-opsin (a marker for M-cone outer segments, **D**). Nuclei were stained with DAPI.

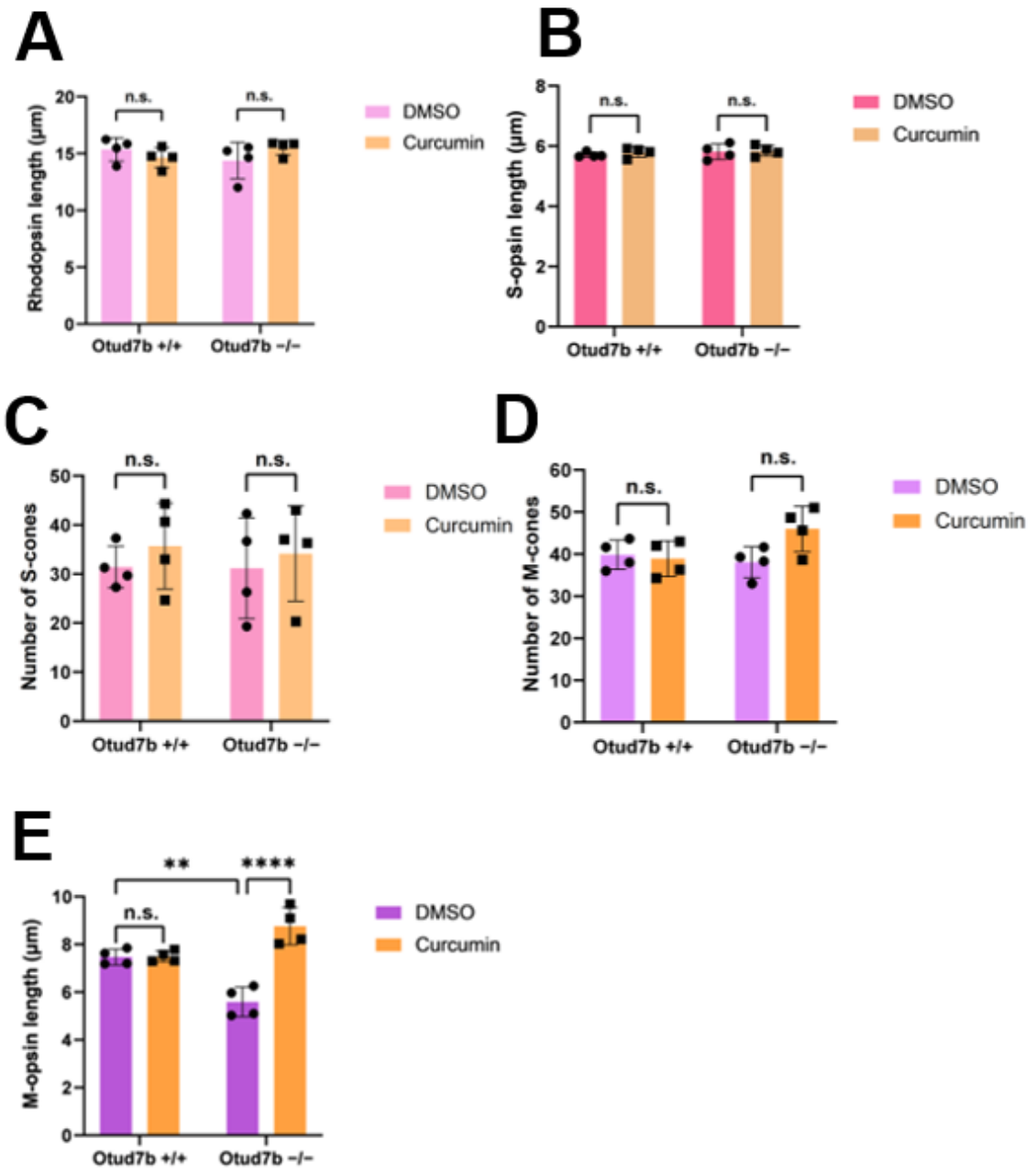

Figure 46. NF-κB pathway inhibition rescues phenotype observed in M-cones. **(A)** Rod outer segment lengths measured. **(B)** S-cone outer segment lengths measured. **(C–D)** The number of S-cones **(C)** and M-cones **(D)** of DMSO or curcumin-treated mice after light exposure was counted. n.s. not significant (two-way ANOVA followed by Tukey's multiple comparisons test) n = 4 per genotype. **(E)** M-cone outer segment lengths measured. $^{**}p < 0.01$, $^{****}p < 0.0001$, n.s. not significant (two-way ANOVA followed by Tukey's multiple comparisons test), n = 4 per genotype.

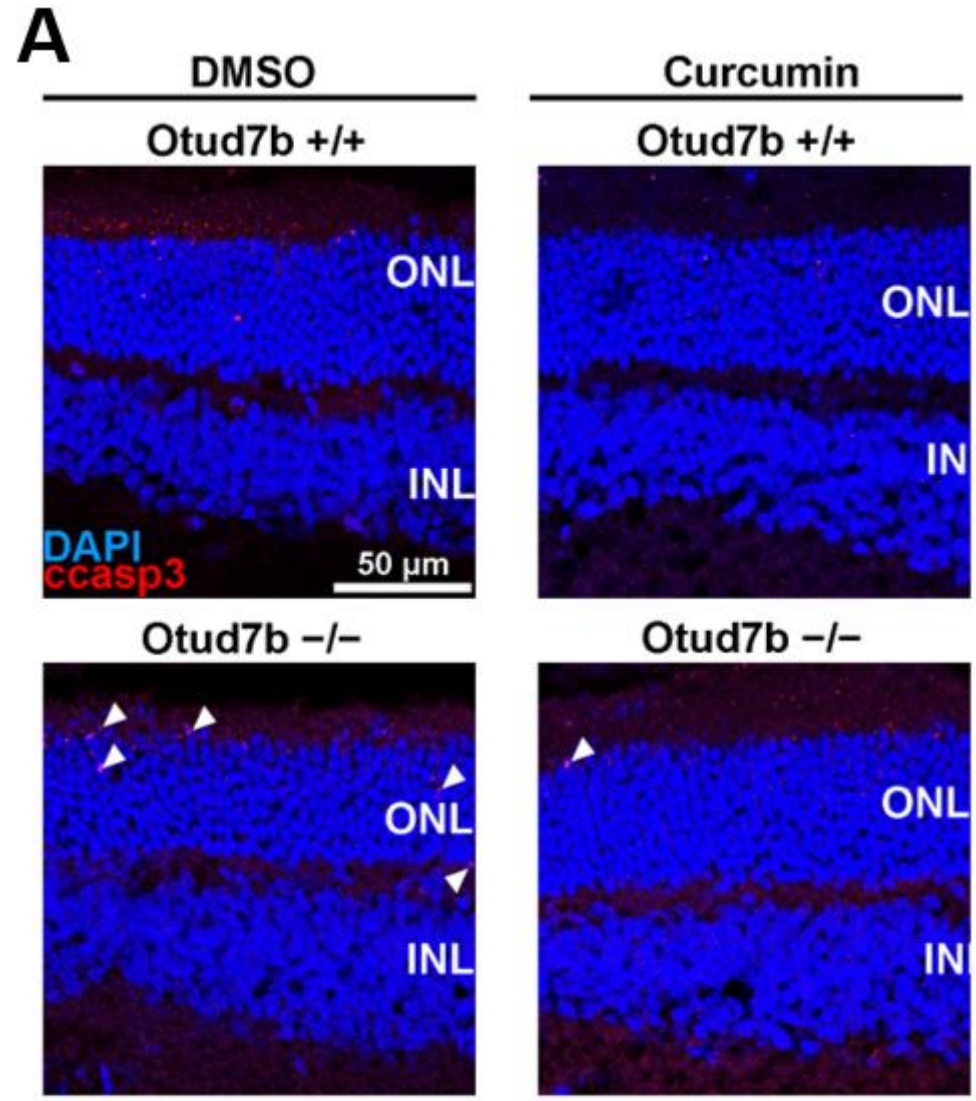
A
DMSO
Curcumin
Otud7b +/+
Otud7b +/+
ONL
INL
DAPI
ccasp3
50 µm
ONL
IN
Otud7b −/−
Otud7b −/−
ONL
INL
ONL
IN

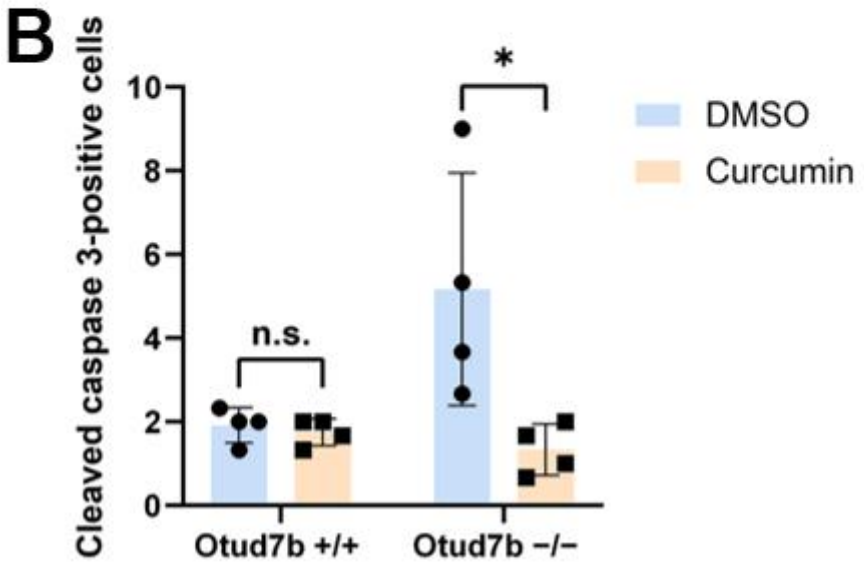
B
Cleaved caspase 3-positive cells
10
8
6
4
2
0
n.s.
*
DMSO
Curcumin
Otud7b +/+
Otud7b −/−

Figure 47. Increase in cleaved caspase3 cells of *Otud7b*$^{-/-}$ mice after light exposure.

(A) Immunofluorescence analysis of retinal sections from curcumin-treated *Otud7b*$^{+/+}$ and *Otud7b*$^{-/-}$ mice after light exposure using an anti-cleaved caspase 3 antibody. Nuclei were stained with DAPI. White arrows indicate cleaved caspase 3-positive cells. **(B)** The number of cleaved caspase 3-positive cells was counted. Curcumin treatment significantly reduced the number of cleaved caspase 3-positive cells in the *Otud7b*$^{-/-}$ retina. *$p < 0.05$, n.s. not significant (two-way ANOVA followed by Tukey's multiple comparisons test), n = 4 per genotype.

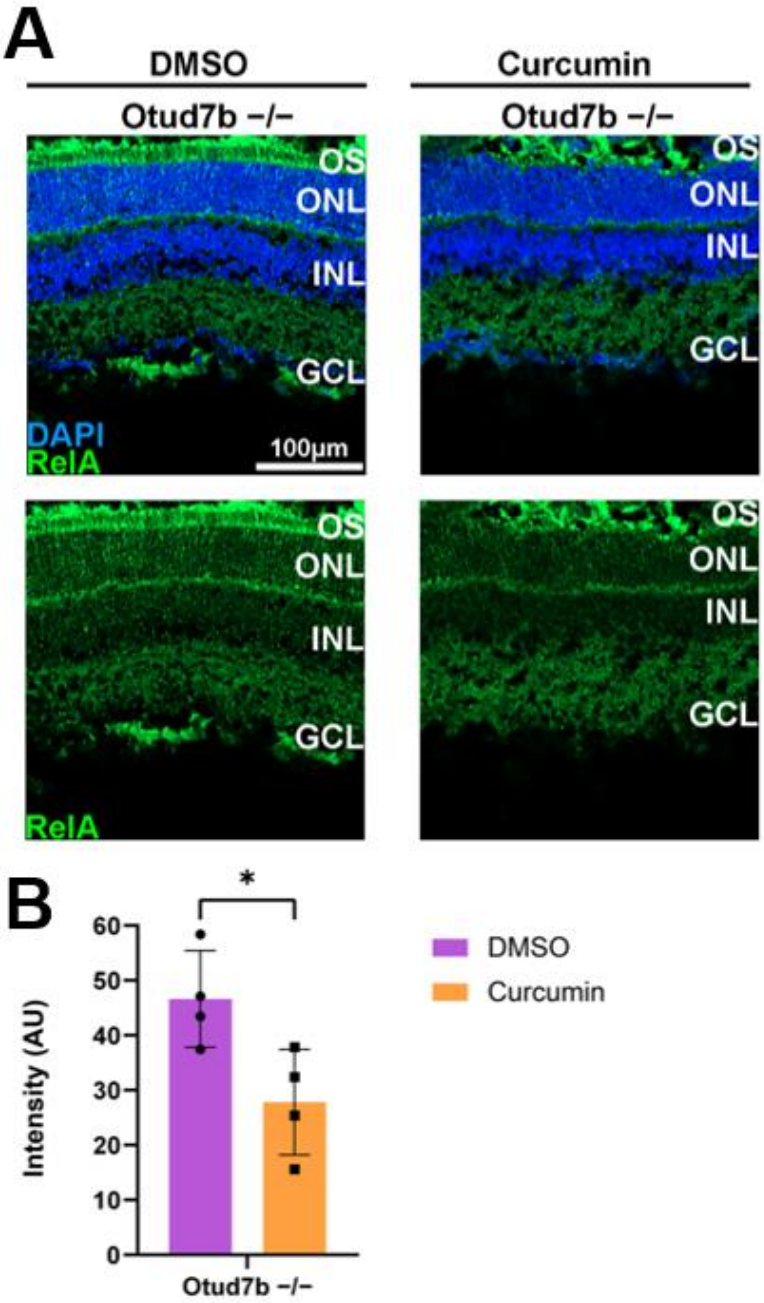

Figure 48. NF-κB pathway inhibition confirmation.
(A) Immunofluorescence analysis of retinal sections from DMSO or curcumin-treated *Otud7b*$^{-/-}$ mice after light exposure using an anti-RelA antibody. Nuclei were stained with DAPI. **(R)** RelA intensity in the ONL of DMSO or curcumin-treated *Otud7b*$^{-/-}$ mice after light exposure was measured. RelA signal intensity in the ONL decreased in the curcumin-treated *Otud7b*$^{-/-}$ retina. Data are presented as the mean ± SD. *$p < 0.05$ (unpaired t-test). n = 4 experiments.

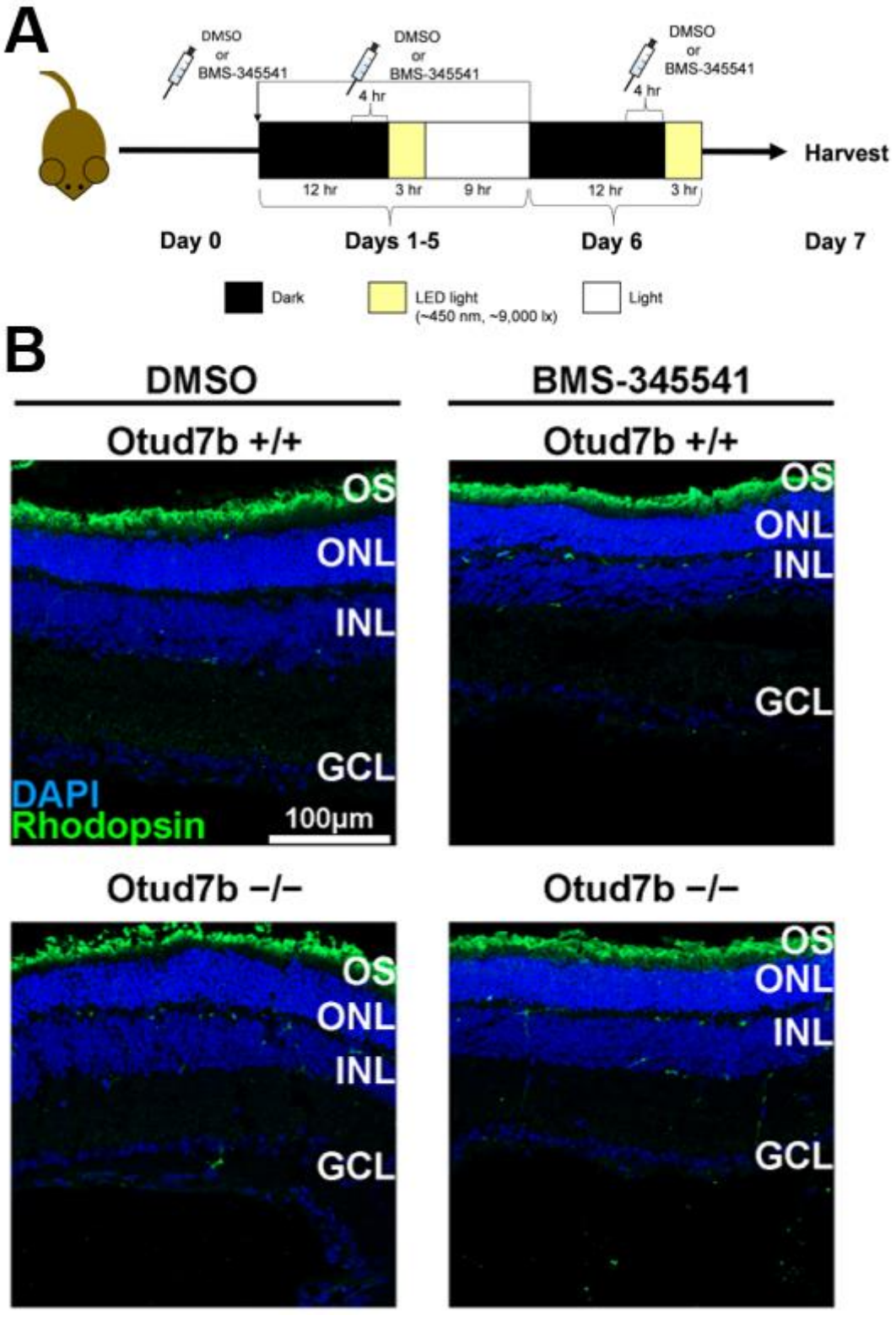
A
DMSO
or
BMS-345541
DMSO
or
BMS-345541
DMSO
or
BMS-345541
4 hr
4 hr
Harvest
12 hr
3 hr
9 hr
12 hr
3 hr
Day 0
Days 1-5
Day 6
Day 7
Dark
LED light
(~450 nm, ~9,000 lx)
Light
B
DMSO
BMS-345541
Otud7b +/+
Otud7b +/+
OS
ONL
INL
GCL
DAPI
Rhodopsin
100μm
Otud7b −/−
Otud7b −/−

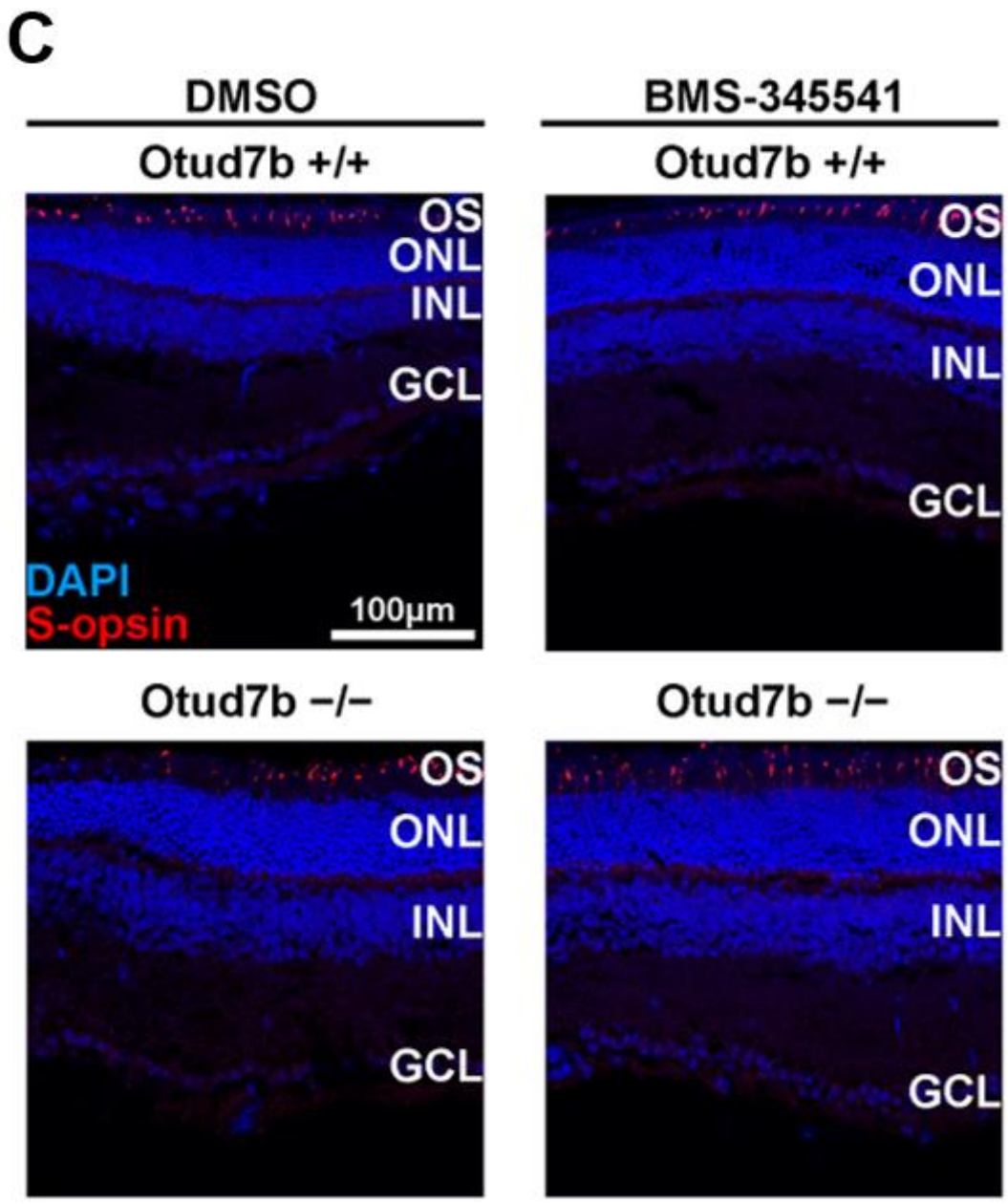
C
DMSO
BMS-345541
Otud7b +/+
Otud7b +/+
OS
ONL
INL
GCL
DAPI
S-opsin
100μm
Otud7b −/−
Otud7b −/−

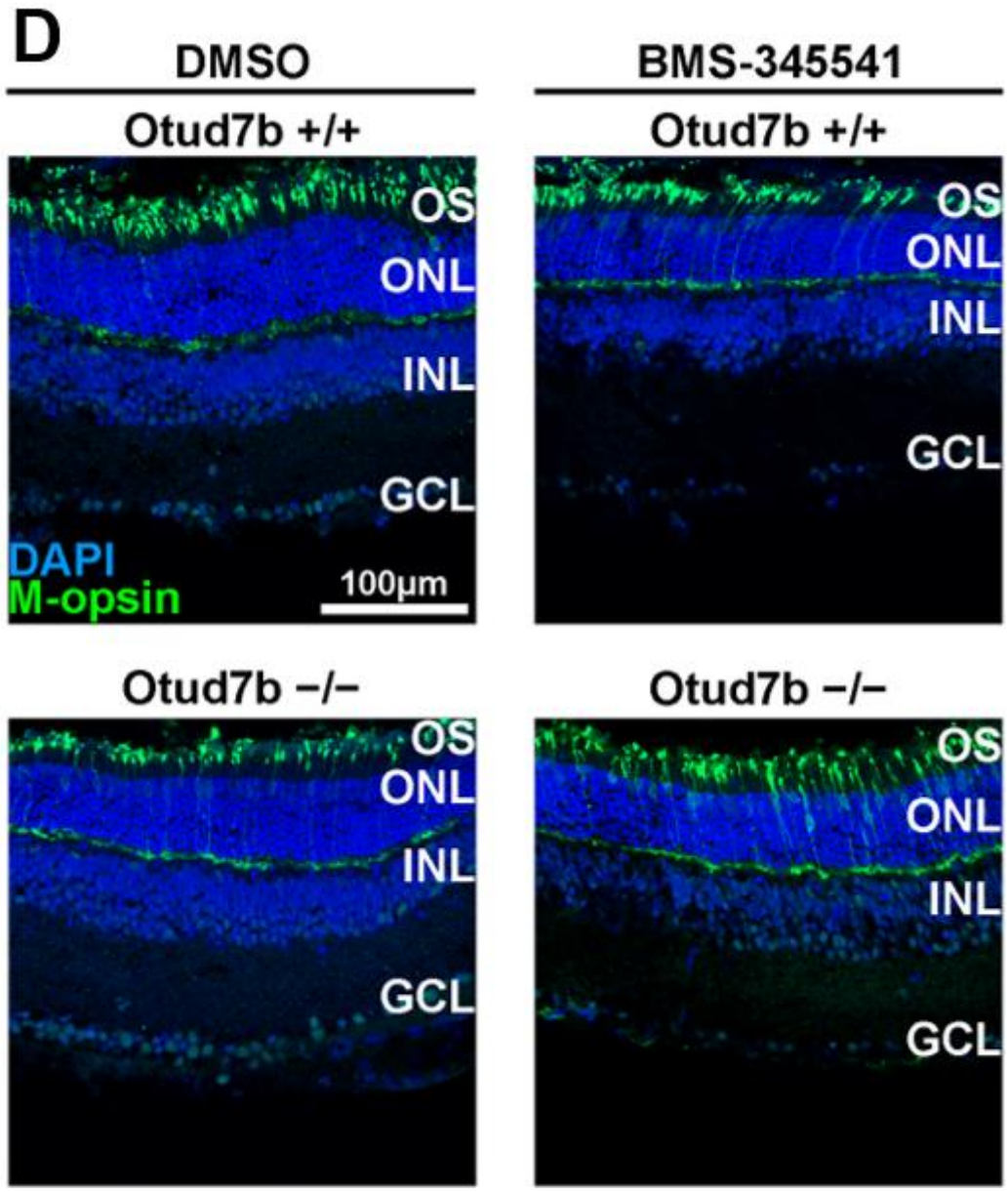

Figure 49. NF-κB pathway inhibition by BMS-345541 suppresses light-induced retinal damage in *Otud7b*$^{-/-}$ mice.

(A) Schematic representation of LED light exposure to mice treated with BMS-345541. BMS-345541 was injected into mice every day for 7 days. **(B–D)** Immunofluorescence analysis of retinal sections from BMS-345541-treated *Otud7b*$^{+/+}$ and *Otud7b*$^{-/-}$ mice after light exposure using the following antibodies: Rhodopsin (a marker for rod outer segments, **B**), S-opsin (a marker for S-cone outer segments, **C**), and M-opsin (a marker for M-cone outer segments, **D**). Nuclei were stained with DAPI.

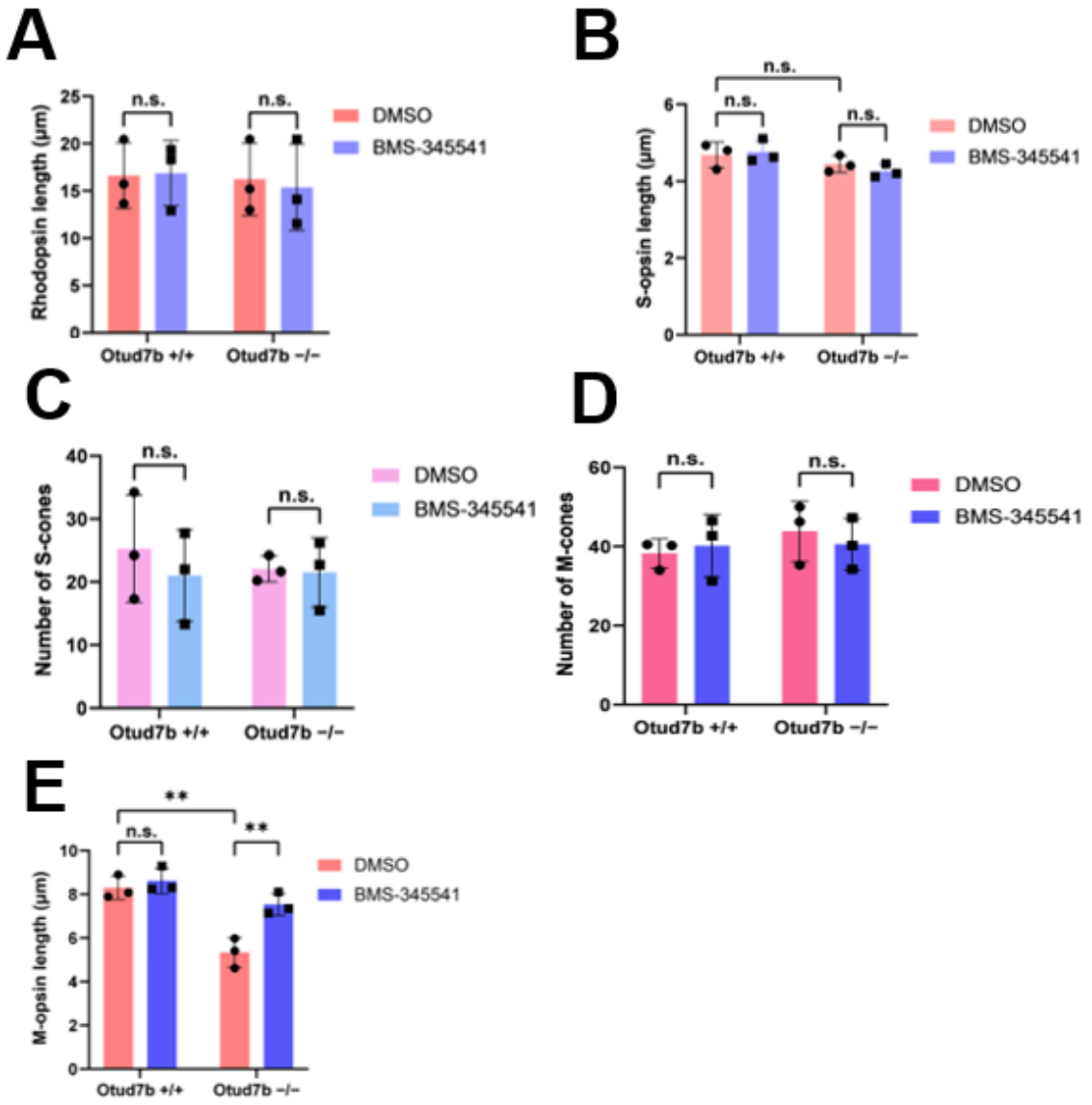

Figure 50. BMS-345541 rescues phenotype observed in *Otud7b*$^{-/-}$ mice after light exposure.

(A) Rod outer segment length was measured. **(B)** S-cone outer segment **(C, D)** The number of S-cones **(C)** and M-cones **(D)** of DMSO or BMS-345541-treated mice after light exposure was counted. Data are presented as the mean ± SD. n.s., not significant (two-way ANOVA followed by Tukey's multiple comparisons test), n = 3 per genotype. **(E)** M-cone outer segment lengths measured in BMS-345541-treated *Otud7b*$^{+/+}$ and *Otud7b*$^{-/-}$ mice after light exposure. The M-cone outer segments were longer in BMS-345541-treated *Otud7b*$^{-/-}$ retina compared to DMSO-treated *Otud7b*$^{-/-}$ retina. *$p < 0.05$, n.s. not significant (two-way ANOVA followed by Tukey's multiple comparisons test), n = 3 per genotype

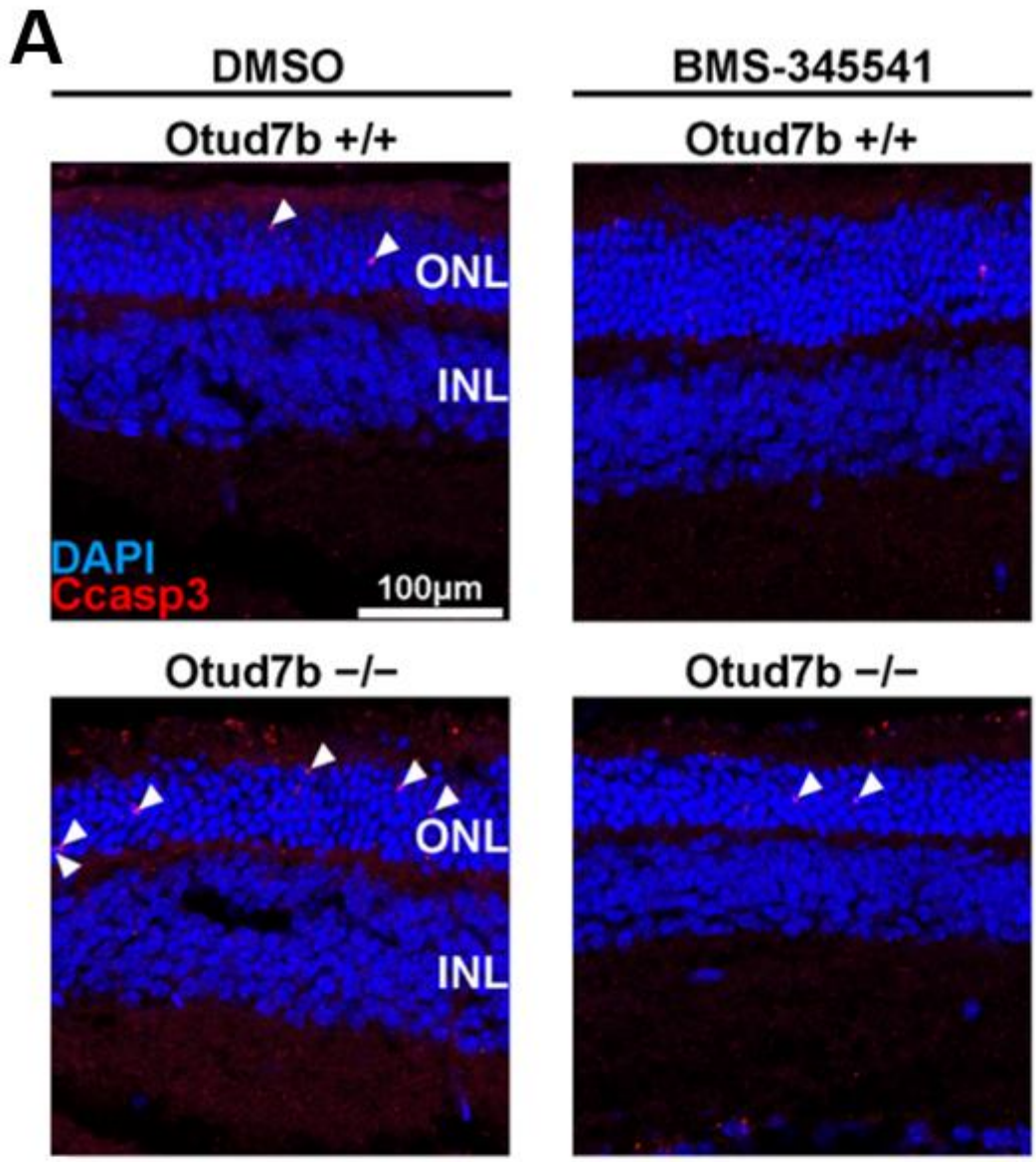
A
DMSO
BMS-345541
Otud7b +/+
Otud7b +/+
ONL
INL
DAPI
Ccasp3
100μm
Otud7b −/−
Otud7b −/−
ONL
INL

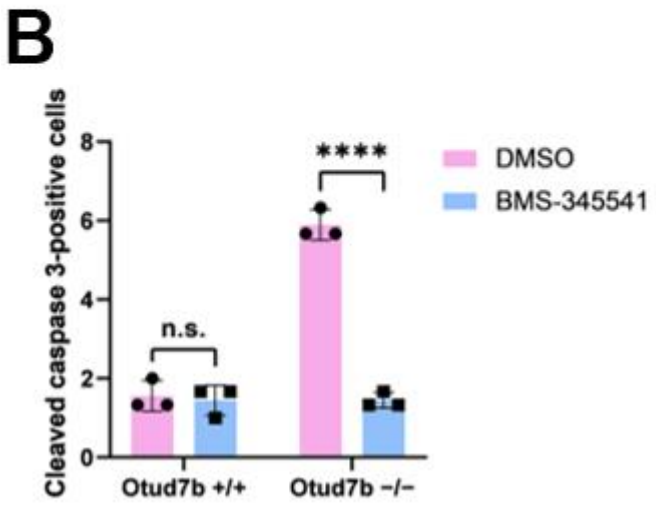
B
Cleaved caspase 3-positive cells
8
6
4
2
0
n.s.
****
DMSO
BMS-345541
Otud7b +/+
Otud7b −/−

Figure 51. BMS-345541 decreased cleaved caspase3.

(A) Immunofluorescence analysis of retinal sections from BMS-345541-treated *Otud7b*$^{+/+}$ and *Otud7b*$^{-/-}$ mice after light exposure using anti-cleaved caspase 3 antibody. Nuclei were stained with DAPI. White arrows indicate cleaved caspase 3-positive cells. **(B)** The number of cleaved caspase 3-positive cells was counted. BMS-345541 treatment significantly reduced the number of cleaved caspase 3-positive cells in the *Otud7b*$^{-/-}$ retina. **** $p < 0.0001$, n.s. not significant (two-way ANOVA followed by Tukey's multiple comparisons test), n = 3 per genotype.

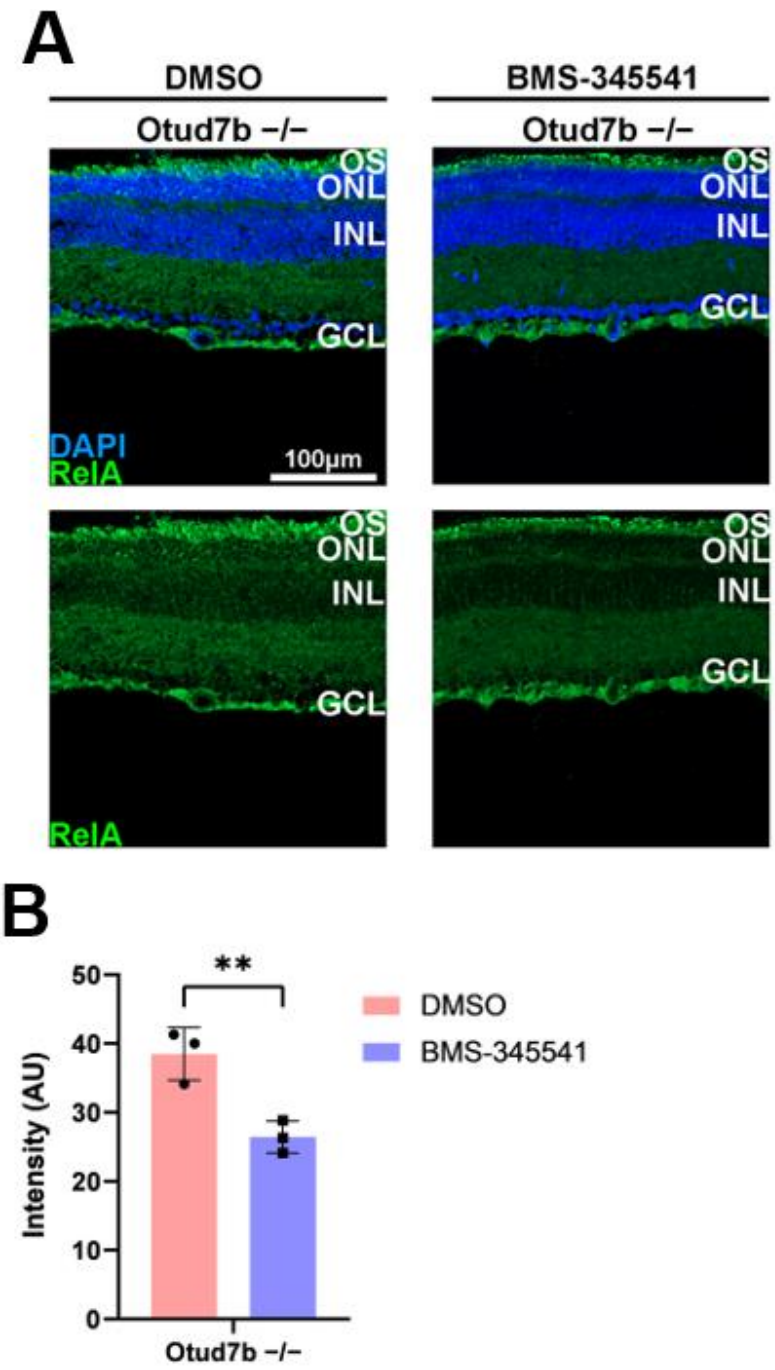

Figure 52. NF-κB pathway inhibition by BMS-345541.

(A) Immunofluorescence analysis of retinal sections from DMSO or BMS-345541-treated *Otud7b*$^{-/-}$ mice after light exposure using an anti-RelA antibody. Nuclei were stained with DAPI. **(B)** RelA intensity in the ONL of DMSO or BMS-345541-treated *Otud7b*$^{-/-}$ mice after light exposure was measured. RelA intensity decreased in the BMS-345541-treated Data are presented as the mean ± SD. $^{**}p < 0.01$ (unpaired t-test). n = 3 experiments.

Discussion

In this study, we found that Otud7b was highly expressed in retinal photoreceptor cells. We did not observe that ablation of *Otud7b* affects retinal photoreceptor development and function; however, cone photoreceptor damage was enhanced in the retinas of *Otud7b*$^{-/-}$ mice subjected to stress conditions by exposure to intense light or mating with the *Mak*$^{-/-}$ RP model mice. We also found that *Otud7b* knockdown in cultured neuronal cells subjected to serum starvation increased cell death. RNA-seq analysis and reporter gene assay showed that NF-κB is activated by *Otud7b* deficiency. Inhibition of the NF-κB pathway ameliorated cone degeneration and neuronal cell death caused by the loss of *Otud7b* in the retina and *Otud7b* knockdown in cultured cells, respectively. These findings suggest that Otud7b protects cone photoreceptor cells from degeneration through the inhibition of the NF-κB in the retina.

The M-cone outer segments, but not the S-cone outer segments, were shorter in light-exposed *Otud7b*$^{-/-}$ mouse retinas than in light-exposed *Otud7b*$^{+/+}$ mouse retinas. M-cone and S-cone photoreceptor cells are mainly located on the dorsal/superior and ventral/inferior sides of the retina, respectively[63]. Given that light-induced damage, an AMD model[62,64], has been reported to significantly impact the dorsal/superior side of the retina compared to the ventral/inferior side[48,65], phenotypic differences between M-cone and S-cone outer segment lengths in the light-exposed *Otud7b*$^{-/-}$ retina might be due to the locations of M-cone and S-cone photoreceptor cells in the retina. In addition, photopic ERG amplitudes indicated greater impairment in cone photoreceptor function in light-exposed *Otud7b*$^{-/-}$ mice than in light-exposed *Otud7b*$^{+/+}$ mice. In contrast to cone photoreceptor cells, the outer segments of rod photoreceptors in *Otud7b*$^{+/+}$ and *Otud7b*$^{-/-}$ mouse retinas exposed to intense light did not exhibit a significant difference.

Furthermore, scotopic ERG amplitudes were almost unchanged in *Otud7b*$^{+/+}$ and *Otud7b*$^{-/-}$ mice subjected to light-damage experiments. Taken together, these results suggest that Otud7b functions more in cone photoreceptor cells than in rod photoreceptor cells under intense light.

We also investigated the effects of *Otud7b* ablation in an RP model *Mak*$^{-/-}$ mice. In this model, progressive retinal deterioration of rods and cones begins at approximately 1 month[54]. A significant decrease in ONL thickness was observed in the *Otud7b*$^{-/-}$; *Mak*$^{-/-}$ mouse retina compared to that in the *Otud7b*$^{+/+}$; *Mak*$^{-/-}$ mouse retina; however, scotopic ERG did not indicate a significant difference between the *Otud7b*$^{+/+}$; *Mak*$^{-/-}$ and *Otud7b*$^{-/-}$; *Mak*$^{-/-}$ mouse retinas, suggesting that rod photoreceptor cell function is not drastically altered by *Otud7b* deficiency. Notably, the outer segments of cone photoreceptor cells were significantly shorter in *Otud7b*$^{-/-}$; *Mak*$^{-/-}$ retinas than in *Otud7b*$^{+/+}$; *Mak*$^{-/-}$ retinas. In addition, photopic ERG indicated decreased cone photoreceptor function in *Otud7b*$^{-/-}$; *Mak*$^{-/-}$ retinas. These results imply that Otud7b mitigates cone photoreceptor degeneration under stress conditions. Given that *OTUD7B* was also found to be expressed in the human retina, mutations and/or variants of the *OTUD7B* gene may be disease modifiers of AMD and RP.

The cleaved caspase 3-positive cells significantly increased in the ONL of the light-exposed *Otud7b*$^{-/-}$ mice compared with that of the light-exposed *Otud7b*$^{+/+}$ mice. However, we observed no significant change in the number of cone photoreceptor cells between the light-exposed *Otud7b*$^{+/+}$ and *Otud7b*$^{-/-}$ mice. One possible explanation of this result may be that more time is needed after light exposure to observe significant cone photoreceptor cell loss. Another possible explanation may be that the percentage of cone photoreceptor cells that expressed cleaved caspase 3 is too low to impact the cell

number.

We found that RelA, a member of the NF-κB family of transcription factors, was activated in the *Otud7b*$^{-/-}$ mouse retina that underwent light-induced damage. The IPA networks also predicted the upregulation of RelB, another NF-κB family transcription factor, as a result of RelA activation. For this reason, we focused on NF-κB for further experiments. In addition, we confirmed that NF-κB activity was upregulated by *Otud7b* knockdown in Neuro2A cells that had undergone serum starvation using a luciferase reporter assay. Furthermore, we showed that inhibition of NF-κB reduced neuronal cell death and photoreceptor damage resulting from *Otud7b* deficiency. While previous studies showed that several compounds suppressed the NF-κB pathway and ameliorated retinal damage[66-68], the causal relationship between the suppression of the NF-κB pathway and the amelioration of retinal damage has not been investigated. Furthermore, it is not clear in which retinal cell types inhibition of NF-κB can suppress photoreceptor degeneration. We observed that Otud7b is predominantly expressed in photoreceptor cells of the retina, strongly suggesting that the degeneration of photoreceptor cells observed in *Otud7b*$^{-/-}$ retinas under stress is induced by the activated NF-κB pathway in retinal photoreceptor cells. However, we cannot exclude the possibility that NF-κB signaling pathway activation in other retinal cell types lacking *Otud7b* contributes to promoting retinal photoreceptor degeneration. It would be helpful to evaluate the effects of *Otud7b* loss in rod and/or cone photoreceptor cells on retinal damage under stress using conditional approaches, such as the Cre/loxP system.

Immunohistochemical analysis showed that Otud7b is expressed in both rod and cone photoreceptor cells. Why are cone photoreceptor cells more damaged than rod photoreceptor cells because of *Otud7b* deficiency under stress conditions? The first

possibility is the difference in the expression levels of Otud7b between rod and cone photoreceptor cells. A previous comprehensive transcriptomic analysis showed that Otud7b expression is increased in the *Nrl*$^{-/-}$ mouse retina in which the absence of rod photoreceptor cells is accompanied by an increase in S-cone-like cells[69,70], suggesting that Otud7b is more highly expressed in cone photoreceptor cells than in rod photoreceptor cells. A second possibility is that cone photoreceptor cells may have increased activation of NF-κB compared with rod photoreceptor cells, resulting in further degradation. We previously performed a microarray analysis of a wild-type mouse retina and *Samd7*$^{-/-}$ mouse retina, in which deletion of *Samd7* caused rod photoreceptor cells to express cone genes[71]. We found that rod-enriched genes were downregulated in the *Samd7*$^{-/-}$ mouse retina, while cone-enriched genes were upregulated in the *Samd7*$^{-/-}$ mouse retina[71]. *Nfkb1*, a gene that encodes the NF-κB family transcription factor p105, was reported to be one of the cone-enriched genes that were upregulated in the *Samd7*$^{-/-}$ mouse retina[71]. In addition, another microarray analysis showed that *Nfkb1* expression increased in the *Nrl*$^{-/-}$ mouse retina from P2 to 2M[72]. *Nfkb1* expression increase was corroborated by other studies that performed RNA-seq analysis on the *Nrl*$^{-/-}$ mouse retina[73,74]. These previous studies suggest that the expression level of *Nfkb1* in cone photoreceptor cells is higher than that in rod photoreceptor cells. When the canonical NF-κB pathway is triggered, p105 undergoes partial degradation and generates p50, which forms dimers with the other NF-κB family transcription factor, translocates to the nucleus, and transactivates NF-κB target genes[75]. Taken together, we speculate that the enriched expression of *Nfkb1* in cone photoreceptor cells results in increased NF-κB activity, leading to greater degeneration than that in rod photoreceptor cells. A third possibility is that the additional deubiquitinase suppresses rod photoreceptor degeneration. Several comprehensive transcriptomic

analyses have shown that the expression of *Tnfaip3*, also known as *Otud7c*, is reduced in *Nrl*$^{-/-}$ retina[73,74,76], suggesting that the expression level of *Tnfaip3* in rod photoreceptor cells is higher than that in cone photoreceptor cells. In addition, Tnfaip3 is an anti-inflammatory protein that negatively regulates the NF-κB pathway by deubiquitinating RIP1 kinase or TRAF6[77,78]. Thus, Tnfaip3 in addition to Otud7b may suppress rod photoreceptor degeneration through the inhibition of the NF-κB pathway.

Otud7b was independently identified as a negative regulator of the noncanonical NF-κB pathway as it prevents the degradation of TRAF3[79] and of the canonical NF-κB pathway through deubiquitination of RIP1 kinase or TRAF6[80-82]. Under the steady-state, TRAF3 binds to NF-κB-inducing kinase (NIK), resulting in the ubiquitination and degradation of NIK[80-82,79]. Activation of the noncanonical pathway leads to TRAF3 proteolysis, which allows for NIK accumulation. Accumulation of NIK induces phosphorylation of the inhibitor of kappa-B kinase α (IKKα), leading to the ubiquitination and processing of p100[80-82,79]. The inactive precursor protein p100 undergoes proteasome-mediated processing to generate active protein p52, which binds to RelB and translocates to the nucleus[80-82]. The deubiquitination of TRAF3 by Otud7b inhibits NF-κB activation by preventing TRAF3 proteolysis and NIK accumulation[79]. Alternatively, the canonical pathway relies on ubiquitination of RIP1 kinase or TRAF6. RIP1 and TRAF6 ubiquitination promotes the activation of TAK1, which phosphorylates and activates the inhibitor of kappa-B kinase (IKK)[80-82,80-82]. IKK activation triggers phosphorylation of IκBα, resulting in IκBα degradation. Then, the dimer p50/RelA, which is bound to IκBα, is released for nuclear translocation[80-82,80-82]. Otud7b inhibits the activation of NF-κB by deubiquitinating RIP1 kinase and TRAF6[80-82,80-82]. In addition, TRAF3 was reported to suppress the canonical NF-κB pathway in the *Traf3*-deficient mouse thymus[83].

Collectively, these previous reports support the idea that the loss of *Otud7b* can activate both canonical and noncanonical NF-κB pathways in retinal photoreceptor cells.

We cannot exclude the possibility that Otud7b is involved in other signaling pathway(s). It was previously reported that Otud7b is a deubiquitinase that deubiquitinates and stabilizes Sox2 and promotes the maintenance of neural progenitor cells[84]. *Otud7b* silencing decreases Sox2 levels and promotes neuronal differentiation in cultured cells. Several studies have revealed that Sox2 is expressed in Müller glia and a subset of amacrine cells in the adult vertebrate retina[85-87]. In addition, the fate determination of retinal progenitor cells depends on the levels of Sox2[85]. Specifically, a decrease in Sox2 levels results in thinning of the retina and loss of ganglion cells, suggesting that the reduction in Sox2 expression results in defective retinal development[85]. However, we did not observe any gross abnormalities in *Otud7b*$^{-/-}$ mouse retinas under normal conditions. Our results imply that Otud7b is not crucial for Sox2 expression in the retina. Defects in the maintenance of neural progenitor cells caused by the loss of Otud7b function may be compensated *in vivo*. Another pathway possibly affected by *Otud7b* deficiency in the retina may be the mTOR pathway. mTOR is the catalytic subunit of two complexes, mTORC1 and mTORC2[88]. mTORC1 comprises mTOR, a regulatory protein associated with mTOR (Raptor) and mammalian lethal with Sec13 protein 8 (mLST8, also referred to as GβL)[88]. In contrast, mTORC2 comprises mTOR, rapamycin insensitive companion of mTOR (Rictor), and GβL[88]. Otud7b has been reported to promote mTORC2 signaling through the deubiquitination of GβL[89]. The deletion of *Otud7b* in mouse embryonic fibroblasts elevates mTORC1 formation while reducing mTORC2 formation, resulting in impaired activation of mTORC2 signaling[89]. Notably, loss of *Raptor* accelerates cone death in a mouse model of RP; however, loss of *Rictor* does not affect cone death in that

model[90]. Taken together, GβL does not seem to be a functional substrate of Otud7b in the retina. Future studies identifying the target proteins of Otud7b in the retina would deepen our understanding of the molecular mechanisms underlying cone photoreceptor cell protection in retinal degenerative diseases, including AMD and RP, and lead to the development of therapeutic strategies to treat these diseases.

Materials and Methods

Animal care

All procedures conformed to the ARVO Statement for the Use of Animals in Ophthalmic and Vision Research, and these procedures were approved by the Institutional Safety Committee on Recombinant DNA Experiments (approval ID 04913) and the Animal Experimental Committees of Institute for Protein Research (approval ID R04-02-0), Osaka University, and were performed in compliance with the institutional guidelines. Mice were housed in a temperature-controlled room at 22°C with a 12 hr light/dark cycle. Fresh water and rodent diet were available at all times. All animal experiments were performed with mice of either sex at 1 month, 2 months, or 6 months.

Cell lines

HEK293T (RIKEN RCB, RCB1637) and Neuro2A (JCRB Cell Bank, IFO50081) cells were cultured in Dulbecco's modified Eagle's medium (DMEM) containing 10% fetal bovine serum supplemented with penicillin (100 μg/mL) and streptomycin (100 μg/mL) at 37°C with 5% CO_2.

Generation of *Otud7b*$^{-/-}$ mice

Otud7b$^{-/-}$ mice were generated using the CRISPR/Cas9 system. Two gRNAs were designed within exon 2 of the *Otud7b* gene using CRISPR Design (http://crispr.mit.edu/). Oligo DNAs for the gRNA sequence were cloned into the pX330 vector[91]. The plasmid constructs were co-injected into B6C3F1 fertilized eggs, which were then transferred into the uteri of pseudopregnant ICR females. Mutated individuals were selected using PCR and subjected to sequencing analyses. *Otud7b*$^{-/-}$ mice were crossed with *Mak*$^{-/-}$ mice[92] to

generate *Otud7b*$^{-/-}$; *Mak*$^{-/-}$ mice. The primer sequences for the gRNA expression plasmid and genotyping are listed in Table 1.

Plasmid construction

Plasmids expressing enhanced green fluorescent protein (EGFP) have been previously constructed[54,93]. The full-length cDNA fragment of mouse *Otud7b* was amplified by PCR using mouse retinal cDNA as a template and subcloned into the pCAGGSII-N-3xFLAG vector[94]. For *Otud7b* knockdown, the Otud7b-shRNA and shRNA-control cassettes were subcloned into the pBAsi-mU6 vector (Takara Bio). The target sequences were as follows: Otud7b-shRNA1, 5′-GTGCTGAGGAAAGCGCTGTAT-3′ and shRNA-control, 5′-GACGTCTAACGGATTCGAGCT-3′[95]. Primer sequences used for amplification are listed in Table 1.

Chemicals

Curcumin (Sigma, C7727) was dissolved in DMSO at 200 mg/mL or 5 mM and stored at -20°C. BMS-345541 (Sigma-Aldrich, B9935-5MG) was dissolved in DMSO at 25 mg/mL or 50 mM and stored at -20°C.

Drug administration

Curcumin was dissolved in DMSO (200 mg/mL) and diluted with sunflower seed oil (Sigma-Aldrich). Curcumin (100 mg/kg) was administered to the mice daily by subcutaneous injection 4 h before light exposure. BMS-3455341 was dissolved in DMSO (25 mg/mL) and diluted with sunflower seed oil. BMS-345541 (30 mg/kg) was administered to the mice daily by subcutaneous injection 4 h before light exposure.

Cell culture and transfection

Transfection was performed using the calcium phosphate method for HEK293T cells. Neuro2A cell transfection was performed using Lipofectamine 3000 (Thermo Fisher Scientific) for shRNA and Lipofectamine RNAiMAX (Life Technologies) for siRNA. To induce cellular stress in transfected cells, the medium was replaced with a serum-free medium 24 or 48 h after transfection, and the cells were cultured for 14 h in a serum-free medium. To examine the effects of curcumin and BMS-345541 on cellular stress, Neuro2A cells were incubated with serum-supplemented medium containing 5 μM curcumin or 2 μM BMS-345541 for 4 h before and 24 h after transfection and further incubated with serum-free medium containing 5 μM curcumin or 2 μM BMS-345541 for 24 h. For knockdown experiments, the cells were transfected with siGENOME non-targeting siRNA pool #2 or mouse Otud7b siRNA (Dharmacon-Horizon Discovery). The following are the catalog numbers and siRNA sequences: nontargeting control #2, catalog no. D-001206-14-05, target sequences: UAAGGCUAUGAAGAGAUAC, AUGUAUUGGCCUGUAUUAG, AUGAACGUAGAAUUGCUCAA, and UGGUUUACAUGUCGACUAA; siGENOME_ mouse_Otud7b, catalog no. D-050018-03; target sequence: GCCGGUAUAUGAAAGCCUA; siGENOME_mouse_Otud7b, catalog no. D-050018-04; target sequence, GCAAUGGCGGGAGCAAGUA.

RT-PCR analysis

RT-PCR was performed as described previously[96,97]. Total RNA was extracted from tissues dissected from ICR mice at 4 weeks using TRIzol (Ambion). Total RNA (2 μg) was reverse-transcribed into cDNA with random hexamers using PrimescriptII (TaKaRa).

Human cDNA was purchased from Clontech (Mountain View, CA, USA). The cDNA was used for PCR with rTaq polymerase (TaKaRa).

Immunofluorescence analysis of retinal sections and cells

Immunofluorescence analysis of retinal sections was performed as described previously[98]. Mouse eyes and eyecups were fixed in 4% paraformaldehyde (PFA) in phosphate-buffered saline (PBS) for 5 or 30 min. Samples were placed in 30% sucrose in PBS overnight at 4°C and embedded in TissueTec OCT Compound 4583 (Sakura). Frozen 20-μm sections placed on slides were dried overnight at room temperature. Tissue sections from eyecups were washed three times with PBS. Eye cryosections were fixed in methanol for 5 min before washing three times with PBS. The samples were then incubated with blocking buffer (5% normal donkey serum and 0.1% Triton X-100 in PBS) for 1 h at room temperature and immunostained with primary antibodies in blocking buffer overnight at 4°C. After washing with PBS, the samples were incubated with fluorescent dye-conjugated secondary antibodies and DAPI (1:1,000, Nacalai Tesque). Neuro2A cells were washed with PBS, fixed with 4% PFA in PBS for 5 min at room temperature, and incubated with blocking buffer for 1 h at room temperature. Cells were immunostained with primary antibodies in blocking buffer overnight at 4°C, washed with PBS, and incubated with fluorescent dye-conjugated secondary antibodies and DAPI in blocking buffer for 2 h at room temperature. The samples were washed three times with PBS and then coverslipped with gelvatol.

The primary antibodies used in this study were as follows: mouse anti-Rhodopsin (1:1,000, Sigma, O4886), mouse anti-Pax6 (1:500, DSHB), mouse anti-S100β (1:200, Sigma, S-2532), mouse anti-Ctbp2 (1:500, BD Biosciences, 612044), rabbit anti-M-opsin

(1:500, Millipore, AB5405), rabbit anti-Pikachurin (1:300)[99], rabbit anti-Gnat2 (1:500, Abcam, ab97501), rabbit anti-Chx10 (1:200)[100], rabbit anti-Calbindin (1:200, Calbiochem, PC253L), rabbit anti-Otud7b (1:500, Proteintech, 16605-1-AP), rabbit anti-GFP (1:2,500, MBL, 598), rabbit anti-cleaved caspase 3 (1:500, Cell Signaling, 9661), goat anti-S-opsin (1:500, Santa Cruz, sc-14363 or 1:500, ROCKLAND, 600-101-MP7S), rabbit anti-IbaI (1:500, WAKO, 019-19741), mouse anti-GFAP (1:500, Sigma, G3893-.2ML), and guinea pig anti-Rbpms (1:1,000, Millipore, ABN1376). Cy3-conjugated (1:500; Jackson ImmunoResearch Laboratories) and Alexa Fluor 488-conjugated (1:500; Sigma-Aldrich) secondary antibodies were used. DAPI was used for nuclear staining. The specimens were observed under a laser confocal microscope (LSM700 or LSM900; Carl Zeiss). Rhodamine-labeled peanut agglutinin (PNA) (1:250) (RL-1072, Vector Laboratories) was used to stain cone photoreceptor synapses. The thicknesses and lengths of the ONL, INL+IPL+GCL, M-opsin, S-opsin, and Gnat2 were measured using ZEN imaging software (ZEN (black edition) or ZEN (blue edition), Carl Zeiss).

Exposure to LED light

Exposure to LED light was performed as described previously[45]. Animals were maintained in the dark for 12 h. Thirty minutes before LED light (~450 nm) exposure, the pupils were dilated using 1% cyclopentolate hydrochloride eye drops (Santen Pharmaceuticals, Osaka, Japan). The non-anesthetized mice were exposed to ~9,000 lux LED light for 3 h in a mirrored box with clear partitions to separate the mice while allowing for light reflection. The ambient temperature was maintained at 25 ± 1.5°C during the light exposure. The mice were returned to their cages after light exposure and

kept under normal light conditions for 9 h before the next 12 h dark cycle. Light exposure was repeated for 6 days. ERG recordings and/or retinal dissections were performed on day 7. *Otud7b*$^{+/-}$ mice were backcrossed with 129S6/*SvEvTac* mice to generate *Otud7b*$^{+/+}$ and *Otud7b*$^{-/-}$ mice homozygous for the variant encoding Leu450 in the *Rpe65* gene, which was used for the experiment[101]. *Otud7b*$^{+/+}$ and *Otud7b*$^{-/-}$ mice treated with curcumin were also subjected to the experiment.

ERG recordings

Electroretinograms (ERGs) were recorded as described previously[102]. The mice were adapted to the dark overnight. Ketamine (100 mg/kg) and xylazine (10 mg/kg) diluted in saline (Otsuka) were injected intraperitoneally to anesthetize the mice. Pupils were dilated with topical 0.5% tropicamide and 0.5% phenylephrine HCl. The ERG responses were measured using the PuREC system with LED electrodes (Mayo Corporation). Scotopic ERGs were recorded at four stimulus intensities ranging from –4.0 to 1.0 log cd s/m^2. The mice were light-adapted for 10 min before photopic ERGs were recorded on a rod-suppressing white background of 1.3 log cd s/m^2. Photopic ERGs were recorded at four stimulus intensities ranging from –0.5 to 1.0 log cd s/m^2. Eight and four responses were averaged for the scotopic recordings (–4.0 and –3.0 log cd s/m^2, respectively). Sixteen responses were averaged for the photopic recordings.

Western blotting

Western blotting was performed as previously described[103]. Neuro2A cells were washed with PBS twice and lysed in a lysis buffer supplemented with protease inhibitors (buffer A: 20 mM Tris-HCl pH 7.4, 150 mM NaCl, 1% Nonidet P-40, 1 mM EDTA, 1 mM PMSF,

2 μg/mL leupeptin, 5 μg/mL aprotinin, and 3 μg/mL pepstatin A). Mouse retinas were lysed in lysis buffer supplemented protease inhibitors (buffer B: 20 mM Tris-HCl pH 7.4, 150 mM NaCl, 1% Nonidet P-40, 0.5 mM EDTA, 1 mM PMSF, 2 μg/mL leupeptin, 5 μg/mL aprotinin, and 3 μg/mL pepstatin A). Samples were resolved by SDS-PAGE and transferred to PVDF membranes (Millipore) using a semi-dry transfer cell (Bio-Rad) or the iBlot system (Invitrogen). The membranes were blocked with blocking buffer (3% skim milk and 0.05% Tween 20 in Tris-buffered saline (TBS)) for 1 h and incubated with primary antibodies overnight at 4°C. The membranes were washed with 0.05% Tween 20 in TBS three times for 10 min each and then incubated with secondary antibodies for 2–5 h at room temperature. Signals were detected using a Chemi-Lumi One L (Nacalai) or Pierce Western Blotting Substrate Plus (Thermo Fisher Scientific). The following primary antibodies were used: mouse anti-FLAG M2 (1:5,000, Sigma, F1804), mouse anti-α-tubulin (Cell Signaling Technology, DM1A, 1:5,000, T9026), rabbit anti-GFP (1:2,500, MBL, 598), rabbit anti-cleaved caspase 3 (1:100, Cell Signaling, 9661), and rabbit anti-Otud7b (1:500, Proteintech, 16605-1-AP). The following secondary antibodies were used: horseradish peroxidase-conjugated anti-mouse IgG (1:10,000; Zymed) and anti-rabbit IgG (1:10,000; Jackson Laboratory).

Cell Viability

Neuro2A cells transfected with shRNA or siRNA were cultured in serum-free medium for 14 h. Viability was assayed using a ReadyProbes Cell Viability Imaging Kit (Blue/Red) based on Hoechst 33342 for live cells and propidium iodide nucleic acid stain for dead cells (Thermo Fischer Scientific). Cell viability was determined as the percentage of live cells among the total cells counted in six fluorescence images of each sample under

a laser confocal microscope (LSM700 or LSM900; Carl Zeiss).

RNA-seq and data analysis

RNA-seq analysis was performed as previously described[104] with certain modifications. Total retinal RNAs from three *Otud7b*$^{+/+}$ and three *Otud7b*$^{-/-}$ mice after light exposure were isolated using TRIzol RNA extraction reagent (Invitrogen). Sequencing was performed on an Illumina NovaSeq 6000 platform in 101-base single-end mode. Raw reads were mapped to mouse reference genome sequences (mm10) using TopHat ver. 2.1.1, in combination with Bowtie2 ver. 2.2.8 and SAMtools ver. 0.1.18. The number of fragments per kilobase of exon per million mapped fragments (FPKMs) was calculated using Cuffdiff ver. 2.2.1. Upstream regulator analysis was performed using IPA (Qiagen). The RNA-seq analysis datasets are available in the Gene Expression Omnibus (GEO) database of NCBI (Accession Number GSE239573).

Luciferase reporter assay

Reporter gene assays were performed using the Nano-Glo Dual-Luciferase Reporter Assay System (Promega), according to the manufacturer's protocol. To generate the reporter construct, a minimal promoter (5′-AGACACTAGAGGGTATATAATGGAAGCTCGACTTCCAG-3′) and 5x NF-κB response element (5′-GGGAATTTCCGGGGACTTTCCGGGAATTTCCGGGGACTTTCCGGGAATTTCC-3′) were cloned into the pGL3-Basic vector (Promega) in which *Firefly luciferase* was replaced with *NanoLuc luciferase* amplified from the pNLF-N [CMV/Hygro] vector (Promega) by PCR. The pGL3-Basic vector containing the minimal promoter was co-

transfected to measure transfection efficiency. A plasmid expressing Otud7b-shRNA1 was transfected with the reporter construct into Neuro2A cells. After 48 h of transfection, the cells were incubated in the serum-free medium for 14 h, washed with TBS, and lysed with buffer A. Luminescence signal was detected using the GloMax® Multi+ Detection System (Promega).

Statistical Analysis

Statistical analyses were performed using GraphPad Prism version 9 (GraphPad Software). Data are represented as the mean ± SD. Statistical analyses were performed using unpaired t-test, one-way ANOVA, or two-way ANOVA, as indicated in the figure legends. Asterisks indicate significance as follows: *$p < 0.05$, **$p < 0.01$, ***$p < 0.001$, and ****$p < 0.0001$.

Acknowledgements

We thank Dr. Y. Shinkai for the *Mak*$^{-/-}$ mouse, M. Kadowaki, A. Tani, M. Wakabayashi, K. Yoshida, and S. Okochi for technical assistance, and Editage for English language editing. This work was supported by Grant-in-Aid for Scientific Research (21H02657, 20K07326) and Grant-in-Aid for Challenging Research (Exploratory) (23K18199) from the Japan Society for the Promotion of Science, AMED-CREST (21gm1510006) from the Japan Agency for Medical Research and Development, Japan Science and Technology Agency Moonshot R&D (JPMJMS2024), The Takeda Science Foundation, and The Uehara Memorial Foundation.

References

1. Scott, A.W., Bressler, N.M., Ffolkes, S., Wittenborn, J.S., and Jorkasky, J. (2016). Public Attitudes About Eye and Vision Health. JAMA Ophthalmol *134*, 1111-1118. 10.1001/jamaophthalmol.2016.2627.
2. Enoch, J., McDonald, L., Jones, L., Jones, P.R., and Crabb, D.P. (2019). Evaluating Whether Sight Is the Most Valued Sense. JAMA Ophthalmol *137*, 1317-1320. 10.1001/jamaophthalmol.2019.3537.
3. Rehman, I., Hazhirkarzar, B., and Patel, B.C. (2024). Anatomy, Head and Neck, Eye. In StatPearls.
4. Hejtmancik, J.F., and Shiels, A. (2015). Overview of the Lens. Prog Mol Biol Transl Sci *134*, 119-127. 10.1016/bs.pmbts.2015.04.006.
5. Boulton, M., and Dayhaw-Barker, P. (2001). The role of the retinal pigment epithelium: topographical variation and ageing changes. Eye (Lond) *15*, 384-389. 10.1038/eye.2001.141.
6. Nguyen, K.H., Patel, B.C., and Tadi, P. (2024). Anatomy, Head and Neck: Eye Retina. In StatPearls.
7. Jeon, C.J., Strettoi, E., and Masland, R.H. (1998). The major cell populations of the mouse retina. J Neurosci *18*, 8936-8946. 10.1523/JNEUROSCI.18-21-08936.1998.
8. Nadal-Nicolas, F.M., Kunze, V.P., Ball, J.M., Peng, B.T., Krishnan, A., Zhou, G., Dong, L., and Li, W. (2020). True S-cones are concentrated in the ventral mouse retina and wired for color detection in the upper visual field. Elife *9*. 10.7554/eLife.56840.

9. Vecino, E., Rodriguez, F.D., Ruzafa, N., Pereiro, X., and Sharma, S.C. (2016). Glia-neuron interactions in the mammalian retina. Prog Retin Eye Res *51*, 1-40. 10.1016/j.preteyeres.2015.06.003.

10. Yang, S., Zhou, J., and Li, D. (2021). Functions and Diseases of the Retinal Pigment Epithelium. Front Pharmacol *12*, 727870. 10.3389/fphar.2021.727870.

11. Masland, R.H. (2012). The neuronal organization of the retina. Neuron *76*, 266-280. 10.1016/j.neuron.2012.10.002.

12. Hartong, D.T., Berson, E.L., and Dryja, T.P. (2006). Retinitis pigmentosa. Lancet *368*, 1795-1809. 10.1016/S0140-6736(06)69740-7.

13. Hamel, C. (2006). Retinitis pigmentosa. Orphanet J Rare Dis *1*, 40. 10.1186/1750-1172-1-40.

14. Gagliardi, G., Ben M'Barek, K., and Goureau, O. (2019). Photoreceptor cell replacement in macular degeneration and retinitis pigmentosa: A pluripotent stem cell-based approach. Prog Retin Eye Res *71*, 1-25. 10.1016/j.preteyeres.2019.03.001.

15. Verbakel, S.K., van Huet, R.A.C., Boon, C.J.F., den Hollander, A.I., Collin, R.W.J., Klaver, C.C.W., Hoyng, C.B., Roepman, R., and Klevering, B.J. (2018). Non-syndromic retinitis pigmentosa. Prog Retin Eye Res *66*, 157-186. 10.1016/j.preteyeres.2018.03.005.

16. Brunet, A.A., Harvey, A.R., and Carvalho, L.S. (2022). Primary and Secondary Cone Cell Death Mechanisms in Inherited Retinal Diseases and Potential Treatment Options. Int J Mol Sci *23*. 10.3390/ijms23020726.

17. Newton, F., and Megaw, R. (2020). Mechanisms of Photoreceptor Death in Retinitis Pigmentosa. Genes (Basel) *11*. 10.3390/genes11101120.

18. Ferri, C., Luparini, R.L., Giarrizzo, G., Valentino, S., Cammarella, I., Musca, A., and Santucci, A. (1989). [Effects of active orthostatism on blood levels of atrial natriuretic peptide in the healthy subject]. Medicina (Firenze) *9*, 172-173.

19. Daiger, S.P., Bowne, S.J., and Sullivan, L.S. (2014). Genes and Mutations Causing Autosomal Dominant Retinitis Pigmentosa. Cold Spring Harb Perspect Med *5*. 10.1101/cshperspect.a017129.

20. O'Neal, T.B., and Luther, E.E. (2024). Retinitis Pigmentosa. In StatPearls.

21. Campochiaro, P.A., and Mir, T.A. (2018). The mechanism of cone cell death in Retinitis Pigmentosa. Prog Retin Eye Res *62*, 24-37. 10.1016/j.preteyeres.2017.08.004.

22. Mitchell, P., Liew, G., Gopinath, B., and Wong, T.Y. (2018). Age-related macular degeneration. Lancet *392*, 1147-1159. 10.1016/S0140-6736(18)31550-2.

23. Stahl, A. (2020). The Diagnosis and Treatment of Age-Related Macular Degeneration. Dtsch Arztebl Int *117*, 513-520. 10.3238/arztebl.2020.0513.

24. Wong, W.L., Su, X., Li, X., Cheung, C.M., Klein, R., Cheng, C.Y., and Wong, T.Y. (2014). Global prevalence of age-related macular degeneration and disease burden projection for 2020 and 2040: a systematic review and meta-analysis. Lancet Glob Health *2*, e106-116. 10.1016/S2214-109X(13)70145-1.

25. Ambati, J., Atkinson, J.P., and Gelfand, B.D. (2013). Immunology of age-related macular degeneration. Nat Rev Immunol *13*, 438-451. 10.1038/nri3459.

26. Rehman, I., Mahabadi, N., Motlagh, M., and Ali, T. (2024). Anatomy, Head and Neck, Eye Fovea. In StatPearls.

27. Galuszka, M., Pojda-Wilczek, D., and Karska-Basta, I. (2023). Age-Related Macular or Retinal Degeneration? Medicina (Kaunas) *59*.

10.3390/medicina59050920.

28. Zhang, Z., Liang, F., Chang, J., Shan, X., Yin, Z., Wang, L., and Li, S. (2024). Autophagy in dry AMD: A promising therapeutic strategy for retinal pigment epithelial cell damage. Exp Eye Res *242*, 109889. 10.1016/j.exer.2024.109889.

29. Heesterbeek, T.J., Lores-Motta, L., Hoyng, C.B., Lechanteur, Y.T.E., and den Hollander, A.I. (2020). Risk factors for progression of age-related macular degeneration. Ophthalmic Physiol Opt *40*, 140-170. 10.1111/opo.12675.

30. Shang, F., and Taylor, A. (2012). Roles for the ubiquitin-proteasome pathway in protein quality control and signaling in the retina: implications in the pathogenesis of age-related macular degeneration. Mol Aspects Med *33*, 446-466. 10.1016/j.mam.2012.04.001.

31. Goldstein, G., Scheid, M., Hammerling, U., Schlesinger, D.H., Niall, H.D., and Boyse, E.A. (1975). Isolation of a polypeptide that has lymphocyte-differentiating properties and is probably represented universally in living cells. Proc Natl Acad Sci U S A *72*, 11-15. 10.1073/pnas.72.1.11.

32. Clague, M.J., Coulson, J.M., and Urbe, S. (2012). Cellular functions of the DUBs. J Cell Sci *125*, 277-286. 10.1242/jcs.090985.

33. Swatek, K.N., and Komander, D. (2016). Ubiquitin modifications. Cell Res *26*, 399-422. 10.1038/cr.2016.39.

34. Kwon, Y.T., and Ciechanover, A. (2017). The Ubiquitin Code in the Ubiquitin-Proteasome System and Autophagy. Trends Biochem Sci *42*, 873-886. 10.1016/j.tibs.2017.09.002.

35. Harrigan, J.A., Jacq, X., Martin, N.M., and Jackson, S.P. (2018). Deubiquitylating enzymes and drug discovery: emerging opportunities. Nat Rev Drug Discov *17*,

57-78. 10.1038/nrd.2017.152.

36. Du, J., Fu, L., Sui, Y., and Zhang, L. (2020). The function and regulation of OTU deubiquitinases. Front Med *14*, 542-563. 10.1007/s11684-019-0734-4.

37. Komander, D., Clague, M.J., and Urbe, S. (2009). Breaking the chains: structure and function of the deubiquitinases. Nat Rev Mol Cell Biol *10*, 550-563. 10.1038/nrm2731.

38. Li, Y., and Reverter, D. (2021). Molecular Mechanisms of DUBs Regulation in Signaling and Disease. Int J Mol Sci *22*. 10.3390/ijms22030986.

39. Jevtic, P., Haakonsen, D.L., and Rape, M. (2021). An E3 ligase guide to the galaxy of small-molecule-induced protein degradation. Cell Chem Biol *28*, 1000-1013. 10.1016/j.chembiol.2021.04.002.

40. Park, C.W., and Ryu, K.Y. (2014). Cellular ubiquitin pool dynamics and homeostasis. BMB Rep *47*, 475-482. 10.5483/bmbrep.2014.47.9.128.

41. Nijman, S.M., Luna-Vargas, M.P., Velds, A., Brummelkamp, T.R., Dirac, A.M., Sixma, T.K., and Bernards, R. (2005). A genomic and functional inventory of deubiquitinating enzymes. Cell *123*, 773-786. 10.1016/j.cell.2005.11.007.

42. Schauer, N.J., Magin, R.S., Liu, X., Doherty, L.M., and Buhrlage, S.J. (2020). Advances in Discovering Deubiquitinating Enzyme (DUB) Inhibitors. J Med Chem *63*, 2731-2750. 10.1021/acs.jmedchem.9b01138.

43. Friedman, J.S., Ray, J.W., Waseem, N., Johnson, K., Brooks, M.J., Hugosson, T., Breuer, D., Branham, K.E., Krauth, D.S., Bowne, S.J., et al. (2009). Mutations in a BTB-Kelch protein, KLHL7, cause autosomal-dominant retinitis pigmentosa. Am J Hum Genet *84*, 792-800. 10.1016/j.ajhg.2009.05.007.

44. Campello, L., Esteve-Rudd, J., Cuenca, N., and Martin-Nieto, J. (2013). The

ubiquitin-proteasome system in retinal health and disease. Mol Neurobiol *47*, 790-810. 10.1007/s12035-012-8391-5.

45. Chaya, T., Tsutsumi, R., Varner, L.R., Maeda, Y., Yoshida, S., and Furukawa, T. (2019). Cul3-Klhl18 ubiquitin ligase modulates rod transducin translocation during light-dark adaptation. EMBO J *38*, e101409. 10.15252/embj.2018101409.

46. Nishida, A., Furukawa, A., Koike, C., Tano, Y., Aizawa, S., Matsuo, I., and Furukawa, T. (2003). Otx2 homeobox gene controls retinal photoreceptor cell fate and pineal gland development. Nat Neurosci *6*, 1255-1263. 10.1038/nn1155.

47. Omori, Y., Katoh, K., Sato, S., Muranishi, Y., Chaya, T., Onishi, A., Minami, T., Fujikado, T., and Furukawa, T. (2011). Analysis of transcriptional regulatory pathways of photoreceptor genes by expression profiling of the Otx2-deficient retina. PLoS One *6*, e19685. 10.1371/journal.pone.0019685.

48. Tanito, M., Kaidzu, S., Ohira, A., and Anderson, R.E. (2008). Topography of retinal damage in light-exposed albino rats. Exp Eye Res *87*, 292-295. 10.1016/j.exer.2008.06.002.

49. Li, T., Snyder, W.K., Olsson, J.E., and Dryja, T.P. (1996). Transgenic mice carrying the dominant rhodopsin mutation P347S: evidence for defective vectorial transport of rhodopsin to the outer segments. Proc Natl Acad Sci U S A *93*, 14176-14181. 10.1073/pnas.93.24.14176.

50. Chrysostomou, V., Stone, J., Stowe, S., Barnett, N.L., and Valter, K. (2008). The status of cones in the rhodopsin mutant P23H-3 retina: light-regulated damage and repair in parallel with rods. Invest Ophthalmol Vis Sci *49*, 1116-1125. 10.1167/iovs.07-1158.

51. Milam, A.H., Li, Z.Y., and Fariss, R.N. (1998). Histopathology of the human

retina in retinitis pigmentosa. Prog Retin Eye Res *17*, 175-205. 10.1016/s1350-9462(97)00012-8.

52. Menghini, M., Jolly, J.K., Nanda, A., Wood, L., Cehajic-Kapetanovic, J., and MacLaren, R.E. (2021). Early Cone Photoreceptor Outer Segment Length Shortening in RPGR X-Linked Retinitis Pigmentosa. Ophthalmologica *244*, 281-290. 10.1159/000507484.

53. Tanimoto, N., Sothilingam, V., Kondo, M., Biel, M., Humphries, P., and Seeliger, M.W. (2015). Electroretinographic assessment of rod- and cone-mediated bipolar cell pathways using flicker stimuli in mice. Sci Rep *5*, 10731. 10.1038/srep10731.

54. Omori, Y., Chaya, T., Katoh, K., Kajimura, N., Sato, S., Muraoka, K., Ueno, S., Koyasu, T., Kondo, M., and Furukawa, T. (2010). Negative regulation of ciliary length by ciliary male germ cell-associated kinase (Mak) is required for retinal photoreceptor survival. Proc Natl Acad Sci U S A *107*, 22671-22676. 10.1073/pnas.1009437108.

55. Chaya, T., and Furukawa, T. (2021). Post-translational modification enzymes as key regulators of ciliary protein trafficking. J Biochem *169*, 633-642. 10.1093/jb/mvab024.

56. Tucker, B.A., Scheetz, T.E., Mullins, R.F., DeLuca, A.P., Hoffmann, J.M., Johnston, R.M., Jacobson, S.G., Sheffield, V.C., and Stone, E.M. (2011). Exome sequencing and analysis of induced pluripotent stem cells identify the cilia-related gene male germ cell-associated kinase (MAK) as a cause of retinitis pigmentosa. Proc Natl Acad Sci U S A *108*, E569-576. 10.1073/pnas.1108918108.

57. Ozgul, R.K., Siemiatkowska, A.M., Yucel, D., Myers, C.A., Collin, R.W., Zonneveld, M.N., Beryozkin, A., Banin, E., Hoyng, C.B., van den Born, L.I., et

al. (2011). Exome sequencing and cis-regulatory mapping identify mutations in MAK, a gene encoding a regulator of ciliary length, as a cause of retinitis pigmentosa. Am J Hum Genet *89*, 253-264. 10.1016/j.ajhg.2011.07.005.

58. Lee, S.B., Kim, J.J., Kim, T.W., Kim, B.S., Lee, M.S., and Yoo, Y.D. (2010). Serum deprivation-induced reactive oxygen species production is mediated by Romo1. Apoptosis *15*, 204-218. 10.1007/s10495-009-0411-1.

59. White, E.Z., Pennant, N.M., Carter, J.R., Hawsawi, O., Odero-Marah, V., and Hinton, C.V. (2020). Serum deprivation initiates adaptation and survival to oxidative stress in prostate cancer cells. Sci Rep *10*, 12505. 10.1038/s41598-020-68668-x.

60. Caamano, J., and Hunter, C.A. (2002). NF-kappaB family of transcription factors: central regulators of innate and adaptive immune functions. Clin Microbiol Rev *15*, 414-429. 10.1128/CMR.15.3.414-429.2002.

61. Oeckinghaus, A., and Ghosh, S. (2009). The NF-kappaB family of transcription factors and its regulation. Cold Spring Harb Perspect Biol *1*, a000034. 10.1101/cshperspect.a000034.

62. Zeng, H.Y., Tso, M.O., Lai, S., and Lai, H. (2008). Activation of nuclear factor-kappaB during retinal degeneration in rd mice. Mol Vis *14*, 1075-1080.

63. Warwick, R.A., Kaushansky, N., Sarid, N., Golan, A., and Rivlin-Etzion, M. (2018). Inhomogeneous Encoding of the Visual Field in the Mouse Retina. Curr Biol *28*, 655-665 e653. 10.1016/j.cub.2018.01.016.

64. Wu, T., Chen, Y., Chiang, S.K., and Tso, M.O. (2002). NF-kappaB activation in light-induced retinal degeneration in a mouse model. Invest Ophthalmol Vis Sci *43*, 2834-2840.

65. Ranchon, I., LaVail, M.M., Kotake, Y., and Anderson, R.E. (2003). Free radical trap phenyl-N-tert-butylnitrone protects against light damage but does not rescue P23H and S334ter rhodopsin transgenic rats from inherited retinal degeneration. J Neurosci *23*, 6050-6057. 10.1523/JNEUROSCI.23-14-06050.2003.

66. Kim, J., Jin, H.L., Jang, D.S., Jeong, K.W., and Choung, S.Y. (2018). Quercetin-3-O-alpha-l-arabinopyranoside protects against retinal cell death via blue light-induced damage in human RPE cells and Balb-c mice. Food Funct *9*, 2171-2183. 10.1039/c7fo01958k.

67. Wang, K., Xiao, J., Peng, B., Xing, F., So, K.F., Tipoe, G.L., and Lin, B. (2014). Retinal structure and function preservation by polysaccharides of wolfberry in a mouse model of retinal degeneration. Sci Rep *4*, 7601. 10.1038/srep07601.

68. Cho, H.M., Lee, S.J., and Choung, S.Y. (2023). Protective effects of Panax ginseng berry extract on blue light-induced retinal damage in ARPE-19 cells and mouse retina. J Ginseng Res *47*, 65-73. 10.1016/j.jgr.2022.04.002.

69. Mears, A.J., Kondo, M., Swain, P.K., Takada, Y., Bush, R.A., Saunders, T.L., Sieving, P.A., and Swaroop, A. (2001). Nrl is required for rod photoreceptor development. Nat Genet *29*, 447-452. 10.1038/ng774.

70. Esquerdo-Barragan, M., Brooks, M.J., Toulis, V., Swaroop, A., and Marfany, G. (2019). Expression of deubiquitinating enzyme genes in the developing mammal retina. Mol Vis *25*, 800-813.

71. Omori, Y., Kubo, S., Kon, T., Furuhashi, M., Narita, H., Kominami, T., Ueno, A., Tsutsumi, R., Chaya, T., Yamamoto, H., et al. (2017). Samd7 is a cell type-specific PRC1 component essential for establishing retinal rod photoreceptor identity. Proc Natl Acad Sci U S A *114*, E8264-E8273. 10.1073/pnas.1707021114.

72. Mo, A., Luo, C., Davis, F.P., Mukamel, E.A., Henry, G.L., Nery, J.R., Urich, M.A., Picard, S., Lister, R., Eddy, S.R., et al. (2016). Epigenomic landscapes of retinal rods and cones. Elife *5*, e11613. 10.7554/eLife.11613.

73. Brooks, M.J., Rajasimha, H.K., Roger, J.E., and Swaroop, A. (2011). Next-generation sequencing facilitates quantitative analysis of wild-type and Nrl(-/-) retinal transcriptomes. Mol Vis *17*, 3034-3054.

74. Yoshida, S., Mears, A.J., Friedman, J.S., Carter, T., He, S., Oh, E., Jing, Y., Farjo, R., Fleury, G., Barlow, C., et al. (2004). Expression profiling of the developing and mature Nrl-/- mouse retina: identification of retinal disease candidates and transcriptional regulatory targets of Nrl. Hum Mol Genet *13*, 1487-1503. 10.1093/hmg/ddh160.

75. Sun, S.C. (2017). The non-canonical NF-kappaB pathway in immunity and inflammation. Nat Rev Immunol *17*, 545-558. 10.1038/nri.2017.52.

76. Kim, J.W., Yang, H.J., Brooks, M.J., Zelinger, L., Karakulah, G., Gotoh, N., Boleda, A., Gieser, L., Giuste, F., Whitaker, D.T., et al. (2016). NRL-Regulated Transcriptome Dynamics of Developing Rod Photoreceptors. Cell Rep *17*, 2460-2473. 10.1016/j.celrep.2016.10.074.

77. Sun, S.C. (2008). Deubiquitylation and regulation of the immune response. Nat Rev Immunol *8*, 501-511. 10.1038/nri2337.

78. Catrysse, L., Vereecke, L., Beyaert, R., and van Loo, G. (2014). A20 in inflammation and autoimmunity. Trends Immunol *35*, 22-31. 10.1016/j.it.2013.10.005.

79. Hu, H., Brittain, G.C., Chang, J.H., Puebla-Osorio, N., Jin, J., Zal, A., Xiao, Y., Cheng, X., Chang, M., Fu, Y.X., et al. (2013). OTUD7B controls non-canonical

NF-kappaB activation through deubiquitination of TRAF3. Nature *494*, 371-374. 10.1038/nature11831.

80. Enesa, K., Zakkar, M., Chaudhury, H., Luong le, A., Rawlinson, L., Mason, J.C., Haskard, D.O., Dean, J.L., and Evans, P.C. (2008). NF-kappaB suppression by the deubiquitinating enzyme Cezanne: a novel negative feedback loop in pro-inflammatory signaling. J Biol Chem *283*, 7036-7045. 10.1074/jbc.M708690200.

81. Ji, Y., Cao, L., Zeng, L., Zhang, Z., Xiao, Q., Guan, P., Chen, S., Chen, Y., Wang, M., and Guo, D. (2018). The N-terminal ubiquitin-associated domain of Cezanne is crucial for its function to suppress NF-kappaB pathway. J Cell Biochem *119*, 1979-1991. 10.1002/jcb.26359.

82. Luong le, A., Fragiadaki, M., Smith, J., Boyle, J., Lutz, J., Dean, J.L., Harten, S., Ashcroft, M., Walmsley, S.R., Haskard, D.O., et al. (2013). Cezanne regulates inflammatory responses to hypoxia in endothelial cells by targeting TRAF6 for deubiquitination. Circ Res *112*, 1583-1591. 10.1161/CIRCRESAHA.111.300119.

83. Zarnegar, B., Yamazaki, S., He, J.Q., and Cheng, G. (2008). Control of canonical NF-kappaB activation through the NIK-IKK complex pathway. Proc Natl Acad Sci U S A *105*, 3503-3508. 10.1073/pnas.0707959105.

84. Cui, C.P., Zhang, Y., Wang, C., Yuan, F., Li, H., Yao, Y., Chen, Y., Li, C., Wei, W., Liu, C.H., et al. (2018). Dynamic ubiquitylation of Sox2 regulates proteostasis and governs neural progenitor cell differentiation. Nat Commun *9*, 4648. 10.1038/s41467-018-07025-z.

85. Taranova, O.V., Magness, S.T., Fagan, B.M., Wu, Y., Surzenko, N., Hutton, S.R., and Pevny, L.H. (2006). SOX2 is a dose-dependent regulator of retinal neural progenitor competence. Genes Dev *20*, 1187-1202. 10.1101/gad.1407906.

86. Surzenko, N., Crowl, T., Bachleda, A., Langer, L., and Pevny, L. (2013). SOX2 maintains the quiescent progenitor cell state of postnatal retinal Muller glia. Development *140*, 1445-1456. 10.1242/dev.071878.

87. Lin, Y.P., Ouchi, Y., Satoh, S., and Watanabe, S. (2009). Sox2 plays a role in the induction of amacrine and Muller glial cells in mouse retinal progenitor cells. Invest Ophthalmol Vis Sci *50*, 68-74. 10.1167/iovs.07-1619.

88. Melick, C.H., and Jewell, J.L. (2020). Regulation of mTORC1 by Upstream Stimuli. Genes (Basel) *11*. 10.3390/genes11090989.

89. Wang, B., Jie, Z., Joo, D., Ordureau, A., Liu, P., Gan, W., Guo, J., Zhang, J., North, B.J., Dai, X., et al. (2017). TRAF2 and OTUD7B govern a ubiquitin-dependent switch that regulates mTORC2 signalling. Nature *545*, 365-369. 10.1038/nature22344.

90. Venkatesh, A., Ma, S., Le, Y.Z., Hall, M.N., Ruegg, M.A., and Punzo, C. (2015). Activated mTORC1 promotes long-term cone survival in retinitis pigmentosa mice. J Clin Invest *125*, 1446-1458. 10.1172/JCI79766.

91. Cong, L., Ran, F.A., Cox, D., Lin, S., Barretto, R., Habib, N., Hsu, P.D., Wu, X., Jiang, W., Marraffini, L.A., and Zhang, F. (2013). Multiplex genome engineering using CRISPR/Cas systems. Science *339*, 819-823. 10.1126/science.1231143.

92. Shinkai, Y., Satoh, H., Takeda, N., Fukuda, M., Chiba, E., Kato, T., Kuramochi, T., and Araki, Y. (2002). A testicular germ cell-associated serine-threonine kinase, MAK, is dispensable for sperm formation. Mol Cell Biol *22*, 3276-3280. 10.1128/MCB.22.10.3276-3280.2002.

93. Chaya, T., Omori, Y., Kuwahara, R., and Furukawa, T. (2014). ICK is essential for cell type-specific ciliogenesis and the regulation of ciliary transport. EMBO J *33*,

1227-1242. 10.1002/embj.201488175.

94. Irie, S., Sanuki, R., Muranishi, Y., Kato, K., Chaya, T., and Furukawa, T. (2015). Rax Homeoprotein Regulates Photoreceptor Cell Maturation and Survival in Association with Crx in the Postnatal Mouse Retina. Mol Cell Biol *35*, 2583-2596. 10.1128/MCB.00048-15.

95. Itoh, Y., Moriyama, Y., Hasegawa, T., Endo, T.A., Toyoda, T., and Gotoh, Y. (2013). Scratch regulates neuronal migration onset via an epithelial-mesenchymal transition-like mechanism. Nat Neurosci *16*, 416-425. 10.1038/nn.3336.

96. Okamoto, S., Chaya, T., Omori, Y., Kuwahara, R., Kubo, S., Sakaguchi, H., and Furukawa, T. (2017). Ick Ciliary Kinase Is Essential for Planar Cell Polarity Formation in Inner Ear Hair Cells and Hearing Function. J Neurosci *37*, 2073-2085. 10.1523/JNEUROSCI.3067-16.2017.

97. Tsutsumi, R., Chaya, T., and Furukawa, T. (2018). Enriched expression of the ciliopathy gene Ick in cell proliferating regions of adult mice. Gene Expr Patterns *29*, 18-23. 10.1016/j.gep.2018.04.005.

98. Chaya, T., Ishikane, H., Varner, L.R., Sugita, Y., Maeda, Y., Tsutsumi, R., Motooka, D., Okuzaki, D., and Furukawa, T. (2022). Deficiency of the neurodevelopmental disorder-associated gene Cyfip2 alters the retinal ganglion cell properties and visual acuity. Hum Mol Genet *31*, 535-547. 10.1093/hmg/ddab268.

99. Sato, S., Omori, Y., Katoh, K., Kondo, M., Kanagawa, M., Miyata, K., Funabiki, K., Koyasu, T., Kajimura, N., Miyoshi, T., et al. (2008). Pikachurin, a dystroglycan ligand, is essential for photoreceptor ribbon synapse formation. Nat Neurosci *11*, 923-931. 10.1038/nn.2160.

100. Koike, C., Nishida, A., Ueno, S., Saito, H., Sanuki, R., Sato, S., Furukawa, A.,

Aizawa, S., Matsuo, I., Suzuki, N., et al. (2007). Functional roles of Otx2 transcription factor in postnatal mouse retinal development. Mol Cell Biol *27*, 8318-8329. 10.1128/MCB.01209-07.

101. Wenzel, A., Reme, C.E., Williams, T.P., Hafezi, F., and Grimm, C. (2001). The Rpe65 Leu450Met variation increases retinal resistance against light-induced degeneration by slowing rhodopsin regeneration. J Neurosci *21*, 53-58. 10.1523/JNEUROSCI.21-01-00053.2001.

102. Tsutsumi, R., Chaya, T., Tsujii, T., and Furukawa, T. (2022). The carboxyl-terminal region of SDCCAG8 comprises a functional module essential for cilia formation as well as organ development and homeostasis. J Biol Chem *298*, 101686. 10.1016/j.jbc.2022.101686.

103. Kubo, S., Yamamoto, H., Kajimura, N., Omori, Y., Maeda, Y., Chaya, T., and Furukawa, T. (2021). Functional analysis of Samd11, a retinal photoreceptor PRC1 component, in establishing rod photoreceptor identity. Sci Rep *11*, 4180. 10.1038/s41598-021-83781-1.

104. Chaya, T., Maeda, Y., Sugimura, R., Okuzaki, D., Watanabe, S., Varner, L.R., Motooka, D., Gyoten, D., Yamamoto, H., Kato, H., and Furukawa, T. (2022). Multiple knockout mouse and embryonic stem cell models reveal the role of miR-124a in neuronal maturation. J Biol Chem *298*, 102293. 10.1016/j.jbc.2022.102293.

Table1. Primer sequences

Experiment	Primer name	Sequence (5' to 3')
CRISPR	Otud7b-gRNA1-F	CACCGTGGAACGAACAAAATCCGAC
	Otud7b-gRNA1-R	AAACGTCGGATTTTGTTCGTTCCAC
	Otud7b-sgRNA2-F	CACCGCAGCCCTGGCTCTGCACCTG
	Otud7b-sgRNA2-R	AAACCAGGTGCAGAGCCAGGGCTGC
Otud7b –/– genotyping	Otud7b-PCR-51	CTGGTTAGGTGAGCCTTGTGCATGCA
	Otud7b-PCR-31	CATACAAGGTGACCAGGGAATCTGTG
RT-PCR	Otud7b-RT-PCR-52	CAGCTTCATAGAGCGAGACCTCATTGA
	Otud7b-RT-PCR-32	TCCTCAGCACCAAGTCTCTATCATGGA
	beta-actin-RT-PCR-51	CGTGCGTGACATCAAAGAGAA
	beta-actin-RT-PCR-31	TGGATGCCACAGGATTCCAT
	human Otud7b RT-PCR-51	TGAGCAGTCCATGCTGGTTGCCTTGGA
	human Otud7b RT-PCR-31	GCTTTCCGCAGCATCAAGTCCCGATCA
	human beta-actin RT-PCR-51	CACCACACCTTCTACAATGAGCTG
	human beta-actin RT-PCR-31	GAGTCCATCACGATGCCAGTGGTA
Construct pCAGGSII-N-3x-FLAG mouse Otud7b	mOtud7b-ORF-SalI-51	GGGGTCGACATGACCCTGGACATGGATGCTGTC
	mOtud7b-ORF-EcoRI-31	ACATGGAATTCCTCTAGGCTTTCA
	mOtud7b-ORF-kozak-SalI-51	GGGGTCGACGCCACCATGACCCTGGACATGGATGCTGTC
	mOtud7b-ORF-NotI-31	GGGGCGGCCGCTCAGAACCTGTGTGCCAGCAGTTC